Mechanistic Studies of NO Sensing and Detoxification by Bacterial Iron-Containing Proteins

By

Erik Thomas Yukl

A DISSERTATION

Presented to the Department of Science and Engineering
and the Oregon Health & Science University
School of Medicine
In partial fulfillment of
the requirements for the degree of

Doctor of Philosophy

December 2009

Department of Science and Engineering
School of Medicine
Oregon Health and Science University

CERTIFICATE OF APPROVAL

This is to certify that the Ph.D. dissertation of
Erik Thomas Yukl
has been approved

Dr. Pierre Moënne-Loccoz, Thesis Advisor
Associate Professor

Dr. Michiko M. Nakano
Research Associate Professor

Dr. David L. Farrens
Associate Professor

Dr. Mario Rivera
Professor, University of Kansas

TABLE OF CONTENTS

LIST OF TABLES

LIST OF FIGURES

ACKNOWLEDGEMENTS

I would like to begin by thanking my research advisor, Dr. Pierre Moënne-Loccoz for his patience, guidance, and support during my graduate studies. The learning environment in his laboratory provided the perfect balance of independent experimentation and guided instruction. Further, outside of the laboratory, his hospitality and friendship were greater than I ever could have expected. I would also like to thank Takahiro Hayashi for his fresh insights and many interesting discussions. Of course, this research would have been impossible without the hard work of our collaborators in the research groups of Profs. Paul Ortiz de Montellano, Mario Rivera, Michiko Nakano, and Simon de Vries. Their contributions of samples and thought-provoking discussions were indispensible. I am also grateful to the instructors under whom I have had the privilege to study including Profs. Pierre Moënne-Loccoz, Peter Zuber, Gebretateos Woldegiorgis, Ninian Blackburn, and James Whittaker as well as the entire faculty of the Department of Science and Engineering. I must also thank my committee members, Drs. Pierre Moënne-Loccoz, Michiko Nakano, David Farrens, and Mario Rivera for carefully reviewing my dissertation. Finally, special thanks are due to my family and friends, particularly to my parents whose unconditional love and sacrifice have made all of my life's accomplishments possible.

ABSTRACT

Mechanistic Studies of NO Sensing and Detoxification by Bacterial Iron-Containing Proteins

Erik Thomas Yukl, B. S.

Doctor of Philosophy
Division of Environmental and Biomolecular Systems within
the Department of Science and Engineering
and the Oregon Health and Science University
School of Medicine

September, 2009
Thesis Advisor: Pierre Moënne-Loccoz

Our research goal is to understand the mechanisms by which metalloproteins sense and detoxify nitric oxide (NO). We have characterized two different bacterial sensor proteins which employ different metal cofactors to detect NO. Further, we have investigated the NO dioxygenase reaction utilized by the hemoglobin homologues of both mammals and bacteria to detoxify NO. These reactions are important for understanding how NO levels are determined and controlled in both mammalian and bacterial systems.

DevS is a heme-based sensor kinase from *Mycobacterium tuberculosis* (MTB) which senses CO, NO and hypoxia. Upon reception of these signals, DevS autophosphorylates and transfers the phosphate group to the response regulator DevR, which induces a regulon associated with entrance of the bacterium into a dormant state. We use UV-vis and resonance Raman (RR) spectroscopy of full-length and truncated

proteins as well as activity assays of wild type (wt) and variant forms in Fe(II), CO, NO, and O_2-bound states to determine the mechanism by which DevS differentiates exogenous ligands and communicates this information from the heme to the kinase domain. Our results identify a specific hydrogen bond network, stabilized by distal residue Tyr171, which is required to differentiate between the activating ligands CO and NO and the inhibitory ligand O_2. This signal is communicated to the kinase domain by interactions between the heme-binding GAF-A domain and second GAF domain called GAF-B.

We have also investigated the NO-sensing transcriptional repressor NsrR from *Bacillus subtilis*. NO relieves repression of flavohemoglobin and nitrite reductase genes by NsrR. We use UV-vis, EPR, and RR spectroscopy to determine that this protein contains a [4Fe-4S] which is reactive toward NO. Thus, it seems likely that conformational changes caused by the binding of NO to the Fe-S cluster of NsrR are responsible for its NO-sensing ability.

Finally, we investigated the NO dioxygenase mechanism of myoglobin. This reaction represents a major route of NO detoxification for both mammals and bacteria. NO reacts with the oxy-heme, leading to complete conversion to nitrate via a peroxynitrite intermediate. Here we use RR spectroscopy of rapid freeze quench (RFQ) samples to demonstrate that the millisecond intermediate previously thought to be a Fe(III)-peroxynitrite is in fact a Fe(III)-nitrato complex. We show that DevS also efficiently catalyzes this reaction which would provide MTB with another route for resistance to NO.

CHAPTER 1
METALLOPROTEINS AND BIOLOGICAL GAS SENSING

1.1 Role of Diatomic Gas Sensing in Pathogenesis and Metabolism

The ability to detect and respond to changes in the environment is a challenge that all organisms must overcome in order to survive. These environmental changes include fluctuations in redox potential, pH, temperature, light, availability of nutrients, etc. Diatomic gases such as O_2, NO, and CO have been identified as important substrates for sensor proteins involved in the biological response to external stimuli. Although the specific mechanisms of coupling gas sensing to biological response are quite diverse, the general trend is that the binding of the relevant gas leads to a conformational change which alters the activity of the protein or of a partner protein. Metal sites, particularly heme iron sites and iron-sulfur clusters, are commonly used to bind these effector molecules. The changes at the metal center affect the activity of a wide variety of output functions. Table 1.1 summarizes some of the better known metal-based gas sensor proteins and their output activities.

Oxygen sensing is particularly important in facultative aerobic organisms. Oxygen is utilized as the terminal electron acceptor in these organisms when present at sufficient levels due to its abundance, solubility, and the energetic favorability of its reduction. However, under oxygen-limiting conditions, these organisms can utilize other terminal electron acceptors such as nitrate. A sensitive oxygen sensing apparatus is therefore required to prevent the wasteful expression of proteins dedicated to this alternate pathway when oxygen is available. NO sensing is also important in this regard in that it is a toxic byproduct of nitrate respiration. Consequently, systems are required to allow the organism to sense NO and provide the appropriate cellular response, such as

induction of NO detoxifying enzymes like flavohemoglobin (Hmp) and nitric oxide reductase (NOR). Finally, CO levels can also impact metabolism. For example, *Rhodospirillum rubrum*, an organism found in mud, pond and sewer water, is capable of multiple metabolic modes including anaerobic growth on CO as a sole carbon source (Kerby *et al.*, 1995). The expression of genes associated with CO oxidation is dependent upon the presence of CO, and this effect is mediated by a specific sensor (Kerby *et al.*, 1992).

Table 1.1 Characteristics of known metal-containing diatomic gas sensing proteins. Reviewed in [a] (Gilles-Gonzalez *et al.*, 2008) and this work chapters 3 and 4; [b] (Uchida and Kitagawa, 2005); [c] this work chapter 5; [d] (Kiley and Beinert, 2003); [e] (D'Autreaux *et al.*, 2008). nb = no binding

Protein	**Sensing Cofactor / Ligation**	**Activity / Target Function**	**Ligand (Activity)**
DevS[a]	5cHS b-Heme / His	Kinase / DevR Nonreplicating persistence	O_2 (-), CO (++), NO (++), none (+)
FixL[b]	5cHS b-Heme / His	Kinase / FixJ Expression of N_2 fixation genes	O_2 (-), CO (+), NO (+), none (++)
sGC[b]	5cHS b-Heme / His	GTP→cGMP Vasodilation, etc	O_2 (nb), CO (-), NO (++), none (-)
HemAT[b]	5cHS b-Heme / His	Kinase Activaton / CheA Aerotaxis	O_2 (++), CO (-), NO (-), none (-)
EcDos[b]	6cLS b-Heme / His/Met	Phosphodiesterase / cAMP	O_2 (-), CO (-), NO (-), none (++)
CooA[b]	6cLS b-Heme / His/Pro	Transcriptional Activator / *coo* genes CO-dependant growth	O_2 (-), CO (++), NO (-), none (-)
NsrR[c]	4Fe-4S	Transcriptional Repressor / *hmp, nasDEF* NO_3^- metabolism, NO detoxification	NO (-), O_2 (?)
FNR[d]	4Fe-4S	Transcriptional Repressor / *narGHIJK, fnr* NO_3^- metabolism	O_2 (-), NO (-)
SoxR[d]	2Fe-2S	Transcriptional Activator / *soxS* Oxidative repair	NO (+), O_2^- (+)
NorR[e]	Nonheme Fe	Transcription Activator / *hmp,* NO reductase genes NO detox	NO (+)

Diatomic gas sensors have also been implicated in enhancing the virulence and survival of pathogens within the host. *Mycobacterium tuberculosis* provides an excellent example of this phenomenon. Although technically an obligate aerobe, *M. tuberculosis* is capable of surviving for long periods at very low oxygen tensions by shifting to a dormant state (Wayne and Hayes, 1996). It has further been observed that a transcription profile characterizing this state can be induced by hypoxia (Voskuil *et al.*, 2003), NO (Voskuil *et al.*, 2003), and CO (Kumar *et al.*, 2008; Shiloh *et al.*, 2008). The physiological relevance of this is apparent in that it enables the pathogen to survive within granulomas which are microaerobic or anaerobic ((Wayne and Sohaskey, 2001) and references therein), where NO is generated by inducible nitric oxide synthase (iNOS) (Choi *et al.*, 2002), and where CO is generated by the heme metabolizing action of heme oxygenase (HO-1) (Kumar *et al.*, 2008; Shiloh *et al.*, 2008). This phenomenon demonstrates how the sensing of all three physiologically relevant diatomic gases plays a role in pathogen survival and how understanding the mechanisms of diatomic gas sensing can have tremendous impact on the treatment of disease.

1.2 Heme-based Sensors

The high affinity of heme iron for diatomic gases makes this prosthetic group an ideal choice for sensing these molecules. Further, interactions between heme ligands and protein residues in the heme pocket provide a mechanism for signal transduction as well as for differentiating between similar ligands, two critical qualities in any sensor. Therefore, it is not surprising that a large and growing number of heme-based sensor proteins are now known. These proteins exhibit great diversity in structure and function and are typically modular in design, with a sensing domain which houses the heme and an output domain whose activity is dependent on the heme state (Uchida and Kitagawa, 2005). A variety of different folds are utilized as sensing domains, including PAS, GAF, and globin domains as well as several unique heme-binding domains which have been identified in gas sensor proteins. Output domains are also highly variable having DNA binding, kinase, phosphodiestease, and guanylate cyclase activities among others. This

organization allows for tremendous versatility in effector specificity and the physiological response elicited.

Mechanisms of ligand discrimination and signal transduction by heme sensors can be grouped into three general categories: the distal, proximal, and peripheral pathways (Fig. 1.1). Activation via the distal pathway refers to a specific conformational change which occurs as a consequence of the target ligand binding to the distal side of the heme. This may be a result of displacement of an endogenous distal ligand or of electrostatic and/or steric interactions between the bound ligand and residues in the distal pocket. In the proximal pathway mechanism, the conformational change accompanying target ligand binding is mediated by a change in interactions on the proximal side of the heme. Finally, heme peripheral groups (propionate and vinyl groups in the case of b-type hemes) are also capable of changing their orientations in a ligand-dependent manner, making them potential players in the signal transduction and ligand discrimination processes. These pathways are not mutually exclusive and all three may be found to be operating within the same protein. Of critical importance is that the conformational change which occurs at the sensing domain be conveyed to the output domain only when the appropriate signal is received. Examples of how these different pathways are used by known heme-based gas sensors are given below.

Our work with DevS, a heme-based sensor kinase from several mycobacteria including *M. tuberculosis*, is described in detail in chapters 3, 4, and 7. We identify specific electrostatic interaction with effector molecules and conclude that a distal activation pathway is predominant. Briefly, a distal residue forms a hydrogen bond with bound oxygen (off state) that is absent in the Fe(II) unligated, CO-bound, and NO-bound states (on states), making this a specific sensor of oxygen (Ioanoviciu *et al.*, 2007; Podust *et al.*, 2008; Yukl *et al.*, 2007; Yukl *et al.*, 2008).

FixL is a heme-based sensor protein found in *Rhizobia* species which allows the organism to adapt to the microaerobic environment of root nodules (Sciotti *et al.*, 2003). This protein is a histidine kinase which is active in the Fe(II) deoxy state. This activity is severely inhibited when oxygen is bound to heme but is only slightly inhibited when the

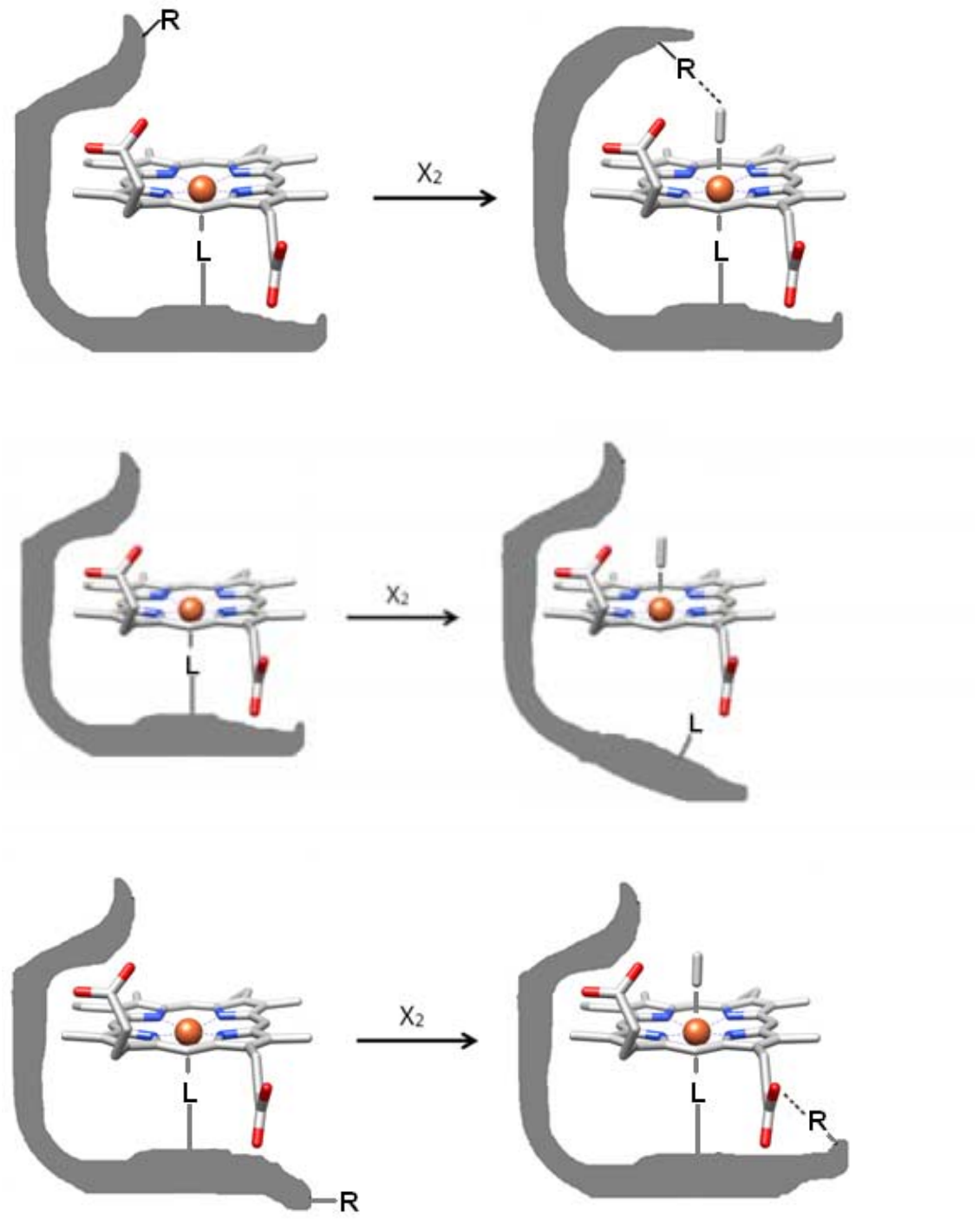

Fig. 1.1 The distal (top), proximal (middle), and peripheral (bottom) pathways of signal transduction in heme-based sensor proteins. L represents the proximal heme ligand, R a protein residue, and exogenous diatomic ligands (X_2) are represented by a gray bar.

heme is bound to NO or CO (Dunham *et al.*, 2003; Tuckerman *et al.*, 2002). As one of the best characterized of the heme-based sensor proteins, crystal structures are available for the heme domain in all of these states (Fig. 1.2), and they reveal a mechanism of ligand discrimination and signal transduction which utilizes both distal and peripheral pathways (Hao *et al.*, 2002). Specifically, in the O_2-bound off-state, a distal arginine residue (Arg220) makes a hydrogen bond with the bound oxygen molecule. Dissociation of this ligand to the deoxy on-state results in a change in the conformation of a propionate peripheral group so that it engages in a hydrogen bond with Arg220, leading to a conformational change and kinase activity. The structures of the NO- and CO-bound forms are similar to the deoxy with the Arg-propionate interaction intact, explaining the relatively mild inhibition these ligands exert on kinase activity. Thus, FixL uses specific interactions between the target ligand and a distal residue (the distal pathway) as well as interactions at a heme propionate group (the peripheral pathway) to specifically sense oxygen.

Another example of mixed peripheral and distal pathways is provided by HemAT, an oxygen sensor involved in the aerotactic response of various bacteria and archaea (Hou *et al.*, 2000). Resonance Raman (RR) studies of wt and mutant HemAT proteins revealed the formation of a hydrogen bond between a histidine residue and heme propionate 6 upon O_2 binding which is absent upon binding of CO or NO (Yoshimura *et al.*, 2006). This interaction induces a conformational change allowing a distal threonine residue to directly hydrogen bond with the bound O_2 ligand, finalizing the signal transduction process. No change occurs at heme propionate 6 upon CO or NO binding, preventing the threonine residue from hydrogen bonding with these ligands (Yoshimura *et al.*, 2006). Thus, HemAT utilizes a stepwise sensing mechanism requiring a specific change at a peripheral group upon binding of target followed by an interaction of a distal residue with the bound O_2. This example also demonstrates the utility of RR to the study of heme-based sensor proteins as this technique allows for the observation of heme spin, coordination, and ligation state as well as interactions between protein residues and exogenous heme ligands and peripheral groups (see section 2.1 for more details).

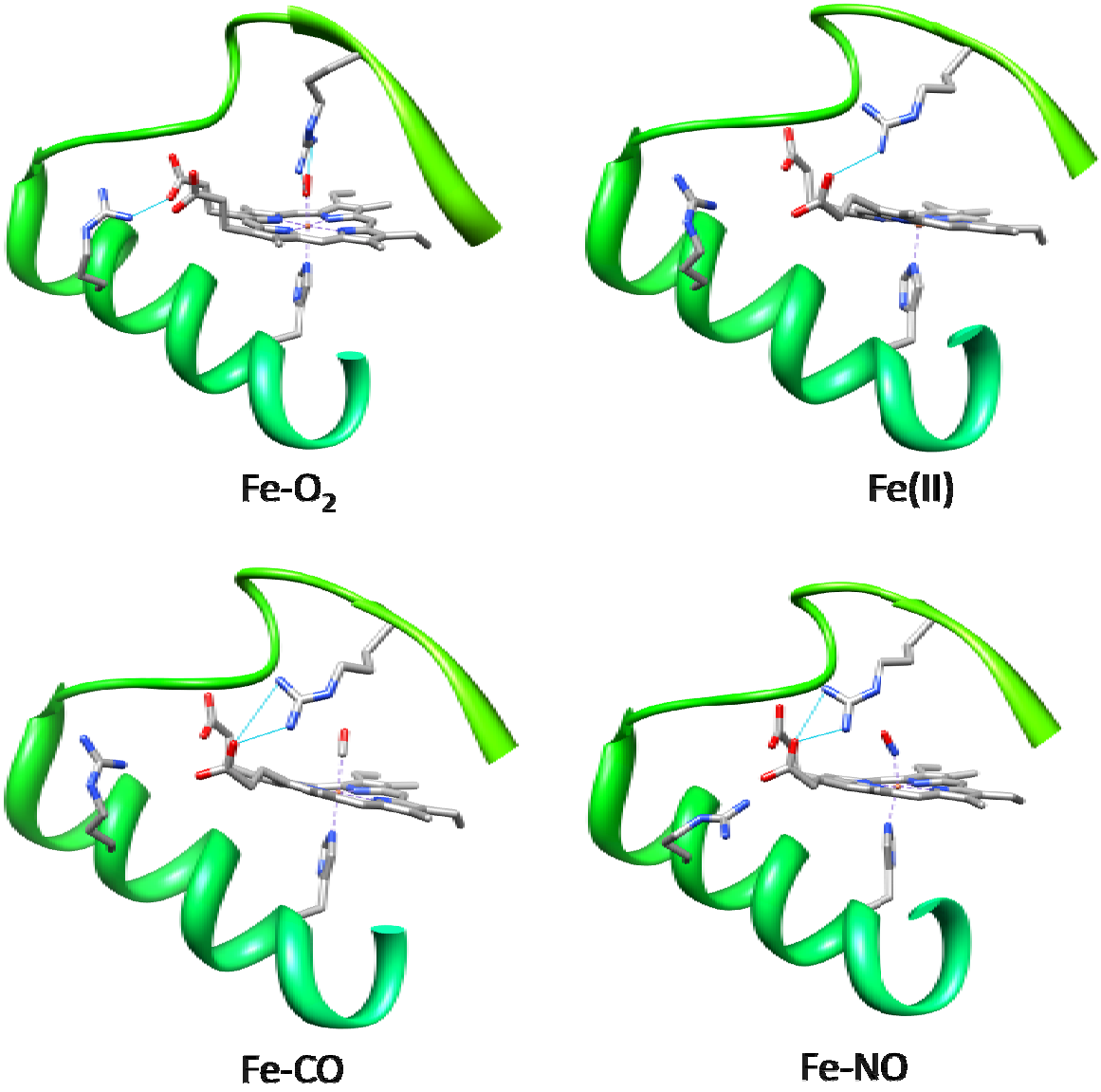

Fig. 1.2 Crystal structures of the *Bradyrhizobium japonicum* FixLH heme binding pocket in the oxy, Fe(II), CO- and NO-bound forms (PDB codes 1DP6, 1LSW, 1LSV, and 1DP8, respectively). Hydrogen bonds are denoted by cyan lines. Adapted from (Hao *et al.*, 2002).

A relatively simple distal mechanism is seen in the CO sensing transcription factor CooA of *R. rubrum* which has an N-terminal heme-binding (sensor) domain and a C-terminal DNA-binding (output) domain (Lanzilotta *et al.*, 2000). Fe(II) CooA is inactive as a transcription factor (Aono *et al.*, 1997), and the heme in this case is 6-coordinate with axial His and Pro ligands (Lanzilotta *et al.*, 2000). Binding of CO forms a 6-coordinate adduct by displacing the proline ligand, (Uchida *et al.*, 2000; Yamamoto *et al.*, 2001) presumably resulting in a significant conformational change which allows the protein to bind the promoters of target genes. A stable O_2 adduct is not formed due to rapid autoxidation (Aono *et al.*, 1996) and, although NO will bind to the heme, it forms a 5-coordinate complex which is inactive (Reynolds *et al.*, 2000). These properties, coupled with the displacement of the ligating proline residue by CO make CooA a specific sensor for CO.

Perhaps the best known example of the proximal activation pathway comes from vertebrate soluble guanylate cyclase (sGC). When activated by NO, this enzyme catalyzes the conversion of GTP to cGMP (Arnold *et al.*, 1977), an important secondary messenger in a variety of physiological processes (Moncada *et al.*, 1991). In its Fe(II) form, the heme of sGC is 5-coordinate with a proximal histidine bond, (Stone *et al.*, 1995). NO specificity is achieved by the formation of a 5-coordinate NO complex where the proximal histidine ligand is ruptured upon NO binding (Stone *et al.*, 1995). Although CO readily binds to the heme, it forms a 6-coordinate complex insufficient to activate sGC. Interestingly, oxygen is not observed to bind to the heme of sGC (Deinum *et al.*, 1996), effectively removing the need to discriminate against this ligand by other means. However, the formation of a 5-coordinate heme-NO adduct is not sufficient for full activation of the enzyme and it has been hypothesized that a second NO site must be occupied for full sGC activation (Cary *et al.*, 2005; Russwurm and Koesling, 2004). Thus, although the proximal pathway is utilized in this enzyme, the detailed mechanism of activation of sGC by NO remains to be elucidated.

1.3 Fe-S Cluster-based Sensors

Fe-S clusters are typically known for their role in electron transport and redox reactions. However, they have also been found to be essential to the regulatory function of some transcription factors. Both NO and O_2 can modify these clusters, causing a change in their DNA binding activity. These clusters are divided into several types depending on the number of iron atoms they contain. Those found in known Fe-S cluster-based sensors are of the [2Fe-2S], [3Fe-4S], or [4Fe-4S] types (Fig. 1.3) and conversions between these states have been observed. The mechanisms of signal transduction are varied but all involve changes occurring at the Fe-S cluster. Below are a few examples of these Fe-S cluster-based sensors and what is known about their signaling mechanisms.

FNR

In *E. coli*, FNR (*Ec*FNR) is a regulator of genes involved in the response to oxygen limitation (Green *et al.*, 2001; Kiley and Beinert, 1998). Under anaerobic conditions, this protein is a homodimer with one $[4Fe\text{-}4S]^{2+}$ cluster per subunit. In this state, *Ec*FNR is an active repressor of genes associated with aerobic respiration and an activator of those required for utilization of alternative electron acceptors such as nitrate or fumarate (Bates *et al.*, 2000). Upon exposure to sufficient levels of oxygen, the

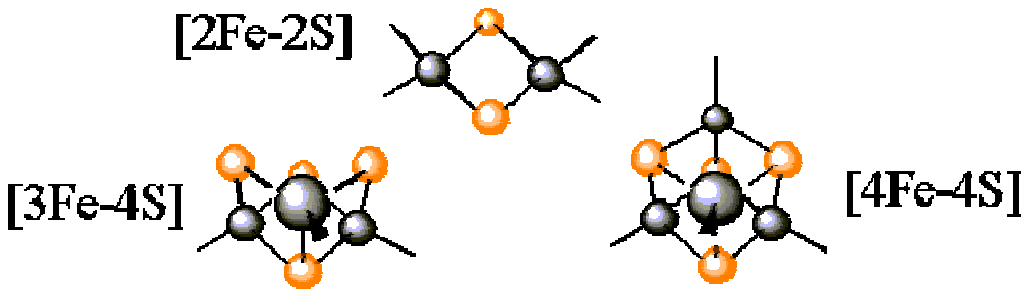

Fig. 1.3 Iron-sulfur cluster types found in known sensor proteins

$[4Fe\text{-}4S]^{2+}$ cluster is converted to a $[2Fe\text{-}2S]^{2+}$ cluster with a concomitant loss in DNA binding activity. This is thought to proceed by a disruption in the dimer interface,

leading to dissociation into monomers which are unable to bind DNA and control gene expression (Khoroshilova *et al.*, 1997). The Fe-S cluster of *Ec*FNR has also been observed to react with NO to produce both monomeric and dimeric, and protein-bound dinitrosyl iron complexes (DNIC). These changes also result in loss of DNA-binding activity causing derepression of *hmp*, a gene coding for a NO detoxifying flavohemoglobin (Cruz-Ramos *et al.*, 2002). In this case, a mechanism is proposed which involves the NO-induced formation of a $[2Fe\text{-}2S]^{2+}$ cluster followed by further reaction to yield the DNIC products. In any case, the end result is the loss of biological activity upon exposure to NO.

Interestingly, the FNR homologue from *B. subtilis* (*Bs*FNR) has a very similar function to that from *E. coli*, yet responds to oxygen via a very different mechanism. In this case, exposure to oxygen results in the formation of apo-protein rather than a relatively stable $[2Fe\text{-}2S]^{2+}$ cluster. DNA binding is lost but not due to dissociation of dimers as the dimerization state of apo-*Bs*FNR is intact (Reents *et al.*, 2006). Rather, a more subtle conformational change must accompany the loss of the Fe-S cluster in *Bs*FNR. The difference may arise as a result of the different binding locations of the clusters in *Ec* and *Bs*FNR and/or the observation that the $[4Fe\text{-}4S]^{2+}$ cluster of *Bs*FNR is ligated by only three cysteine residues whereas four are present in *Ec*FNR (Reents *et al.*, 2006). FNR provides a good example of the potential complexity encountered when dealing with Fe-S cluster based sensor systems.

SoxR

SoxR is responsible for activating the transcription of *soxS* in response to both superoxide (Demple *et al.*, 2002) and NO (Ding and Demple, 2000) stress. Accumulation of the transcription factor SoxS leads to the induction of a set of genes associated with superoxide removal and repair of oxidative damage (Demple *et al.*, 2002). Under normal, aerobic conditions, SoxR is predicted to exist as a homodimer with each subunit containing one $[2Fe\text{-}2S]^{+}$ cluster. In this form SoxR can still bind its target DNA but is unable to stimulate transcription. Upon exposure to superoxide, the $[2Fe\text{-}2S]^{+}$ cluster is likely oxidized to the $[2Fe\text{-}2S]^{2+}$ form, resulting in activation of SoxR and transcription of *soxS* is induced (Demple *et al.*, 2002). A similar outcome is noted during

anaerobic exposure to NO. However, in this case, activation results from the conversion of the $[2Fe\text{-}2S]^{+}$ cluster to a DNIC rather than through oxidation to the $[2Fe\text{-}2S]^{2+}$ state (Ding and Demple, 2000). Thus, the mechanism of SoxR differs from that of FNR in several important aspects. First, oxidation or reaction with NO *activates* the transcriptional activity of SoxR. Secondly, reaction with superoxide or NO does not block DNA binding as the affinity of SoxR for target DNA does not seem to be affected by modification of its Fe-S cluster (Demple *et al.*, 2002). Rather, it would seem to cause a structural change leading to favorable interaction with components of the transcription machinery.

1.4 Mechanisms of NO Detoxification

As previously mentioned, bacteria are exposed to NO either as a result of the host immune response, in the case of pathogens, or as a byproduct of denitrification or nitrate respiration. Although NO decays rapidly upon reaction with superoxide, the product of this reaction, peroxynitrite, is also highly damaging to multiple enzymes and cell structures. Therefore, mechanisms for its remediation which do not result in peroxynitrite formation are essential for these organisms. Routes to detoxification involve either a NO reductase (NOR) or a NO dioxygenase (NOD) mechanism. Here we will focus on the oxygen-dependent NO dioxygenase mechanism.

Microbial homologues of human hemoglobin (Hb) such as flavohemoglobins (flavoHbs) are thought to provide the primary defense against NO toxicity in many diverse microbes (Gardner, 2005). These proteins contain a globin domain and an FAD-binding domain (Fig. 1.4). Oxygen binds to the reduced heme and reacts with NO to quantitatively produce NO_3^- and Fe(III) heme. Electrons from NAD(P)H are funneled through the FAD cofactor to reduce the heme and allow for binding of another oxygen molecule and catalysis.

Human Hb and myoglobin (Mb) have also been shown to possess high NOD activity (Herold *et al.*, 2001) although, in this case, an external reductase is required for catalysis (Fig. 1.4). This reaction is physiologically relevant in mammals considering that NO is used as an important signaling molecule, with low NO fluxes influencing such

diverse functions as immune response, vasodilation, and smooth muscle contraction among others (Moncada *et al.*, 1991). Given the high concentrations of Mb and Hb, these proteins likely have a significant effect on NO signaling. Here, we speculate that this reaction may also play a direct role in diatomic gas sensing. Indeed, if a heme-based sensor protein of the type describe earlier in this chapter can perform the NOD reaction, the NO-mediated conversion of the oxy to the met form of the heme could impact the output activity. We have observed this activity in DevS from *M.* tuberculosis and discuss its potential physiological relevance in chapter 7. Thus, given the importance of the NOD reaction in mammals as well as its apparent ubiquity in bacterial systems as a protective mechanism, a detailed understanding of this reaction could be instrumental to treating a variety of human health concerns.

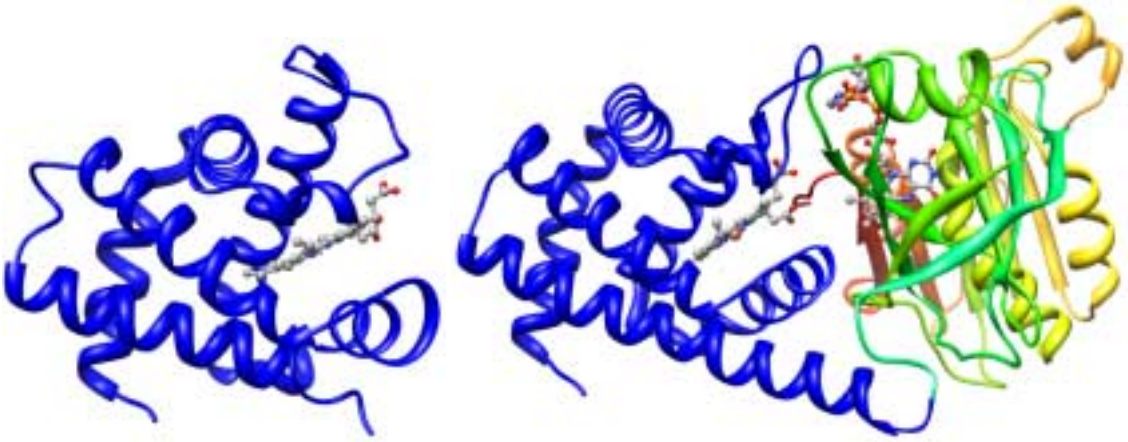

Fig. 1.4 Structural comparison of the α subunit of Hb (left, 2W6V) with flavohemoblogin from *E. coli* (right, 1GVH) . The globin domains are shown as blue ribbons, the FAD-binding domain as multicolored ribbons, and the heme and FAD cofactors are shown as ball and stick colored according to element.

CHAPTER 2
SPECTROSCOPIC CHARACTERIZATION OF HEMOPROTEINS: CASE STUDIES

2.1 Spectroscopic Characterization of Hemoproteins

UV-vis Spectroscopy

A consequence of the highly conjugated nature of the porphyrin molecule is the occurrence of relatively low lying π to π^* electronic transitions that give rise to intense absorption features in the visible region (Makinen and Churg, 1983; McMillin, 2000). The intense absorption near 400 nm is known as the Soret band while weaker bands known as α/β bands are found at higher wavelengths (Fig 2.1). When iron is bound to the porphyrin macrocycle, the splitting of the d orbitals predicted by ligand field theory contributes significantly to the transition energies of the heme (Makinen and Churg, 1983). The presence of ligand-to-metal charge-transfer (LMCT) transitions adds further complexity to the electronic absorption properties of heme cofactors. Thus, the positions and intensities (denoted as extinction coefficient or ε) of these features are sensitive to the heme iron oxidation state, spin state, and coordination number as well as to the type of ligands present and the protein environment of the heme cofactor (Fig 2.1, Table 2.1). Although UV-vis spectra of hemes are not always easily interpreted, changes due to ligand binding or other alterations of the heme environment are easily observed. Thus, UV-vis spectroscopy is a simple yet powerful tool ideally suited to determining the ligand affinity of hemoproteins and for observing subtle conformational changes at the heme group as a result of a perturbation.

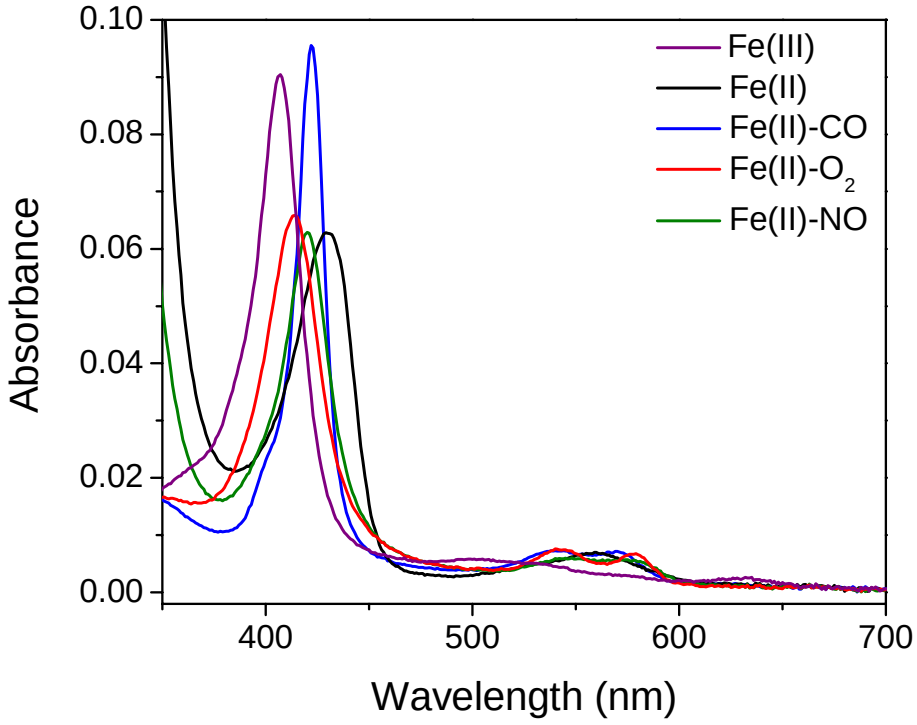

Fig. 2.1 Absorption spectra of wt full-length DevS at equivalent concentrations.

Table 2.1 Peak positions (λ) and extinction coefficients (ε) of wt full-length DevS in various heme states

	Soret Band		Visible Bands	
Heme State	**λ (nm)**	**ε ($mM^{-1}cm^{-1}$)**	**λ (nm)**	**ε ($mM^{-1}cm^{-1}$)**
Fe(III)	407	166	500, 630	10.6, 4.7
Fe(II)	428	116	562	12.9
Fe(II)-O_2	414	121	543, 578	13.7, 12.5
Fe(II)-CO	422	177	540, 570	13.4, 13.2
Fe(II)-NO	420	117	545, 574	11.1, 10.6

The above discussion is in reference to steady state UV-vis spectroscopy. An extremely useful extension of this approach is the determination of kinetic rates using stopped-flow measurements. In this technique, reactants are rapidly mixed and the spectra of the resulting mixtures are recorded on very short time scales. Given the sensitivity of the heme group's absorption spectra to ligation and environment, one can accurately determine the rates of ligand binding or other reactions using this technique. The utility of this approach is demonstrated in section 2.4 where it was used to determine the rates of free heme (hemin) binding and heme transfer between proteins.

RR Spectroscopy

In addition to being absorbed, photons can also be scattered by molecules (Fig 2.2). Most of the photons are scattered elastically, meaning that their energies are identical before and after the scattereing event. This phenomenon is referred to as Rayleigh scattering. However, the photon may be inelastically scattered, imparting energy to the molecule to promote it to an excited state. Consequently, the photon loses energy and is scattered with a lower frequency (Woodward, 1967). The difference in the energies of the scattered and incident photons corresponds to the energy of a molecular bond vibration and is in the IR region of the electromagnetic spectrum. A Raman spectrometer measures this difference to produce a vibrational spectrum of the analyte molecule similar to infrared absorption spectroscopy.

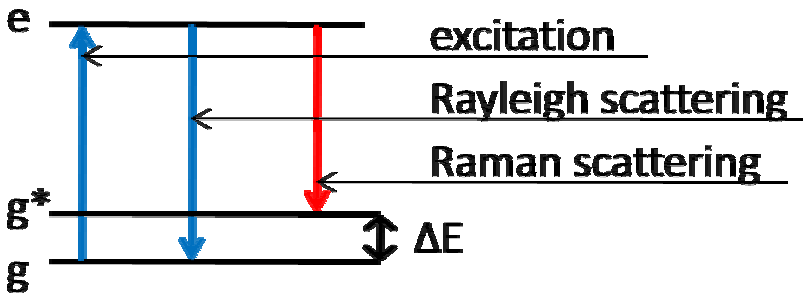

Fig. 2.2 Diagram of scattering processes. g is the ground electronic state, g* is an excited vibrational state, and e is a quantum state. Arrows show the direction of electron travel. ΔE is the energy difference between g and g* and is determined by measuring the difference in energies between incident and Raman scattered photons.

Typically, the probabilities of Raman scattering events are very low, but they can be imporved by a phenomenon known as resonance enhancement. Resonance occurs when the excitation wavelength is near the energy of an electronic transition, causing the enhancement of vibrational modes involving electrons associated with the excited state (Spiro and Czeruszewicz, 2000). For hemoproteins, visible light lasers are used to probe the heme cofactor while vibrational modes from other molecules remain non-resonant. Consequently, by tuning the excitation wavelength, unique selectivity may be achieved.

The RR spectrum of a hemoprotein provides a wealth of information about the heme group. Porphyrin skeletal vibrations in the high-frequency portion of the spectrum are sensitive to the porphyrin core size which in turn depends upon the spin state and coordination number of the Fe atom (Spiro and Li, 1988). Specifically, the frequencies of the modes labeled ν_3, ν_2, and ν_{10} are diagnostic of the heme iron spin and coordination states while the ν_4 mode reports on the occupancy of the porphyrin π^* orbitals which is diagnostic of the heme iron oxidation state (Spiro and Li, 1988). Analysis of the RR spectra of a variety of hemoproteins and model compounds has led to a reliable framework for determining the oxidation, spin, and coordination states of hemes from the frequencies of the their ν_4, ν_3, ν_2, and ν_{10} modes (Table 2.2)

Table 2.2 Frequencies of porphyrin skeletal vibrations for hemes in various oxidation, coordination and spin states (Spiro and Li, 1988).

Oxdiation State	**Coordination and Spin States**	**ν_4 (cm^{-1})**	**ν_3 (cm^{-1})**	**ν_2 (cm^{-1})**	**ν_{10} (cm^{-1})**
Fe(III)	6cHS	1370-1375	1480	1560-1565	1610
	5cHS		1490	1570-1575	1625
	6cLS		1505	1580-1590	1635
Fe(II)	5cHS	1355-1360	1470	1560-1565	1600
	6cLS		1495	1590-1600	1625

Peripheral group vibrations can also be identified, and the frequencies of propionate deformation modes in the low-frequency are characteristic of the degree of hydrogen bonding in which the propionate groups are engaged (Uchida and Kitagawa, 2005). Also available are axial ligand vibrations which are informative as to the strength of the axial bonds as well as the interactions engaged by axial ligands in the heme pocket. A very useful application of this is the measurement of ν(C-O) and ν(Fe-CO) frequencies for CO-bound hemes. An inverse correlation exists between these two frequencies as backbonding from the filled iron d-orbitals to the empty CO π* increases the Fe-C bond order while decreasing the C-O bond order. When proximal ligation remains constant, the degree of backbonding is dependent on electrostatic interactions engaged by the bound CO in the distal pocket (Ray *et al.*, 1994). Positively polar (i.e. hydrogen bonding) interactions with the CO stabilize a partial negative charge on the O atom of CO and enhance backbonding while negatively polar interactions have the opposite effect (Fig 2.3). Thus, CO acts as a probe of the distal pocket environment (Ray *et al.*, 1994). Finally, the ν(N-O) (Tomita *et al.*, 1999) and ν(Fe-O) (Yeh *et al.*, 2000) frequencies of Fe(II) nitrosyl and oxy hemes, respectively, are also sensitive to electrostatic interactions in the distal pocket. Thus, not only is RR an excellent tool for general hemoprotein characterization, but a careful RR analysis of the various forms of a heme-based sensor protein can tell us much about the type of sensing mechanism employed.

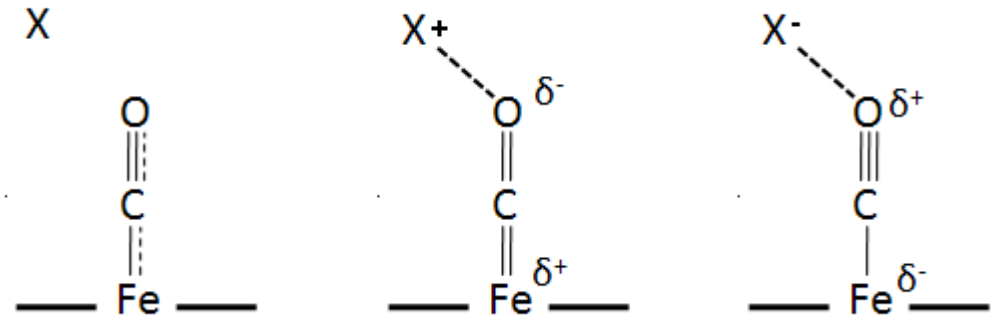

Fig 2.3 Effect of distal environment on the heme Fe to CO backbonding.

The role of RR spectroscopy can be expanded further using rapid freeze quench (RFQ) techniques. The high selectivity and sensitivity of RR to heme group vibrations

make it ideal for the identification of intermediates in ligand binding or catalytic reactions of hemoproteins. The remainder of this chapter is given to the description of several examples illustrating how the above techniques can be applied to the study of hemoprotein structure and function.

2.2 Instrumentation and Methods

Anaerobic Sample Preparation

Samples are purged of oxygen on a Schlenk line with a flow of argon saturated with water to prevent desiccation and transfer to a glovebox with a controlled atmosphere of less than 1 ppm O_2 (Omni-Lab System; Vacuum Atmospheres Co.). Reduction to the Fe(II) state is achieved by adding microliter aliquots of concentrated sodium dithionite solution (35-50 mM). ^{12}CO (Airgas) and ^{13}CO (99% ^{13}C; ICON Stable Isotopes) adducts are obtained by injecting CO through a septum-sealed capillary containing argon-purged, reduced protein (~20 μL). O_2 (Airgas), $^{18}O_2$ (99% ^{18}O; ICON Stable Isotopes), NO (Aldrich), $^{15}N^{16}O$ (99% ^{15}N; ICON Stable Isotopes), and $^{15}N^{18}O$ (98% ^{15}N and 95%^{18}O; Aldrich) adducts are generated using the same procedure after excess dithionite is removed from the reduced sample with desalting spin columns (Zeba 0.5 mL; Pierce) or by dialysis (Slide-A-Lyzer Dialysis Cassettes, Pierce).

UV-vis Spectroscopy

Electronic absorption spectra are obtained using a Cary 50 Varian spectrophotometer using a 1 nm resolution and a scanning rate of 1200 nm/min. Protein solutions are monitored either in cuvettes (sealed for air-sensitive samples) or directly in the capillaries used for RR spectroscopy.

RR Spectroscopy

A typical sample size for RR spectroscopy when using 1 mm capillaries is 20 μL. Concentrations used for hemoproteins vary from 50 to 300 μM whereas those for iron-sulfur cluster proteins approached 1 mM. RR spectra are obtained using a custom McPherson 2061/207 spectrograph (0.67 m with variable gratings) equipped with a

Princeton Instruments liquid N_2-cooled CCD detector (LN-1100PB). Excitation at 413, 351, and 637 nm are provided by a krypton laser (Innova 302, Coherent) while a Liconix 4240NB He/Cd laser is used for excitation at 442 nm. Excitation at 514, 488, and 458 nm are provided by an Innova I90C-3 argon ion laser. A Kaiser Optical supernotch filter is used to attenuate Rayleigh scattering at 413 nm while long-pass filters (RazorEdge, Semrock) are used for all other excitation wavelengths.

RR spectra are collected in a 90° scattering geometry at room temperature on samples mounted on a reciprocating translation stage. Low temperature spectra are obtained in a backscattering geometry on samples maintained at ~ 105 K in a liquid nitrogen cold finger. Other temperatures can be accessed by using different mixtures of solvents cooled with dry ice. Frequencies are calibrated relative to indene and CCl_4 (room temperature) or aspirin (low temperature) and are accurate to ±1 cm^{-1}. CCl_4 is also used to check the polarization conditions. The integrity of the RR samples, before and after laser illumination, is confirmed by direct monitoring of their UV-vis spectra at room temperature in the Raman capillaries.

Stopped-Flow UV-vis Spectroscopy

Proteins and reagents are loaded into a SX20 stopped-flow UV-vis spectrometer (Applied Photophysics) equipped with a variable temperature bath and photodiode array detector. For anaerobic experiments, the sample loading area is kept in a glovebag filled with nitrogen and all lines are purged with anaerobic buffer before loading samples. A separate concern is photochemistry. When mixed with buffer only, Hb undergoes significant photoreduction when the exit slit of the monochrometer is set to 1 mm which is largely eliminated when set to 0.2 mm (Fig 2.4). Thus, the width of the exit slit is optimized to prevent photoreduction or photodissociation of sensitive samples over long acquisitions.

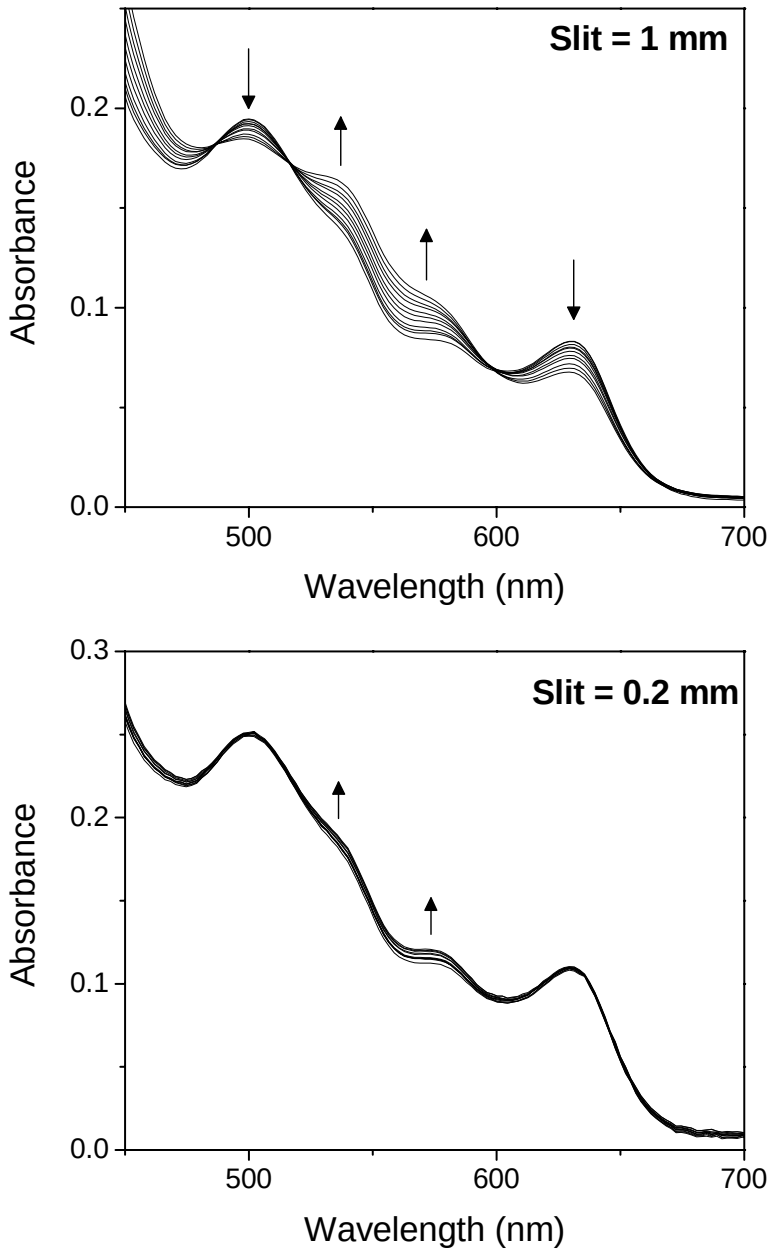

Fig 2.4 Stopped-flow UV-vis spectra of met-Hb mixed with buffer showing photoreduction with the exit slit set to 1 mm (top) or 0.2 mm (bottom). Scans every 50 s for 500 s.

Rapid Freeze Quench (RFQ)

RFQ syringes are loaded at the bench or in the glovebox for anaerobic samples before being mounted in the System 1000 Chemical / Freeze Quench Apparatus (Update Instruments, Inc.) equipped with a water bath (Fig. 2.5). Reaction times are controlled by varying the syringe displacement rate from 2-8 cm/s which varies the speed of solution ejection from the system. In conjunction with variable displament rates, the volume of the reactor hose after the mixer can be varied to achieve different reaction times. 5 ms are added to the calculated reaction time to account for time of flight and freezing in liquid ethane. Samples of 125 – 250 μL are ejected into a glass funnel attached to EPR or NMR tubes filled with liquid ethane at ≤ -120° C. The frozen sample is packed into the tube as the assembly sit within a Teflon block cooled with liquid nitrogen to ≤ -100° C. Once packed the frozen samples are stored in liquid nitrogen until analysis by EPR and/or RR.

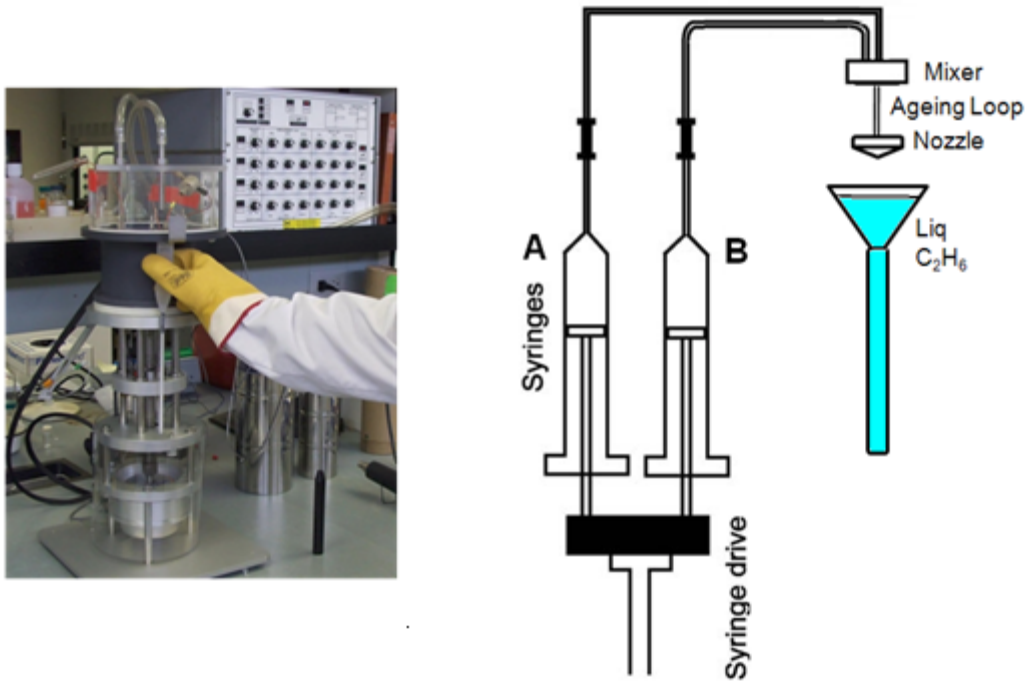

Fig 2.5. Update Instruments Inc. System 1000 Chemical / Freeze Quench apparatus photograph (left) and schematic (right).

2.3 Case Study I: Fungal Heme Oxygenase 1

Heme oxygenases (HO) catalyze the oxidation of heme to biliverdin, CO, and free iron in the presence of a suitable electron donor. Heme serves as both the prosthetic group and the substrate for this enzyme and the overall catalytic process requires three molecules of O_2 and seven electrons (Colas and Ortiz de Montellano, 2003). Heme oxygenases are found in various organisms including bacteria, plants, and mammals. Three heme oxygenase isoforms have been reported in mammals, but only two of these, HO-1 and HO-2, appear to play important roles in heme catabolism (Colas and Ortiz de Montellano, 2003). Recently, several bacterial heme oxygenases have been reported including HemO, HmuO, IsdG/I, BphO, and PigA (Petryka *et al.*, 1962; Schmitt, 1997; Skaar *et al.*, 2004, 2006; Suits *et al.*, 2005; Wegele *et al.*, 2004; Wilks and Schmitt, 1998; Zhu *et al.*, 2000). Most of these bacterial heme oxygenases convert heme to iron, biliverdin IXα and CO, but PigA from *Pseudomonas* is distinct in that its reaction product is a mixture of biliverdin IXδ and β rather than IXα due to a change in the orientation of the heme within the binding pocket (Caignan *et al.*, 2002). All of these bacterial heme oxygenases share structural and amino acid sequence similarity to mammalian heme oxygenses.

The occurrence of heme oxygenases in fungi has been proposed based on genomic information but they have not been characterized at the protein level and their identities and properties remain obscure. The protein encoded by gene *hmx1* from *S. cerevisiae* is expected to present significant sequence similarity with human HO-1 (21%) and bacterial HmuO (19%). Deletion of the Hmx1 gene causes a decrease in heme degradation activity and suggests that Hmx1 is important for heme iron reutilization and also for the homeostasis of regulatory pools of iron and heme (Protchenko and Philpott, 2003). In this work, we use RR spectroscopy to characterize this enzyme and

---

*Material in this chapter has been published in this or similar form in *Biochemistry*, and is used here with permission of the American ChemicalSociety.

Kim, D., Yukl, E. T., Moënne-Loccoz, P., Ortiz de Montellano, P. R. (2006) Fungal Heme Oxygenases: Functional Expression and Characterization of Hmx1 from *Saccharomyces cerevisiae* and CaHmx1 from *Candida albicans*. *Biochemistry* **45**, 14772-14780.

demonstrate that the structural features of the heme binding pocket in mammalian and bacterial heme oxygenases are conserved in this fungal representative.

2.3.1 Materials and Methods

Expression and Purification—Expression and purification of the truncated yeast heme oxygenase was carried out by D. Kim in the laboratory of P. Ortiz de Montellano at University of California San Francisco (UCSF) as previously described with some modifications (Wilks *et al.*, 1995). The *E. coli* strains transformed with pCW(Ori$^+$) vectors were inoculated into TB medium containing 100 μg/ml ampicillin and 1.0 mM IPTG. The expression cultures were grown at 37 °C for 3 h and then at 28 °C with shaking at 200 rpm for 24 h in 1 liter Fernback flasks. The soluble proteins were separated by ultracentrifugation. The solubilized proteins were purified using a Ni^{2+}-nitrilotriacetic acid agarose column eventually eluted with imidazole (400 mM). The eluted fractions were concentrated and dialyzed. The reconstitution with heme was performed as previously described (Wilks *et al.*, 1995). Hemin was added to the purified proteins to give a final 1:1 heme:protein ratio. The samples were applied to a hydroxyapatite Bio-Gel HTP column (Bio-Rad Laboratories, Hercules, CA) preequilibrated with 10 mM potassium phosphate buffer (pH 7.4) and the proteins were eluted with 150 mM potassium phosphate buffer (pH 7.4) after first washing with 10 mM potassium phosphate buffer (pH 7.4).

Spectroscopic Characterization

Formation of the reduced enzyme and spectroscopic procedures were performed as indicated for hemoproteins in section 2.1.

2.3.2 Spectroscopic Results and Dicussion

The high-frequency RR spectrum of the Fe(III) protein is characteristic of a 6-coordinate high-spin (6cHS) species with ν_4, ν_3, and ν_{10} at 1371, 1482, and 1611 cm^{-1}, respectively (Fig 2.5, left). In the reduced protein, the heme iron is in a 5cHS

configuration as revealed by its ν_3 at 1469 cm^{-1} (Fig 2.6, left). Thus, the coordination and spin states of the heme iron in Fe(III) and Fe(II) wt Hmx1 are identical to those of the mammalian and bacterial heme oxygenases and suggest the presence of a proximal histidine and a distal water ligand.

The RR analysis of Hmx1 at different pH values (Fig 2.6, right) identifies a conversion from 6cHS to 6cLS with increasing pH, with the alkaline pH sample exhibiting skeletal vibrations consistent with a 6cLS configuration (Table 2.2). These results argue in favor of the axial coordination of an aqua ligand to the Fe(III) iron. Coordination to the Fe(III) lowers the pK_a value of the coordinated water molecule and facilitates its deprotonation to a hydroxyl ion above pH 8. The stronger ligand field associated with the hydroxyl group changes the Fe(III) configuration from high-spin to low-spin. In the low-frequency RR spectra of the alkaline form of the Fe(III) heme complex, a RR band observed at 554 cm^{-1} in unlabeled water downshifts to 533 cm^{-1} in $H_2{}^{18}O$ (Fig 2.7, left). This vibrational frequency and its ^{18}O-isotope shift is typical of a ν(Fe−OH) in a 6cLS Fe(III)−hydroxo heme complex (Asher *et al.*, 1977; Desbois *et al.*, 1979; Sitter *et al.*, 1988) and is within a few cm^{-1} of those observed in mammalian and bacterial heme oxygenases (Takahashi *et al.*, 1994; Wilks and Moenne-Loccoz, 2000). A 442 nm excitation was used to acquire the low-frequency RR spectrum of Fe(II) Hmx1 at neutral pH to identify the proximal ligand of Hmx1 (Fig 2.7, right). An intense band at 218 cm^{-1} was identified which is within the characteristic range for ν(Fe-N_{His}) vibrations. The ν(Fe-N_{His}) is detectable in 5-coordinate high-spin (5cHS) Fe(II) hemes using this excitation due to the asymmetry of this form as a result of the heme iron moving out of the heme plane (Hoard and Scheidt, 1973). Stretching of the Fe-His bond alters the interaction of Fe orbitals with those of porphyrin π and π^* orbitals (Spiro, 1983) allowing for observation of the ν(Fe-N_{His}) using Soret excitation.

Our RR analysis of the heme−Hmx1 complex shows that, in the oxidized protein, the heme iron is coordinated to a proximal histidine and an aqua ligand with a pK_a around 8. Fe(III)−aqua stretching frequencies are not observable in the RR of hemoproteins, but the Fe(III)−hydroxo stretching frequency suggests a comparable distal environment in Hmx1 and other heme oxygenases. In the reduced protein, the aqua ligand is

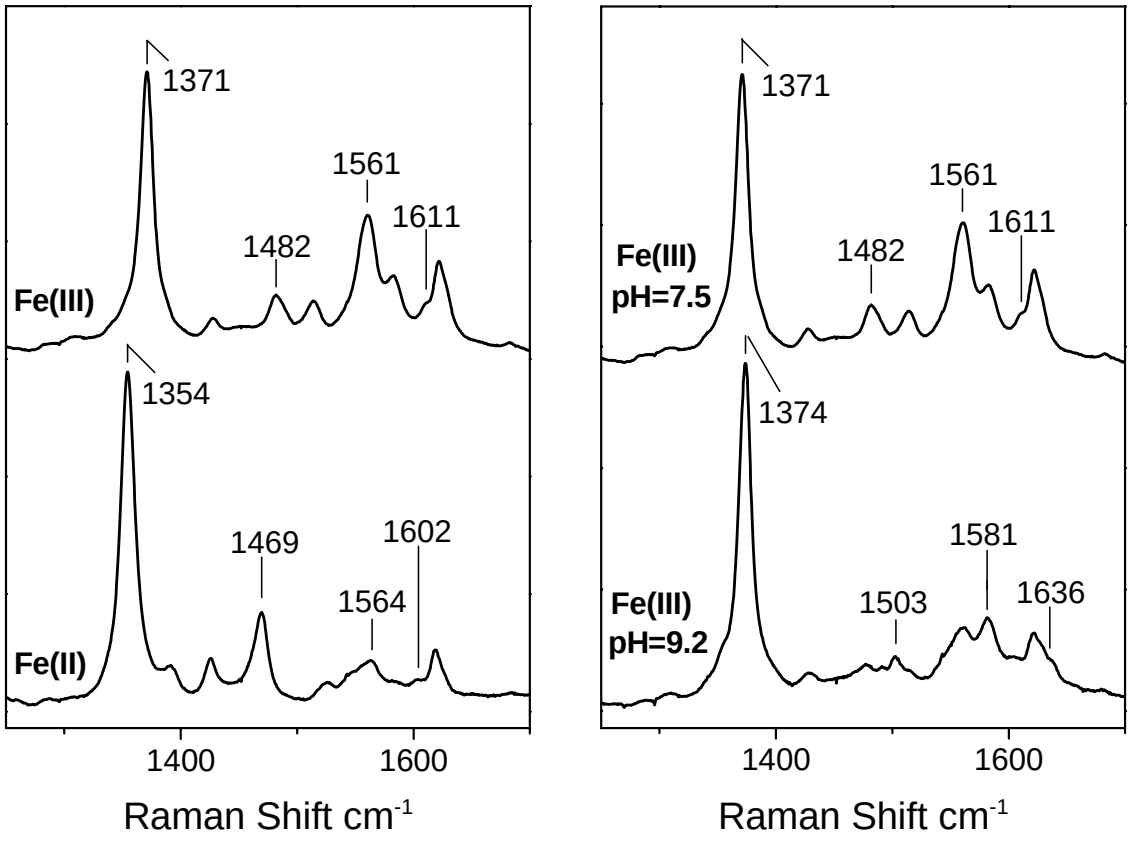

Fig. 2.6 High-frequency RR spectra of Fe(III) and Fe(II) Hmx1 at pH 7.5 (left) and Fe(III) Hmx1 at pH 7.5 and 9.2 (right) at room temperature (λ_{exc} = 413 nm, 5 mW)

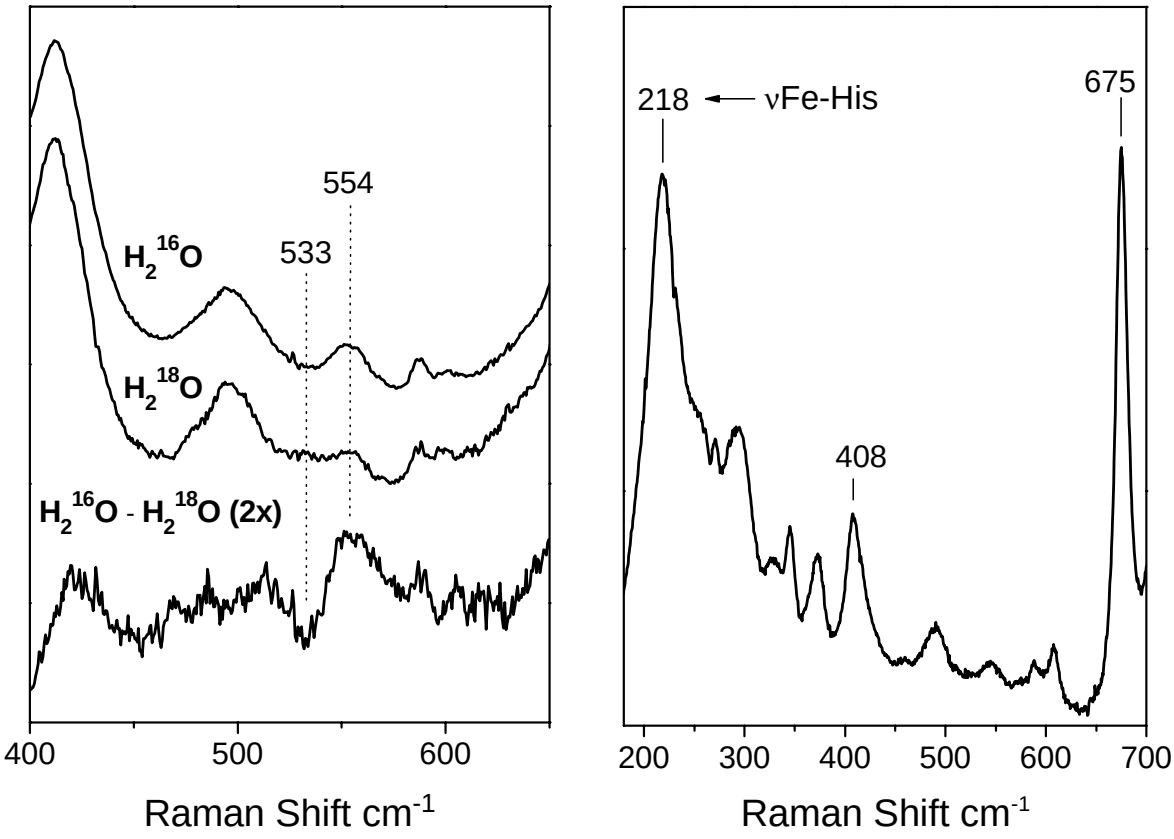

Fig. 2.7 Low-frequency RR spectra of Fe(III) Hmx 1 at pH 9.5 in $H_2{}^{16}O$ and $H_2{}^{18}O$ (λ_{exc} = 413 nm, 5 mW) (left) and Fe(II) Hmx 1 at pH 7.5 (λ_{exc} = 442nm, 15 mW) at room temperature

destabilized and the Fe(II) heme presents an open coordination site *trans* to a neutral proximal histidine identified by a $\nu(Fe\text{-}N_{His})$ at 218 cm^{-1}. The similarity in $\nu(Fe\text{-}N_{His})$ in yeast, mammalian, and bacterial heme oxygenases suggests a common structure of the proximal pocket across species in this family of enzymes.

Fungi require iron, an abundant mineral in nature, to perform their biological functions, including growth and pathogenic infection. Since iron availability is severely limited due to the extreme insolubility of Fe(III) at physiological pH, iron acquisition is crucial for microorganisms and has been implicated in infections by the pathogenic yeast *Candida albicans* (Foury and Talibi, 2001; Han, 2005; Pendrak *et al.*, 2004; Puig *et al.*, 2005). While our understanding of iron and heme metabolism in mammals has advanced greatly in recent years, iron assimilation in yeast is not well understood. Here we have characterized a critical protein responsible for iron utilization, the heme oxygenase from the prototypical eukaryotic microorganism *S. cerevisiae*. Interestingly, a homologue of this protein (CaHmx) exists in *C. albicans*. A heme uptake system exists in *C. albicans* which mediates specific binding of heme at the cell surface, transport into the cell, and subsequent degradation by CaHmx1. The presence of an iron uptake system in *C. albicans* has important implications for pathogenic fungal infection as CaHmx1 allows this organism to use exogenous heme as an iron source (Santos *et al.*, 2003). Thus, characterization of the Hmx1 protein from *S. cerevisiea* could be of value in identifying targets for treatment of *Candida* infections.

2.4 Case Study II: HasAp Hemophore

HasA is an extracellular heme-binding protein secreted by gram-negative bacteria for the purpose of scavenging iron in the form of heme (Letoffe *et al.*, 1994). Once

---

*Material in this chapter has been published in this or similar form in *Biochemistry*, and is used here with permission of the American ChemicalSociety.

Alontaga, A. Y., Rodriguez, J. C., Schonbrunn, E., Becker, A., Funke, T., Yukl, E. T., Hayashi, T., Stobaugh, J., Moënne-Loccoz, P., Rivera, M. (2009) Structural Characterization of the Hemophore HasAp from *Pseudomonas aeruginosa*: NMR Spectroscopy Reveals Protein-Protein Interactions Between Holo-HasAp and Hemoglobin. *Biochemsitry* **48**, 96-109.

bound, the heme is delivered to a specific outer membrane receptor, HasR (Ghigo *et al.*, 1997; Letoffe *et al.*, 1994), and imported into the cell where heme oxygenases degrade the heme, providing the organism with a source of iron. This is particularly important for pathogenic organisms where heme and hemoproteins within the host provide a large reservoir of accessible iron whereas free iron is extremely scarce. Consequently, it is important to determine whether HasA is capable only of sequestering free heme or whether it can actively remove heme from hemoproteins, specifically hemoglobin (Hb), via specific interactions between the two proteins.

Toward this end, we have compared the rates of heme acquisition from Hb for both apo-HasA from *Pseudomonas aeruginosa* (HasAp) and apo-cytochrome b_5 from the mitochondrial outer membrane (OM) using stopped-flow UV-vis spectroscopy. OM apo-cytochrome b_5 was chosen as a control for measuring passive heme dissociation from Hb due to its high affinity for heme driven by an exceedingly slow off-rate (Silchenko *et al.*, 2000). Similar experiments have been conducted using a variant of apo-Mb to measure the rate of heme dissociation from Hb (Hargrove *et al.*, 1997).

Also of interest is the possible observation of intermediates in the heme binding process of HasAp. The Fe(III) heme of HasAp is axially coordinated by His32 and Tyr75 in the resting state where the strength of the Fe-Tyr bond is maximized by a hydrogen bond interaction between Tyr75 and His83 (Fig. 2.8) (Alontaga *et al.*, 2009). Both axial ligands reside on loops and comparison of the crystal structures of apo (open) and holo (closed) HasA from *Serratia marcescens* show that the loop on which His32 resides undergoes a significant conformational change upon heme binding whereas the protein region that carries Tyr75 seems largely unaffected (Wolff *et al.*, 2008) (Fig. 2.8). Further, the hydrogen bond between Tyr75 and His83 is maintained in the apo form. Thus, the model proposed by Wolff *et al* is that heme initially binds to the strongest axial ligand, Tyr75, in the open conformation followed by conversion to the closed conformation upon the binding of His32 to the heme iron. We attempted to trap such an intermediate using RFQ and characterize it using RR spectroscopy.

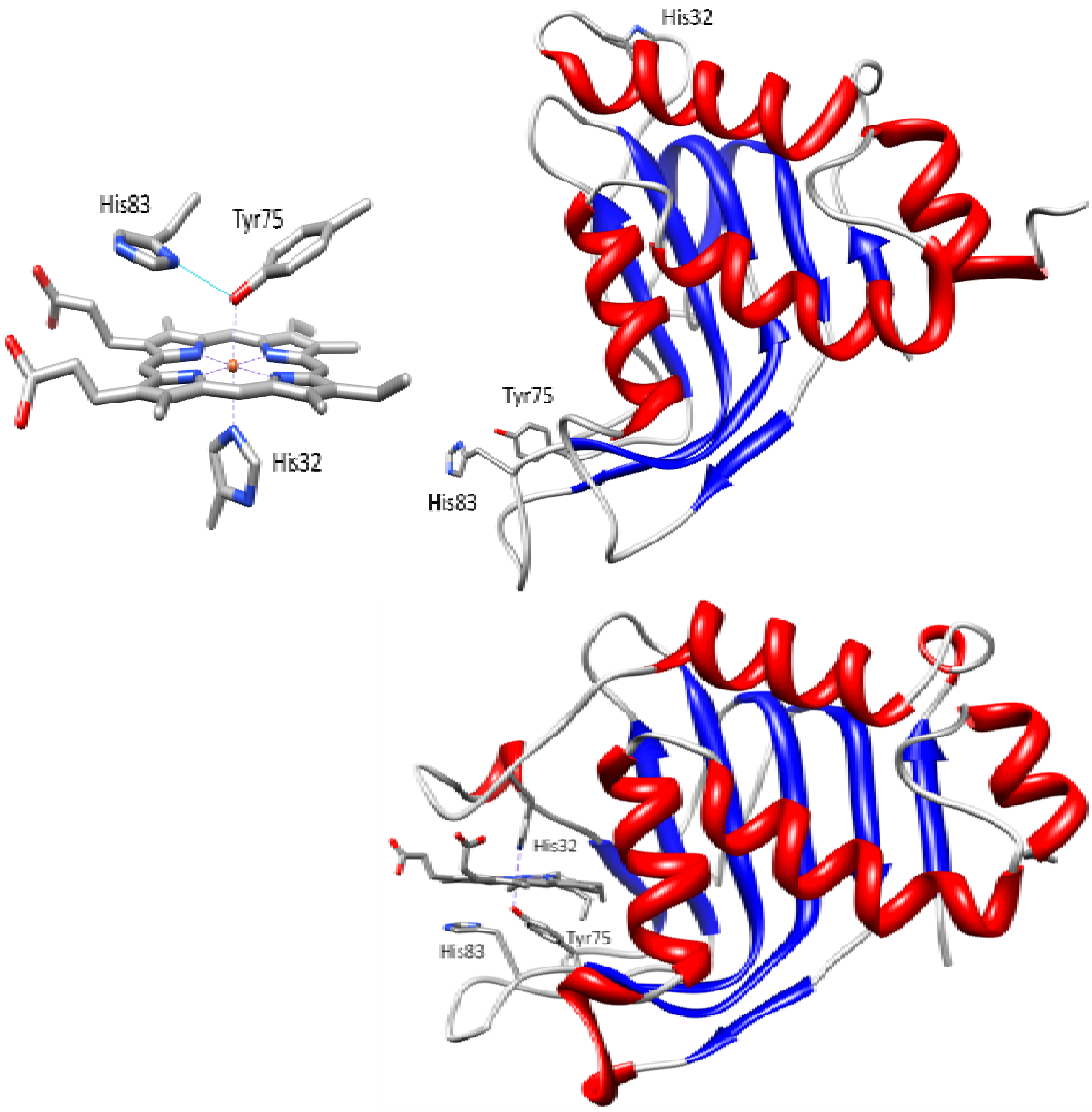

Fig. 2.8 Crystal structure of the heme coordination sphere of HasAp (3ELL) showing hydrogen bond interaction (cyan line) to the axial Tyr ligand (left). Based on (Alontaga *et al.*, 2009). NMR structures (right) of apo-HasA (1YBJ) (top) and holo-HasA (1B2V) (bottom). Adapted from (Wolff *et al.*, 2008)

2.4.1 Materials and Methods

Expression and Purification

HasAp was expressed and purified by Rivera and coworkers at the University of Kansas as follows: A single colony of freshly transformed cells was cultured for 12 h in 10 mL of Luria−Bertani (LB) medium containing 200 μg/mL ampicillin and used to inoculate 1.0 L of M9 minimal medium (200 μg/mL ampicillin). The resultant culture was incubated with continuous shaking at 225 rpm to an OD_{600} of 0.80−0.90, followed by centrifugation at 4000 rpm for 10 min. The cell pellet was resuspended in 1.0 L of fresh minimal M9 medium containing ampicillin and cultured to an OD_{600} of 1.0 before addition of isopropyl β-D-thiogalactopyranoside (IPTG; 1 mM final concentration), followed by culturing at 30 °C for 5 h and harvesting cells by centrifugation at 4000 rpm for 10 min. The cells were lysed by sonication as previously described (Caignan *et al.*, 2002) in 50 mM Tris-HCl (pH 7.8) containing 1 mM EDTA and 1 mM phenylmethanesulfonyl fluoride (PMSF). The resultant suspension was centrifuged at 23500 rpm for 2 h to separate the cell debris and the supernatant dialyzed against 20 mM Tris-HCl (pH 7.8) (3 × 4 L) at 4 °C. The protein was loaded into a Sepharose-Q Fast Flow column (2.6 cm i.d. × 15 cm length) preequilibrated with 20 mM Tris-HCl (pH 7.6) and eluted with the same buffer with a linear gradient of NaCl (50−500 mM); the purity of the protein in the different fractions was determined by SDS−PAGE, and the best fractions were pooled. The apoprotein, which amounts to approximately 80% of total HasAp, was reconstituted where necessary with hemin dissolved in DMSO. To this end, heme was added gradually to the protein solution until the absorbance ratio (A_{280}/A_{407}) no longer changed. The resultant solution was incubated at 4 °C and concentrated to a final volume of 2−3 mL using Amicon ultracentrifuge filters and further purified by size-exclusion chromatography in a Sephacryl S-200 column (2.6 cm i.d. × 90 cm length), equilibrated and eluted with 100 mM Tris-HCl containing 100 mM NaCl (pH 7.6). Fractions with an absorbance ratio (A_{280}/A_{407}) < 0.35 were pooled, dialyzed against phosphate buffer (μ = 0.10, pH 7.0), concentrated by ultrafiltration, and stored at −20 °C.

Lyophilized human Hb (Sigma) was dissolved in phosphate buffer (μ = 0.1, pH 7.0) and purified in a Sephacryl S-200 size exclusion column preequilibrated and eluted

with phosphate buffer (μ = 0.1, pH 7.0). Fractions with purity ratio (A_{280}/A_{406}) < 0.25 were pooled and concentrated using Amicon ultracentrifuge filters to a final concentration of 3.5 mM.

Formation of apo-cytochrome b_5.

Five milligrams of (OM) holo-cyt b_5 was diluted to 15 mL in 100 mM phosphate, pH 7.0. The solution was put on ice and the pH brought to 1.5-2.0 using cold 1 M HCl. Heme extraction was performed in a separatory funnel using several additions of 2-butanone chilled to -20 °C. The apo protein was dialyzed against 2 L of a solution of 0.6 mM $NaHCO_3$ and 1 mM EDTA, pH 10.3 for 1 h. This procedure was followed by three consecutive dialyses against 2 L charges of a solution of 0.6 mM $NaHCO_3$ alone, each for 3 h followed by an equivalent treatment using 20 mM phosphate, pH 7.2. Finally, the protein was dialyzed into 50 mM HEPES, 150 mM NaCl, pH 7.0 and concentrated to ~180 μM using 10 kD MWCO centrifugal concentrators (Millipore). All dialysis steps were performed on ice and concentration performed at 4 °C.

Stopped-flow UV-vis spectroscopy.

The concentrations of apo-HasAp and apo-cyt b_5 were determined by titration with a solution of bovine hemin. Hemin was dissolved in 10 mM NaOH and its concentration in this medium was determined using ε_{385} = 58.4 $mM^{-1}cm^{-1}$ (Dawson, 1986) and was used immediately. Apo proteins were diluted where necessary in 50 mM HEPES, 150 mM NaCl pH 7.0 for reaction with holo-Hb and in 200 mM HEPES pH 7.5 for hemin binding experiments. Human Hb was purified extensively to remove any free or loosely-bound heme (see above) and incubated in 10-fold excess of potassium ferricyanide for 10 min followed by removal of excess ferricyanide using desalting columns. This protein solution was then diluted in the above buffer and immediately loaded along with apo-HasAp into a SX20 stopped-flow UV-vis spectrometer (Applied Photophysics). The exit slit on the monochrometer was set to 0.2 mm to minimize photoreduction of Hb heme to < 5% after 500 s (Fig. 2.4).

RFQ

Concentrations of apo-HasAp and hemin were determined as above and were then diluted to 1 mM in 200 mM HEPES pH 7.5 and 10 mM NaOH, respectively. Solutions were then loaded into the System 1000 Chemical / Freeze Quench Apparatus (Update Instruments, Inc.) maintained at 3 °C. Samples were treated as described in section 2.1. 1:1 mixtures of buffer and 10 mM NaOH were checked to ensure that final pH of RFQ samples remained near 7.5.

2.4.2 Spectroscopic Results and Discussion

Heme Acquisition from Hb

The absorption spectra of the resting states of Hb, holo-cyt b_5, and holo-HasAp at equivalent concentrations illustrate differences which allow us to monitor the transfer of heme between these species (Fig. 2.9) at several wavelengths. Stopped-flow spectra of Hb mixed with a 4-fold excess of apo-cyt b_5 or apo-HasAp over heme is consistent with the unidirectional transfer of heme from Hb to the apo proteins over the course of 10 minutes (Fig. 2.10). The kinetics as measured by the absorbance change at 571 nm fit well to a single exponential function and show very similar rate constants of 1.1×10^{-3} s^{-1} and 1.4×10^{-3} s^{-1} for cyt-b_5 and HasAp, respectively. Combining the analysis of the reaction at this wavelength with that at 500 and 631 nm for cyt b_5 and at 500 and 619 nm for HasAp yields $k_{obs} = 2.2 \pm 1.1$ s^{-1} and 2.0 ± 0.7 s^{-1} for cyt b_5 and HasAp, respectively. The variability in these values may arise from the observation of heme photoreduction which occurs even when the exit slit is set to 2 mm (see Fig. 2.4) over the long time course of the reaction. To circumvent this issue we performed an experiment using the same concentrations of HasAp and Hb mixed in a cuvette and followed the progress of the reaction with a scanning UV-vis instrument (Fig 2.11). The data fit very well to a double exponential with rates of 1.1×10^{-3} s^{-1} and 1.0×10^{-4} s^{-1} having equal amplitudes. These values are identical to those in the literature for heme dissociation from the β and α subunits, respectively, of human Hb at the same concentration (Hargrove *et al.*, 1997). Thus, the UV-vis data indicates that HasAp does not actively remove heme from Hb but acquires heme passively subsequent to its dissociation from Hb.

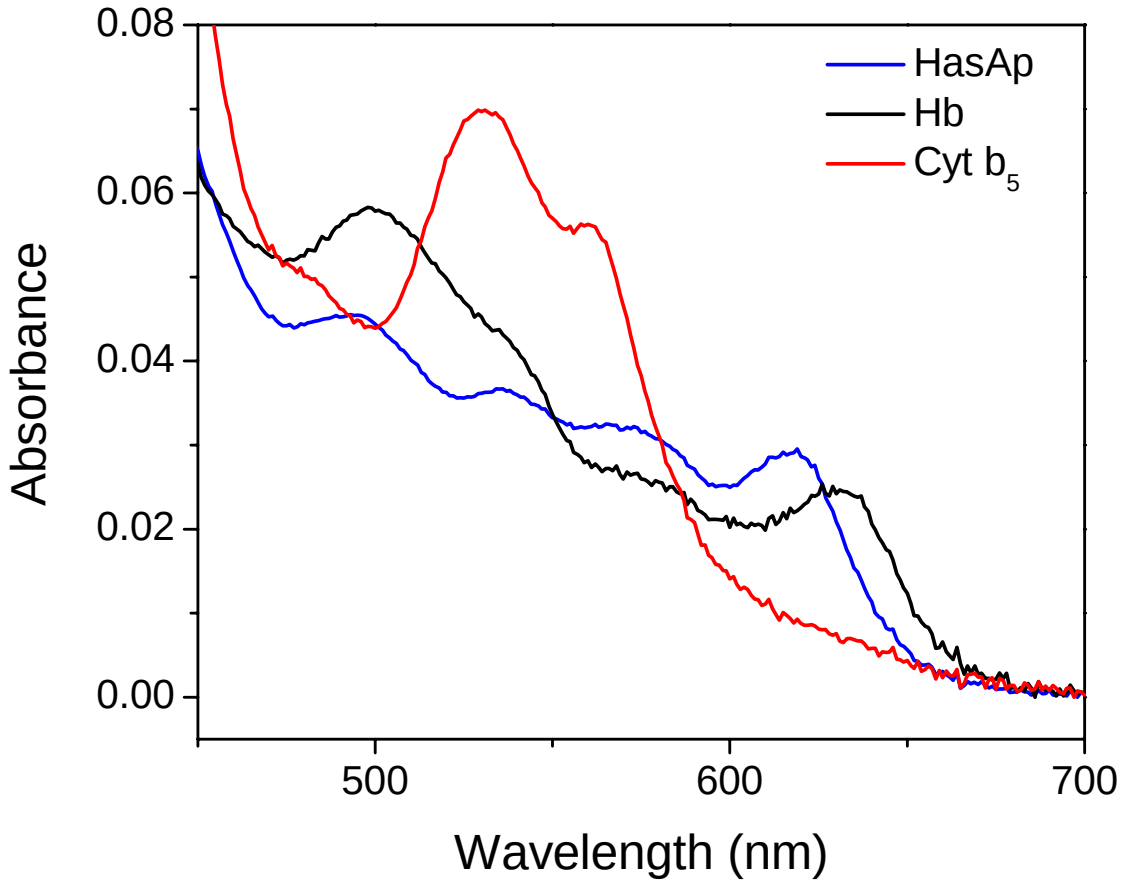

Fig. 2.9 Absorption spectra of holo-HasAp (blue), holo-Hb (black), and holo-cyt b_5 (red) at equivalent concentrations

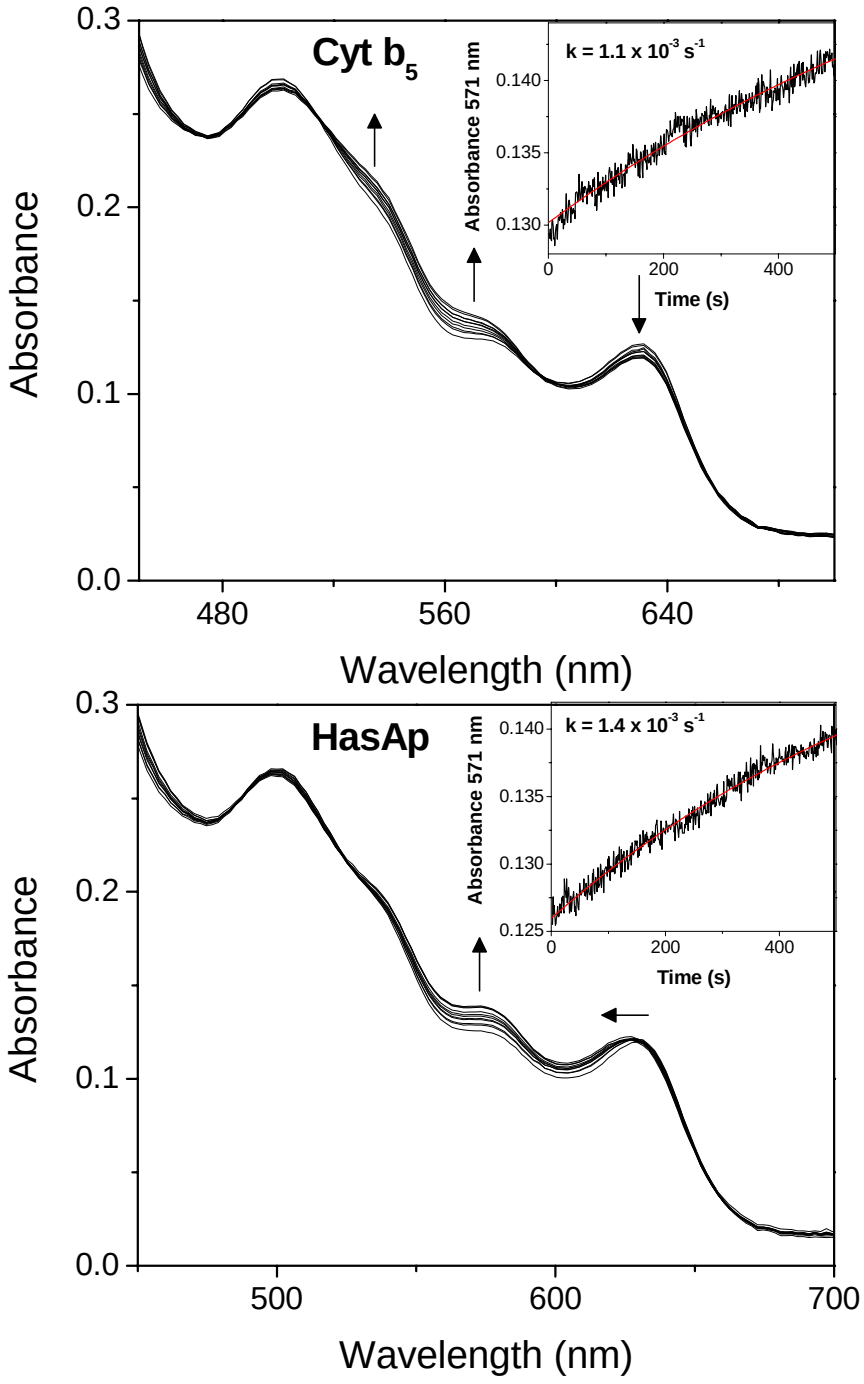

Fig 2.10 Stopped-flow UV-vis spectra of met-Hb mixed with apo-cyt b_5 (top) or apo-HasAp (bottom) . Scans every 50 s for 500 s, exit slit set to 0.2 mm. Absorbance change at 571 nm fit to a single exponential (inset).

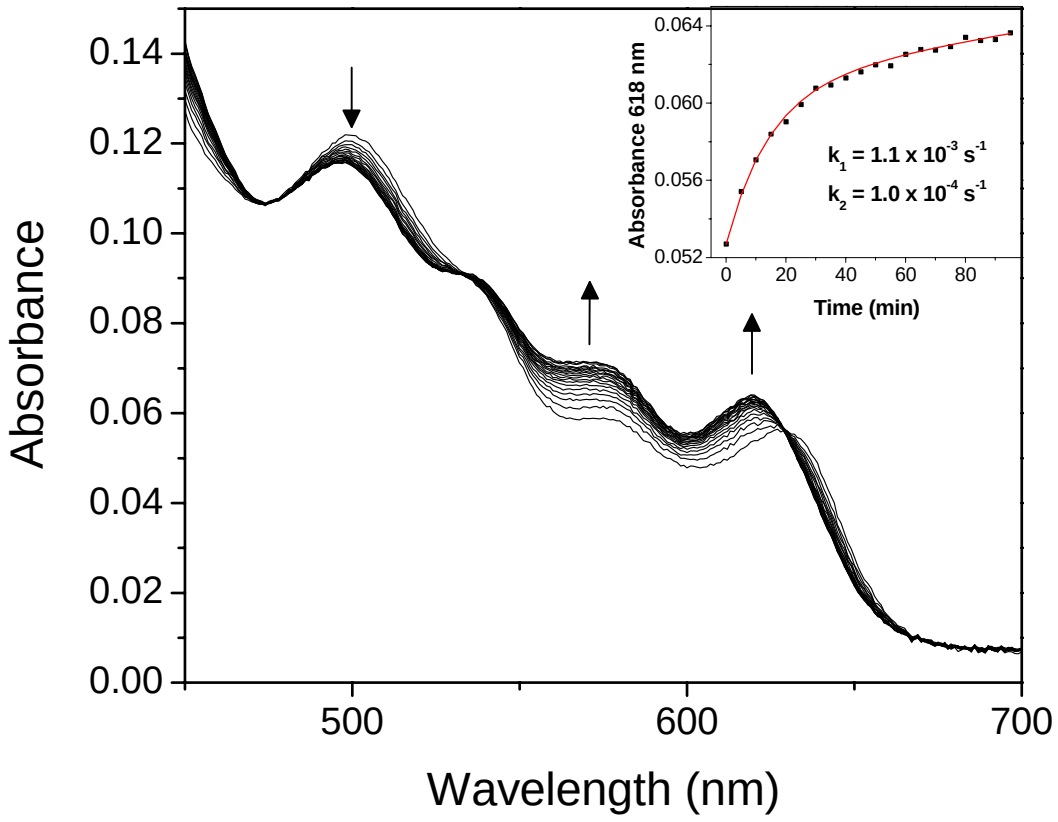

Fig 2.11 UV-vis spectra of met-Hb hand mixed with apo-HasAp. Scans every 5 min for 100 min. Absorbance change at 618 nm fit to a double exponential (inset)

Hemin Binding in HasAp

Stopped-flow spectroscopy of hemin binding to both wt and H32A apo-HasAp illustrates that this reaction is relatively rapid, with significant binding occurring within the dead time of the instrument. Analysis of hemin binding to wt apo-HasAp shows a biphasic reaction with roughly equal amplitudes and rate constants of 10.0 and 2.5 s^{-1} (Fig 2.12) indicating the accumulation of an intermediate prior to conversion to the final product. The same reaction with H32A apo-HasAp fits well to a single exponential with a rate constant of 13.3 s^{-1} (Fig 2.12). This rate is similar to the formation rate of the wt heme binding intermediate. Further, the intermediate of the wt reaction observed at the earliest time point has a UV-vis spectrum very similar to that of holo H32A (Fig 2.13).

To gain further insight into the structure of the wt HasAp heme binding intermediate, we investigated the RR spectra of RFQ samples of wt apo-HasAp plus hemin frozen at 7, 21, 100, and 500 ms (Fig 2.14). The results show that the intermediate coordinates heme in a combination of 6cHS and 5cHS forms as determined by the presence of spin and coordination state sensitive ν_3 modes at 1479 and 1489 cm^{-1}, respectively (Spiro and Li, 1988) (Table 2.2). This same mixture of spin and coordination states is observed for H32A holo-HasA (Fig. 2.15). Conversion of the wt intermediate to the predominantly 6cLS product is shown by the growth of the 6cLS ν_3 modes at 1504 cm^{-1} over time (Spiro and Li, 1988) (Table 2.2). The reaction is essentially complete by 500 ms which is consistent with the stopped-flow analysis. Taken together, the stopped flow and RFQ data suggest that the single heme binding step of H32A HasAp is representative of the initial heme binding step of wt HasAp and that the coordination of heme in the wt intermediate is similar to that in H32A holo-HasAp. This is consistent with initial binding by the Tyr75 ligand and subsequent conversion to the 6cLS product upon binding of His32 in the wt protein.

Concluding Remarks

This study makes use of stopped flow spectroscopy and RFQ to analyze the mechanism of heme acquisition by the hemophore HasAp. Stopped flow analysis shows that apo-HasAp acquires heme from met-Hb at the same rate at which it dissociates from met-Hb, suggesting a passive mechanism of heme acquisition whereby HasAp traps heme

subsequent to its dissociation by virtue of its greater affinity. This is consistent with previous results where a complex between HasA from *S. marcescens* and hemoglobin could not be observed using analytical centrifugation or coimmunoprecipitation techniques (Létoffé *et al.,* 1999; Cescau *et al.,* 2007). However, NMR spectroscopy revealed transient interactions between wt holo-HasAp and Hb which were localized to the loop containing His32 (Alontaga *et al.,* 2009). Our results indicate that, while this interaction does not increase the rate of dissociation from Hb, it may be important for positioning the hemophore for efficient heme capture upon dissociation. Experiments comparing the rates of heme capture by wt apo-HasAp and apo-cyt b_5 where the hemophores are at substoichiometric concentrations relative to Hb-heme may be useful in clarifying this issue.

Stopped flow and RFQ analyses of the hemin binding reaction of wt HasAp are consistent with the mechanism put forward by Wolff *et al.* (Wolff *et al.*, 2008) suggesting that heme initially binds Tyr75 whose ligand strength is optimized by a hydrogen bond with His83. This step occurs rapidly and with similar rates in wt and H32A HasAp. The next step in the mechanism is the closing of the loop and binding of the His32 ligand. Stopped flow analysis of wt HasA binding hemin has allowed us to calculate the apparent rate of this step as being four-fold slower than heme binding to Tyr75, causing the accumulation of a mixed 5cHS/6cHS intermediate. As there is no His32 ligand in the H32A mutant, this step is not observed spectroscopically and heme binding is complete after the rapid initial binding step. Consistent with this is the observed similarity in the UV-vis and RR spectra of the wt HasAp intermediate with the resting state of the H32A variant. Thus, using RR spectroscopy of RFQ samples, we are able to characterize the intermediate in the heme binding reaction of HasAp and confirm that binding to Tyr75 preceeds loop closure and binding of the His32 ligand.

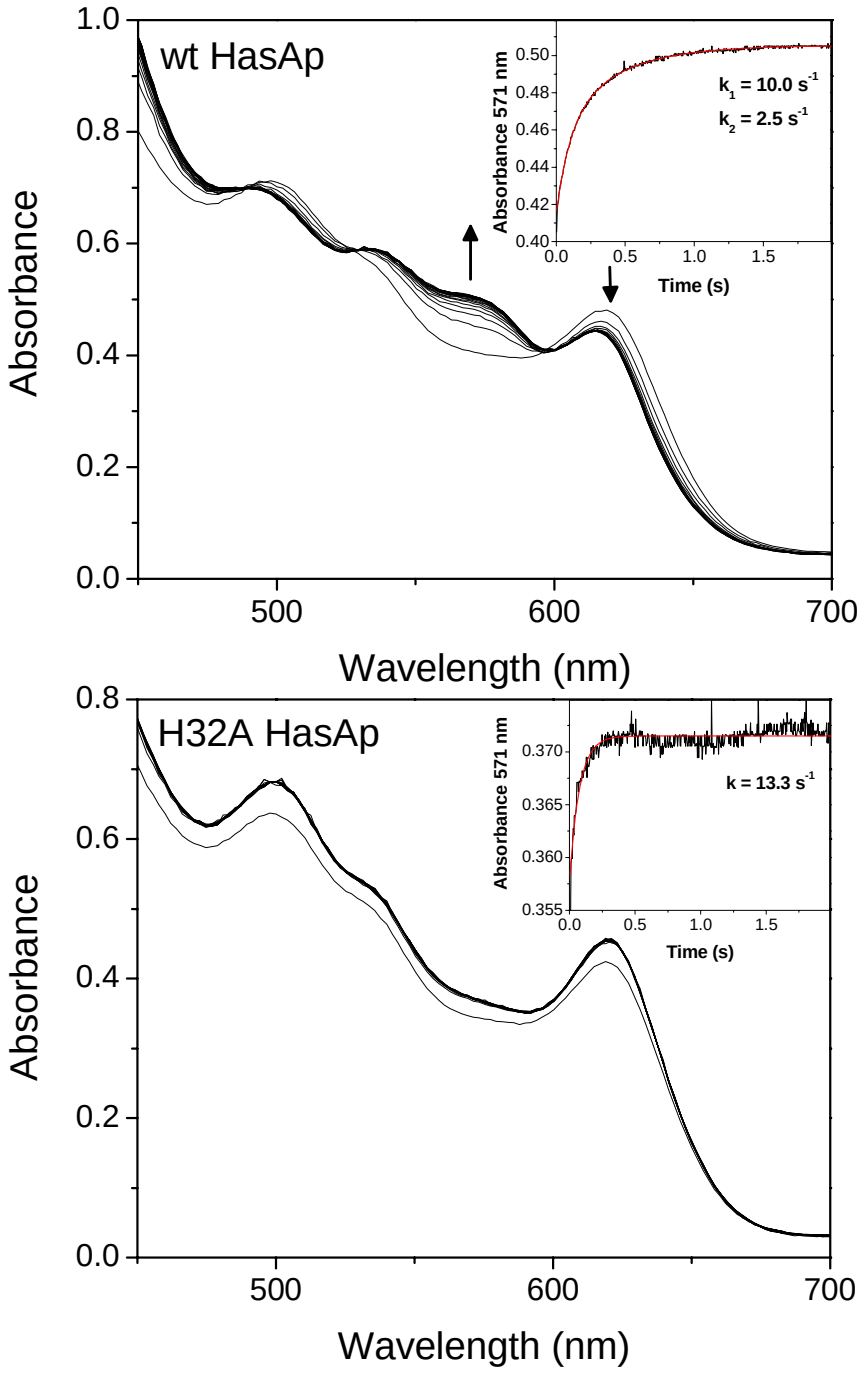

Fig. 2.12 Stopped-flow UV-vis spectra of heme binding to wt (top) and H32A apo-HasAp (bottom). Scans were taken every 100 ms for 2 s. Absorbance change at 571 nm fit to double (wt) and single (H32A) exponentials (inset).

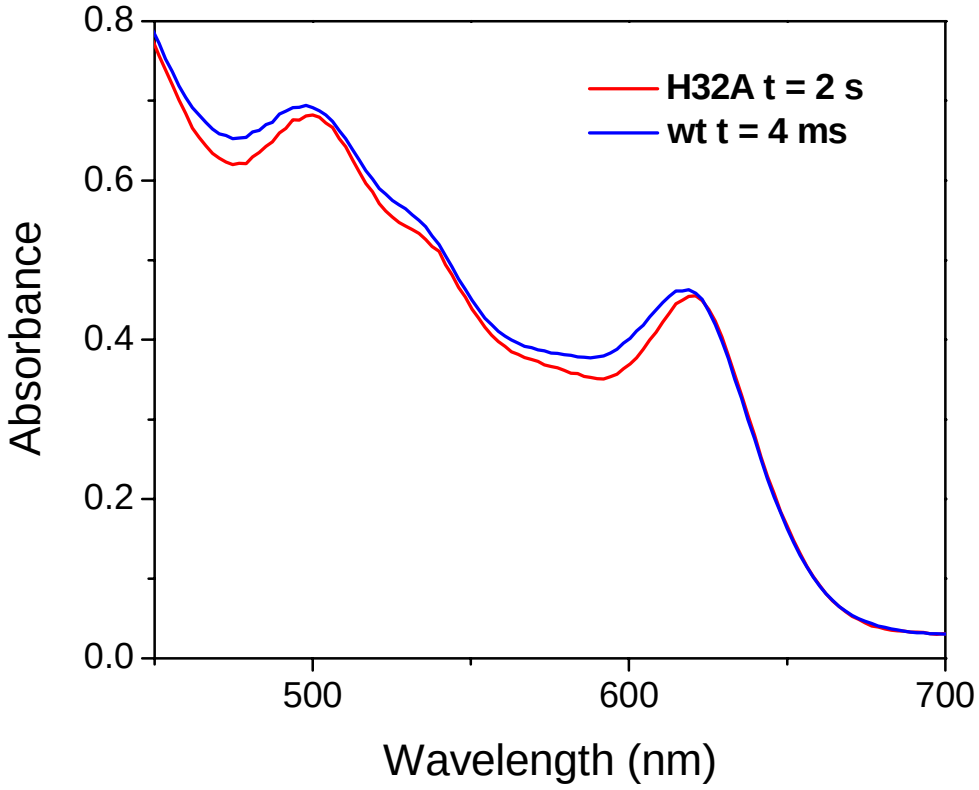

Fig. 2.13 UV-vis spectra of intermediate formed at 4 ms in the reaction of wt apo-HasAp and hemin (Blue) and the product of the reaction of H32A apo-HasAp and hemin at 2 s (Red)

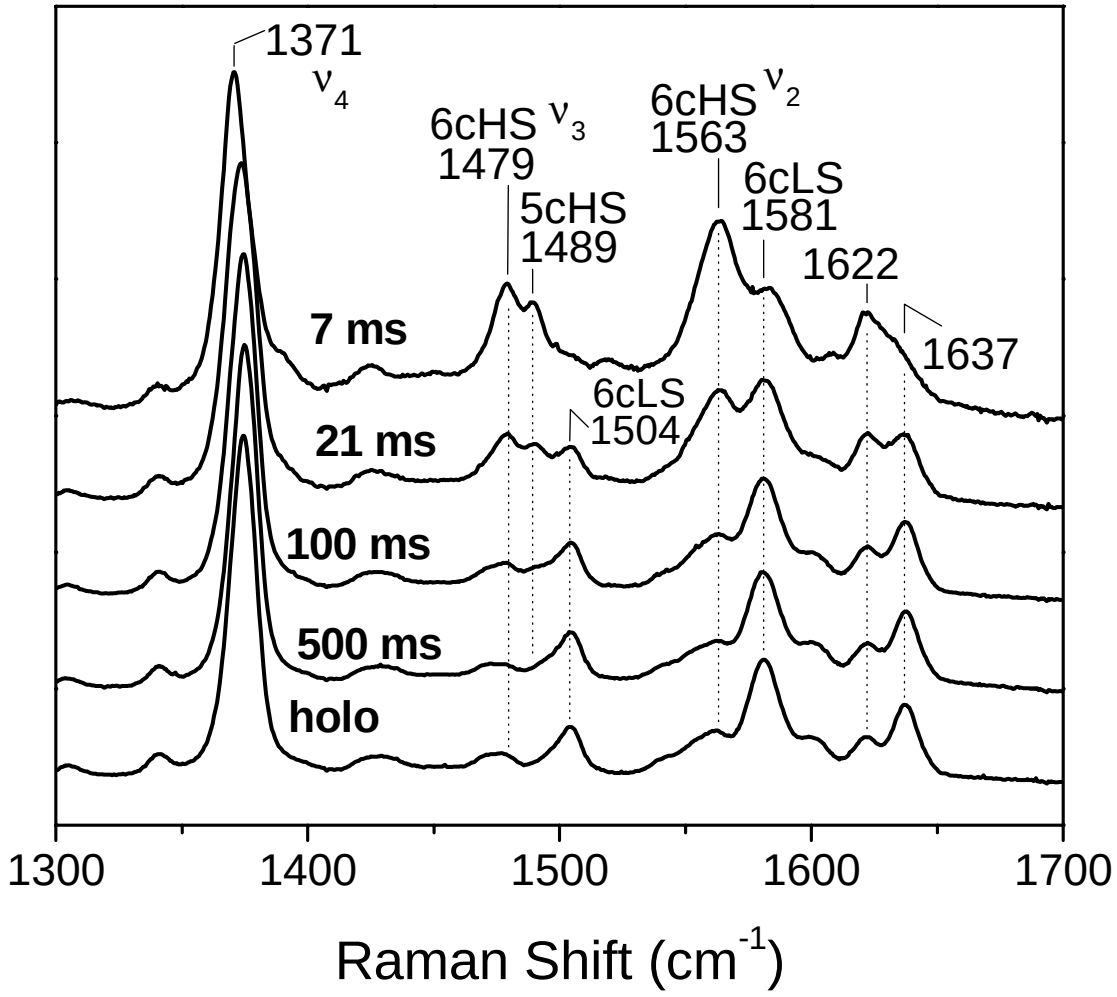

Fig 2.14 RR spectra of RFQ samples of wt apo-HasAp plus hemin frozen at 7, 21, 100, and 500 ms as well as an end point frozen by hand (λ_{exc} = 413 nm, 16.5 mW, 105K)

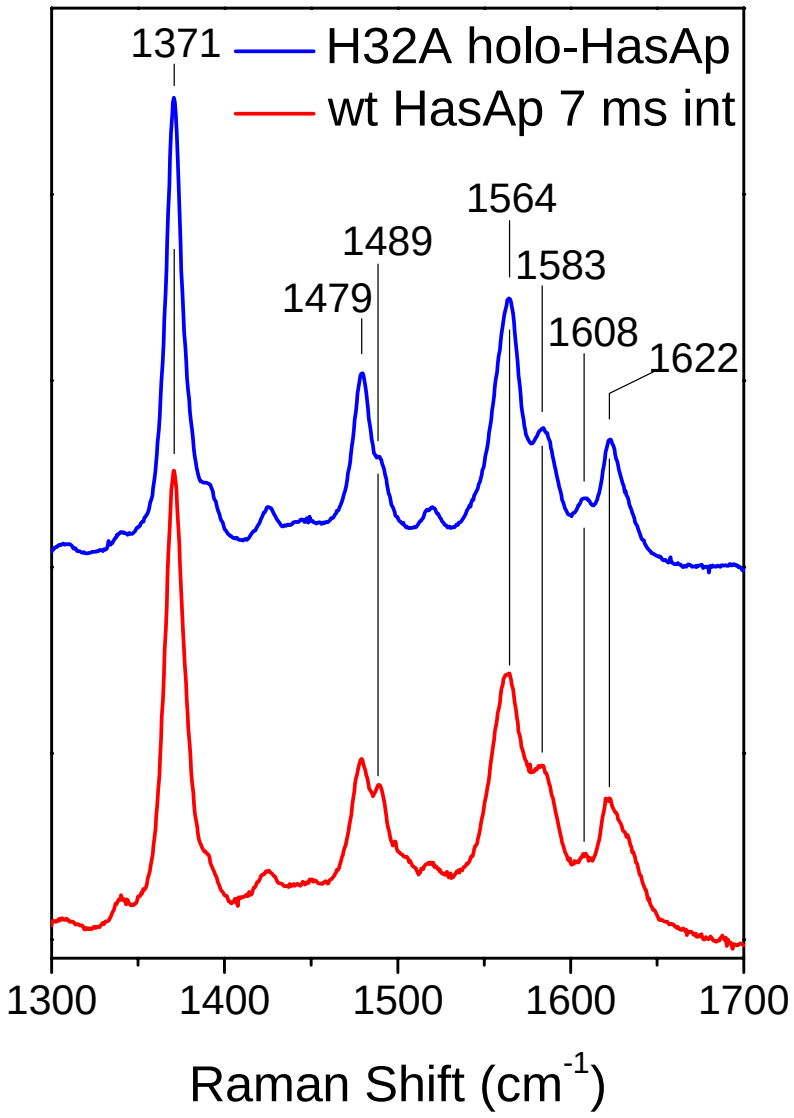

Fig. 2.15 High-frequency RR spectra of the 7 ms RFQ sample of wt apo-HasAp plus hemin (blue) and the resting H32A holo-HasAp. (λ_{exc} = 413 nm, 16.5 mW, 105K)

CHAPTER 3
SIGNAL TRANSDUCTION IN THE HEME-BASED SENSOR PROTEIN DevS

3.1 Non-Replicating Persistence in *Mycobacterium tuberculosis*

Mycobacterium tuberculosis (MTB)[1] is a remarkably successful pathogen thought to have latently infected 2 billion people worldwide (WHO, 2006). Part of the reason for this organism's success is its ability to exist within the host in a state known as "nonreplicating persistence" (NRP) for extended periods, reactivating at any point to cause clinical disease. Current chemotherapies act rapidly on growing bacteria, but subpopulations in the dormant state are phenotypically resistant (Dick, 2001). For this reason, 6 months are often required to cure the disease, making patient compliance difficult. Thus, a detailed understanding of NRP and the signals that initiate it are critical for improvements in the treatment of TB.

NRP is characterized by the induction of a set of 48 genes, the so-called "dormancy regulon". Included in this set is α-crystallin, a heat-shock protein likely involved in the stabilization of essential proteins and cell structures during extended quiescence (Cunningham and Spreadbury, 1998). Hypoxia, NO, and CO are likely environmental cues prompting entrance into NRP as expression of the dormancy regulon

---

*Material in this chapter has been published in this or similar form in *Biochemistry*, and is used here with permission of the American Chemical Society.

Ioanoviciu, A., Yukl, E. T., Moënne-Loccoz, P., Ortiz de Montellano, P. R. (2007) DevS, a Heme-Containing Two-Component Oxygen Sensor of *Mycobacterium tuberculosis*. *Biochemistry* **46**, 4250-4260.

Yukl, E. T., Ioanoviciu, A., Ortiz de Montellano, P. R., Moënne-Loccoz, P. (2007) Interdomain Interactions within the Two-Component Heme-Based Sensor DevS from *Mycobacterium tuberculosis*. *Biochemistry* **46**, 9728-9736.

was found to be induced in response to all three of these conditions (Kumar *et al.*, 2008; Shiloh *et al.*, 2008; Voskuil *et al.*, 2003). These conditions are likely to be relevant for MTB survival within the human host because the granulomas in which MTB cells are sequestered are thought to be largely anoxic (Wayne and Sohaskey, 2001), and host expression of nitric oxide synthases (Choi *et al.*, 2002) and heme oxygenase -1 (HO-1) (Kumar *et al.*, 2008; Shiloh *et al.*, 2008) are upregulated in infected macrophages, leading to increased production of NO and CO, respectively.

Induction of the dormancy regulon depends upon the regulatory system DevR/S/T (also known as DosR/S/T), originally identified by the preferential expression of DevR and DevS in virulent over avirulent MTB strains (Dasgupta *et al.*, 2000). DevR is a response regulator of the LuxR family (Dasgupta *et al.*, 2000). DevS, and its paralog DevT, are histidine protein kinases (HPK) capable of autophosphorylation at a conserved histidine residue and subsequent transfer of the phosphate group to an aspartate residue of DevR (Roberts *et al.*, 2004). Phosphorylation of DevR enhances its affinity for palindromic DNA sequences that precede nearly every MTB gene upregulated in the hypoxic response (Roberts *et al.*, 2004). MTB mutants *ΔdosR* (Voskuil *et al.*, 2003) and *ΔdosS:ΔdosT* (Roberts *et al.*, 2004) are unable to activate gene expression in response to hypoxia, making the DevR/S/T system an attractive target for treatment of persistent MTB infection.

3.2 Domain Architecture of DevS

DevS and DevT are 62% identical in primary sequence and both are modular in nature, consisting of an N-terminal sensing core composed of two tandem GAF domains and a C-terminal kinase core with a HisKA (histidine kinase phosphor-acceptor) domain where autophosphorylation occurs and a HATPase (histidine kinase-like ATPase) domain responsible for binding ATP (Sardiwal *et al.*, 2005) (Fig 3.1). We and others have shown that the N-terminal GAF domain (GAF-A) of DevS binds heme (Ioanoviciu *et al.*, 2007; Sardiwal *et al.*, 2005). Because CN^- prevents induction of the dormancy regulon by NO and hypoxia (Voskuil *et al.*, 2003), and because hemes often present high affinities for diatomic ligands, the GAF-A domain is likely to be responsible for diatomic gas sensing

in DevS. Given the function of DevS in induction of the dormancy regulon in response to hypoxia, NO, and CO, it seems likely that kinase activity will be inhibited when the heme is bound by O_2 and active when in the deoxy, CO- or NO-bound forms. Indeed, autokinase assays confirm this hypothesis (Kumar *et al.*, 2007; Sousa *et al.*, 2007; Yukl *et al.*, 2008). However, the questions of how the protein differentiates between exogenous ligands, and how these signals are communicated to the histidine kinase domain require structural information.

In the first part of this chapter, we characterize the heme environment of the truncated GAF-A domain of DevS (GAF-A DevS) and show that the heme iron is coordinated by a histidine residue (His149). RR investigation of the CO-complex of the truncated protein showed two discrete environments for the bound CO. This prompted us to investigate how the presence of the other domains of DevS may interact with the GAF-A domain to influence the distal heme pocket and perhaps mediate signal transduction. Toward that goal, the second part of this chapter presents the RR characterization of wt full-length DevS (FL DevS), GAF-A DevS, and a construct composed of both GAF domains (GAF-A/B DevS) (Fig 3.1). All constructs in both oxidation states, as well as bound to the exogenous ligands CO, NO, and O_2 were investigated. The results indicate that interaction between the GAF-A and GAF-B domains enhances the specificity of the interaction between exogenous ligands and the heme distal pocket, allowing the protein to distinguish between O_2 and other diatomics such as NO and CO. As such, these interactions may represent a means of signal transduction linking the state of the heme to the activity of the kinase domain. Within the context of signal transduction, the GAF-B domain is proposed to be an actuator domain that couples the sensory and the kinase functions in DevS. Possible mechanisms for differentiating between exogenous ligands are also discussed.

3.3 Materials and Methods

Expression and Purification

Expression and purification of DevS constructs was undertaken by A. Ioanoviciu in the laboratory of P. Ortiz de Montellano at UCSF. The DevS constructs were co-overexpressed with the GroEL/ES complex in BL21DE3 cells. The cells were grown on LB plates containing both ampicillin (50 μg/mL) and chloramphenicol (34 μg/mL). Five starter cultures were then inoculated with one colony each. The five cultures were then pooled and used to inoculate flasks containing 1.5 L LB medium as well as the antibiotics ampicillin (100 μg/mL) and chloramphenicol (34 μg/mL). The cells were grown to an optical density of OD600 0.8 at 37 °C and 230 rpm. Hemin was added before induction (45 mg/4.5 mL NaOH 0.1 N for each 1.5 L culture). Protein expression was induced with IPTG at a final concentration of 1 mM and the flasks were kept at 18 °C for 20 h. The cells were harvested by centrifugation at 5000 rpm for 25 min.

The cells were lysed in phosphate buffer pH 7.6 (50 mM NaH_2PO_4, 10% glycerol, 200 mM NaCl, 1% Triton X-100, 0.5 mg/mL lysozyme, protease inhibitors: antipain 1 μg/mL, leupeptin 1 μM, pepstatin 1 μM, PMSF 0.1 mM). Then the mixture was incubated with shaking at 37 °C for 10 min. The cell membranes were disrupted by repeated sonication cycles at 50% using a Branson sonifier 450 from VWR Scientific, while cooling on ice. The insoluble fraction was isolated by centrifugation at 35000 rpm for 1 h at 4 °C. The cell lysate was applied to a 5 mL His trap column at a rate of 1 mL/min. The column was then washed with 20 and 50 mM imidazole in phosphate buffer (50 mM NaH_2PO_4, 10% glycerol, 500 mM NaCl, 50 mL at a rate of 2 mL/min). The recombinant protein eluted with 200 mM imidazole in phosphate buffer (50 mL, 1 mL/min). The sample was then dialyzed and the fractions that were not pure were repurified on a His trap column to provide the pure protein.

Electronic Absorption and RR Spectroscopy

A 50 mM potassium phosphate buffer at pH 7.5 with 100 mM NaCl was used for all protein samples. Sample treatment and UV-vis and RR spectroscopy were performed as described in section 2.1.

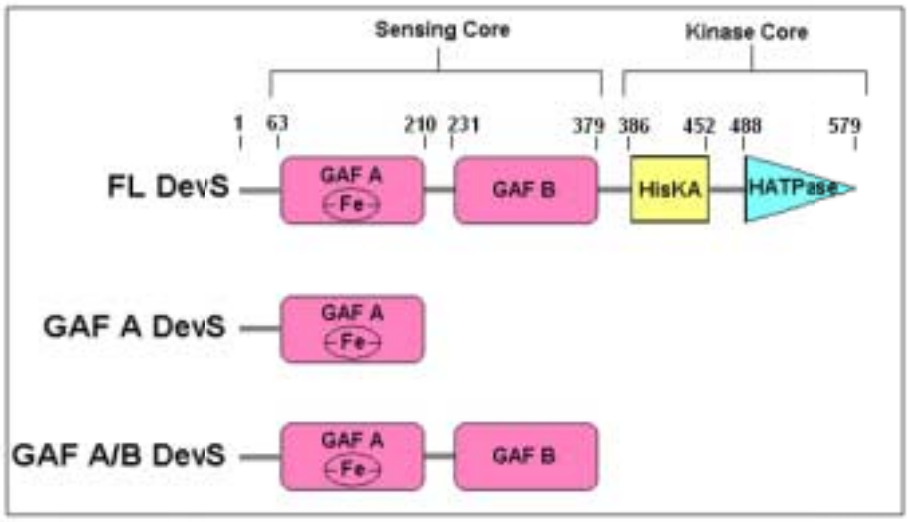


```
DevS MTTGGLVDENDGAAMRPLRHTLSQLRLHELLVEVQDRVEQIVEGRDRLDGLVEAMLVVTA   60
DevT MTHPDRANVNPGSP--PLRETLSQLRLRELLLEVQDRIEQIVEGRDRLDGLIDAILAITS   58
     **   . .: * *:.   ***.*******:***:*****:*************::*:*.:*:

DevS GLDLEATLRAIVHSATSLVDARYGAMEWHDRQHRVLHFVYEGIDEETVRRIGHLPKGLGV   120
DevT GLKLDATLRAIVHTAAELVDARYGALGWRGYDHRLVEFVYEGIDEETRHLIGSLPEGRGV   118
     **.*:********:*:.********:*:. :**::.********* : ** **:* **

DevS IGLLIEDPKPLRLDDVSAHPASIGFPPYHPPMRTFLGVPVRVRDESFGTLCLTDKTNGQP   180
DevT LGALIEEPKPIRLDDISRHPASVGFPLHHPPMRTFLGVPVRIRDEVFGNLYLTEKADGQP   178
     :* ***:***:****:* ****:*** :*************:*** ** .*:**:*::***

DevS FSDDDEVLVQALAAAAGIAVANARLYQQAKARQSWIEATRDIATELLSGTEPATVFRLVA   240
DevT FSDDDEVLVQALAAAAGIAVDNARLFEESRTREAWIEATRDIGTQMLAGADPAMVFRLIA   238
     ******************** ****:::::*::********.*::*:*::** ****:*

DevS AEALKLTAADAALVAVPVDEDMPAADVGELLVIETVGSAVASIVGRTIPVAGAVLREVFV   300
DevT EEALTLMAGAATLVAVPLDDEAPACEVDDLVIVEVAGEISPAVKQMTVAVSGTSIGGVFH   298
      ***.* *. *:*****:*:: **.:*.:*:::*..*.  .::   *:.*:*: :  **

DevS NGIPRRVDRVDLEGLDELADAGPALLLPLRARGTVAGVVVVLSQGGPGAFTDEQLEMMAA   360
DevT DRTPRRFDRLDLA-VDGPVEPGPALVLPLRAADTVAGVLVALRSADEQPFSDKQLDMMAA   357
     :  ***.**:**  :*  .:.****:***** .*****:*.*  ...  .*:*:**:****

DevS FADQAALAWQLATSQRRMRELDVLTDRDRIARDLHDHVIQRLFAIGLALQGAVPHERNPE   420
DevT FADQAALAWRLATAQRQMRELVEILTDRDRIARDLHDHVIQRLFAVGLTLQGAAPRARVPA   417
     *********:***:**:***:::**********.*********:**:****.*:  * *

DevS VQQRLSDVVDDLQDVIQEIRTTIYDLHGASQGITRLRQRIDAAVAQFADSGLRTSVQFVG   480
DevT VRESIYSSIDDLQEIIQEIRSAIFDLHAGPSRATGLRHRLDKVIDQLAIPALHTTVQYTG   477
     *:: : . :****::*****::*:***.... * **:*:* .: *:* ..*:*:**:.*

DevS PLSVVDSALADQAEAVVREAVSNAVRHAKASTLTVRVKVDDDLCIEVTDNGRGLPDEFTG   540
DevT PLSVVDTVLANHAEAVLREAVSNAVRHANATSLAINVSVEDDVRVEVVDDGVGISGDITE   537
     ******.**::****:**********:*::*::.*.*:**: :**.*:* *:..::*

DevS SGLTNLRQRAEQAGGEFTLASVPGASGTVLRWSAPLSQ   578
DevT SGLRNLRQRADDAGGEFTVENMP-TGGTLLRWSAPLR-   573
     *** ******::******: .:* :.**:*******
```

Fig 3.1 (Top) Domain organization of wild-type and truncated *M. tuberculosis* DevS. Domain nomenclatures, symbols, and protein organizations are according to the simple modular architecture research tool (SMART) from the European Molecular Biology Laboratory (Letunic *et al.*, 2002). (Bottom) Sequence alignment of DevS and DevT, proximal heme ligand (red), residues important for signal transduction (blue), and site of autophosphorylation (green) (Dasgupta *et al.*, 2000) for DevS are highlighted.

3.4 Identification of Proximal Ligation in Truncated GAF-A DevS

UV−vis absorption spectra of wt GAF-A DevS (Table 3.1) clearly establish that its heme forms stable complexes with O_2, CO, and NO. The formation of a stable oxy complex is consistent with its potential role as a gas sensor *in vivo*. NO binds to both oxidation states of the iron, while CO and O_2 only bind to the reduced protein. The histidine to alanine substitution in the H149A variant has serious consequences on the heme absorption (Table 3.1). Most importantly, H149A GAF-A DevS does not form a stable oxy complex, as exposure of the reduced form to O_2 leads to autoxidation, producing the oxidized protein. The H149A variant also responds differently to NO than the wt protein. Specifically, the Fe(II) heme in H149A GAF-A DevS binds NO to form a 5-coordinate Fe(II)−NO complex with a characteristic Soret absorption near 400 nm (Table 3.1). When the Fe(III) heme is exposed to NO, the Soret absorption is slightly broader with a maximum at 402 nm which suggests the presence of a transient species with a red-shifted Soret, either an Fe(III)−NO or a 6-coordinate Fe(II)−NO, but the sample quickly evolves to produce the 5-coordinate Fe(II)−NO complex. High-frequency RR spectra of the nitrosyl adducts in the H149A variant confirm the UV−vis analysis (data not shown).

Table 3.1 UV-vis data for wt and H149A GAF-A domains of DevS and their complexes

Heme State	wt DevS		H149A DevS	
	Soret band (nm)	**Visible bands (nm)**	**Soret band (nm)**	**Visible bands (nm)**
Fe(III)	406	500, 630	412	535
Fe(II)	428	562	422	559
Fe(II)-O_2	414	578, 543	unstable	unstable
Fe(II)-CO	422	540, 570	413	533, 567
Fe(II)-NO	419	545, 574	400	541, 568
Fe(III)-NO	420	539, 569	unstable	unstable

The coordination number, spin state, and oxidation state of the heme iron of the wt and H149A proteins are revealed by the frequency of the ν_4, ν_3, ν_2, and ν_{10} modes in the high-frequency region of the RR spectra obtained with Soret excitation (Spiro and Li, 1988). At room temperature and neutral pH, Fe(III) wt GAF-A DevS exhibits ν_4, ν_3, ν_2, and ν_{10} at 1370, 1479, 1557, and 1609 cm^{-1}, respectively (Figure 3.2). The frequencies of these bands are characteristic of a 6-coordinate high-spin (6cHS) heme. A minor 6-coordinate low-spin (6cLS) species is evidenced by a shoulder at 1507 cm^{-1} in the range of ν_3 modes. The intense high-spin charge-transfer marker band at 630 nm in the UV−vis spectrum (Table 3.1) and the dominance of high-spin marker bands in the RR spectra support the assignment of the high-spin state as the major conformer in the wt protein. Upon reduction with dithionite, the Fe(II) wt GAF-A DevS adopts a pure 5-coordinate high-spin (5cHS) configuration with ν_4, ν_3, ν_2, and ν_{10} at 1354, 1470, 1557, and 1603 cm^{-1}, respectively (Figure 3.2).

In contrast to the wt protein, the Fe(III) heme in H149A GAF-A DevS exists as a mixture of 5cHS and 6cLS states with ν_3 at 1491 and 1506 cm^{-1} and ν_{10} at 1624 and 1640 cm^{-1}, respectively (Figure 3.2). The Fe(II) heme−H149A DevS also exists as a mixture of spin and coordination states where a 5cHS species is indicated by ν_4, ν_3, ν_2, and ν_{10} at 1359, 1471, 1557, and 1603 cm^{-1}, respectively (Figure 3.2), and contributions from a 4-coordinate intermediate-spin species are also apparent with ν_3 and ν_{10} at 1501 and 1638 cm^{-1}, respectively (Andersson *et al.*, 1989; Sun *et al.*, 1994; Wilks and Moenne-Loccoz, 2000). Determining spin-state populations from relative intensities in the RR spectra could be misleading since the Fe(III) and Fe(II) variant proteins exhibit broad Soret absorptions, raising the possibility of significant differences in resonance enhancement for individual spin states.

When 442 nm excitation is used, the low-frequency region of the RR spectrum of the reduced wt protein displays a strong RR signal at 214 cm^{-1} (Figure 3.3). The vibrational frequency and the intensity of this band are characteristic of a $\nu(Fe-N_{His})$ mode from a neutral proximal histidine that is free of any strong hydrogen bonds (Kitagawa, 1988). While other low-frequency modes are only marginally perturbed in the Fe(II) H149A variant, the $\nu(Fe-N_{His})$ band is not observed. The weak signal at 218 cm^{-1}

observed in the RR spectrum of the variant protein is likely to correspond to an Fe(II)−$N_{pyrrole}$ stretching mode or an out-of-plane porphyrin deformation mode.

The identification of His149 as the proximal ligand to the iron in the wt protein was further confirmed by the RR characterization of the carbonyl complexes. Vibrations from the [Fe−C−O] unit were unambiguously identified by $^{12}C/^{13}C$ isotopic substitution (Figure 3.4). In wt GAF-A DevS, RR bands at 524 and 490 cm^{-1} that downshift by 4 and 3 cm^{-1} upon ^{13}CO substitution, respectively, are assigned to two distinct ν(Fe−CO) bands. Corresponding ν(C−O) bands appear at 1936 and 1971 cm^{-1}, with $^{12}C/^{13}C$ shifts of −43 and −44 cm^{-1}, respectively. These observed frequencies are characteristic of heme−carbonyl complexes with a neutral histidine coordinating *trans* to the CO group (Ray *et al.*, 1994). Effects of the *trans* ligand on the Fe−C−O vibrations are well understood in terms of competition for σ-bond donation to the iron and are easily visualized in graphs correlating ν(Fe−CO) to ν(C−O) frequencies (Fig. 3.5). The two sets of Fe−C−O vibrations observed in the wt protein fall on the correlation line for complexes with *trans* histidine ligands and, thus, suggest two species with distinct distal pocket conformations. These two conformers appear to be present at equivalent concentration as their respective ν(C−O) vibrations show comparable intensities. The position of a correlation point along the line for an imidazole *trans* ligand is governed by the degree of back-bonding from filled Fe *d* orbitals to the empty π* orbital of the bound CO. The extent of back-bonding is a good indicator of the electrostatic environment in the distal pocket where positive polarity and/or hydrogen-bonding interactions at the CO group promote back-bonding while negative polarity inhibits back-bonding (Ray *et al.*, 1994). The low correlation point originating from the ν(Fe−CO) and ν(C−O) at 490 and 1971 cm^{-1}, respectively, is very similar to that measured with the H64L variant of human Mb (i.e., 490 and 1965 cm^{-1}, respectively) (Li *et al.*, 1994; Ling *et al.*, 1994) suggesting that, in this conformer, the CO group lacks any hydrogen bond interaction. In contrast, the high correlation point with ν(Fe−CO) and ν(C−O) at 524 and 1936 cm^{-1}, respectively, falls nearer to values obtained with the V68N Mb variant (i.e., 526 and 1922 cm^{-1}, respectively) (Anderton *et al.*, 1997; Li *et al.*, 1994), where an additional hydrogen bond donor is substituted for a hydrophobic residue in the distal pocket. These observations suggest that this CO conformer in wt GAF-A DevS engages strong hydrogen bond

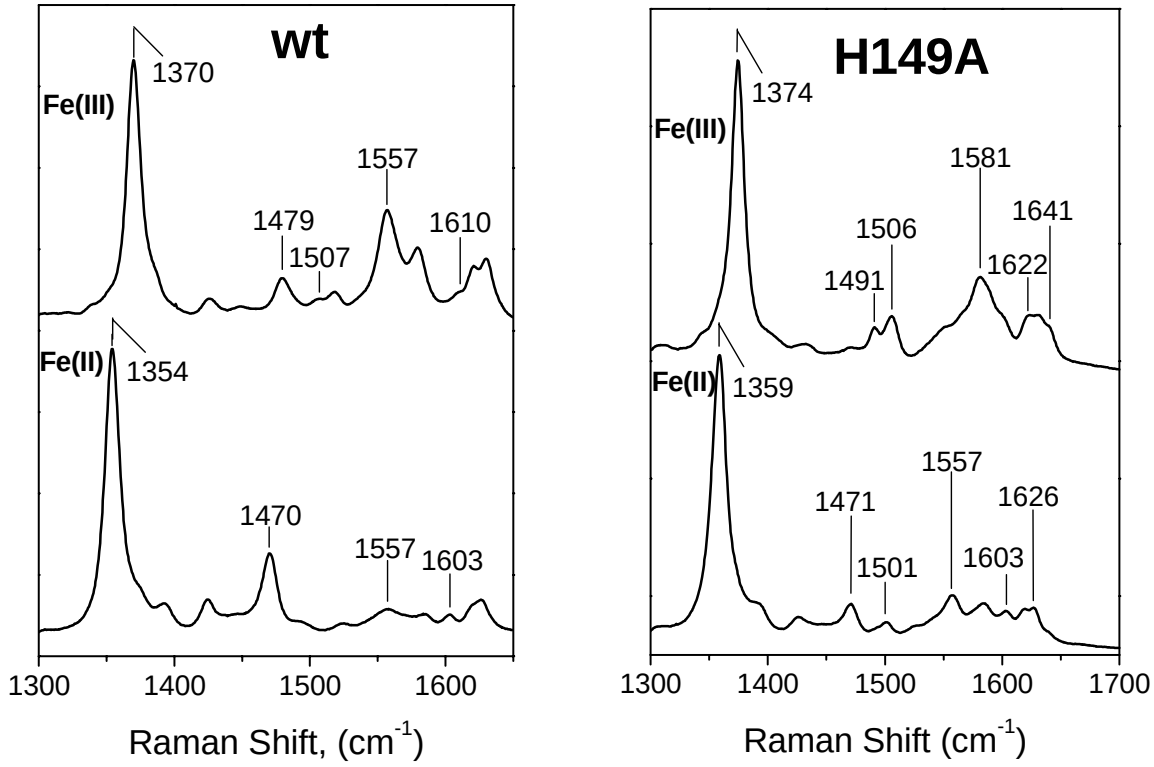

Fig. 3.2 High-frequency RR spectra of Fe(III) and Fe(II) wt (left) and H149A (right) GAF-A DevS at room temperature (λ_{exc} = 413 nm; 5 mW)

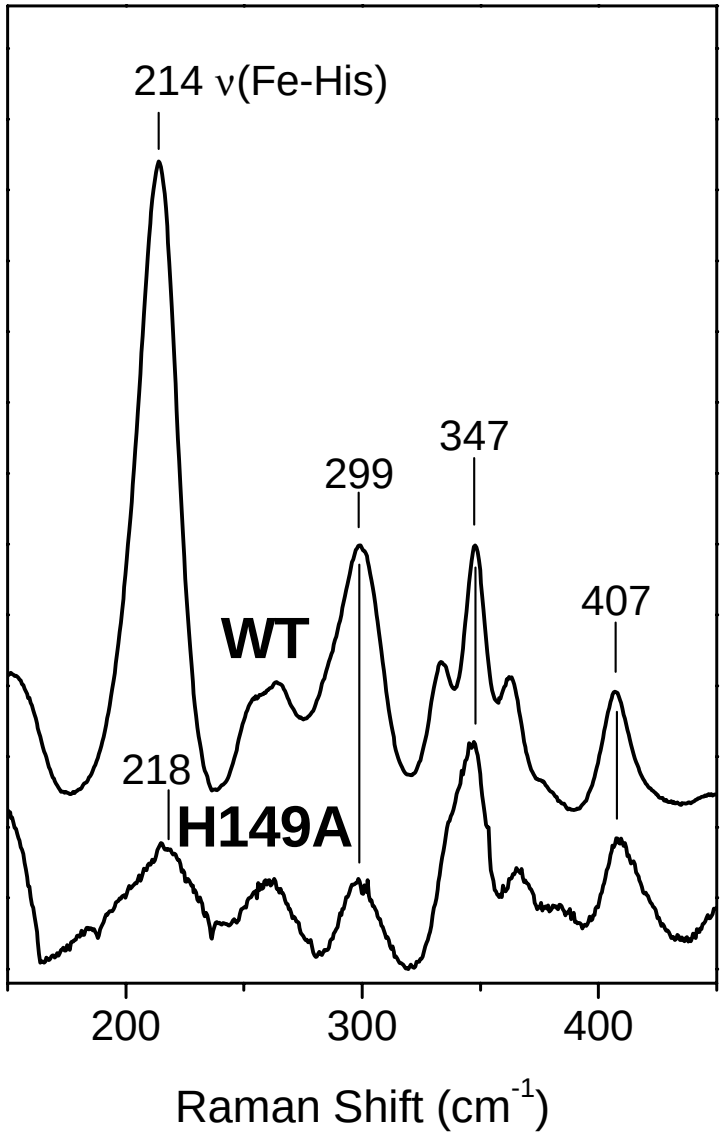

Fig. 3.3 Low-frequency RR spectra of Fe(II) wt and H149A GAF-A DevS at room temperature (λ_{exc} = 442 nm; 15 mW).

interaction(s) with distal pocket residue(s). This conformational heterogeneity is further discussed in the following section.

The RR spectra of the carbonyl complex in the H149A variant reveal a single conformer, with a ν(Fe−CO) at 533 cm^{-1} ($\Delta^{13}C = -4$ cm^{-1}) and a ν(C−O) at 1956 cm^{-1} ($\Delta^{13}C = -46$ cm^{-1}) (Fig. 3.4). These Fe−C−O stretching frequencies are characteristic of a complex with a very weak or no proximal ligand (Fig. 3.5), supporting the identification of His149 as the proximal histidine ligand in the wt protein.

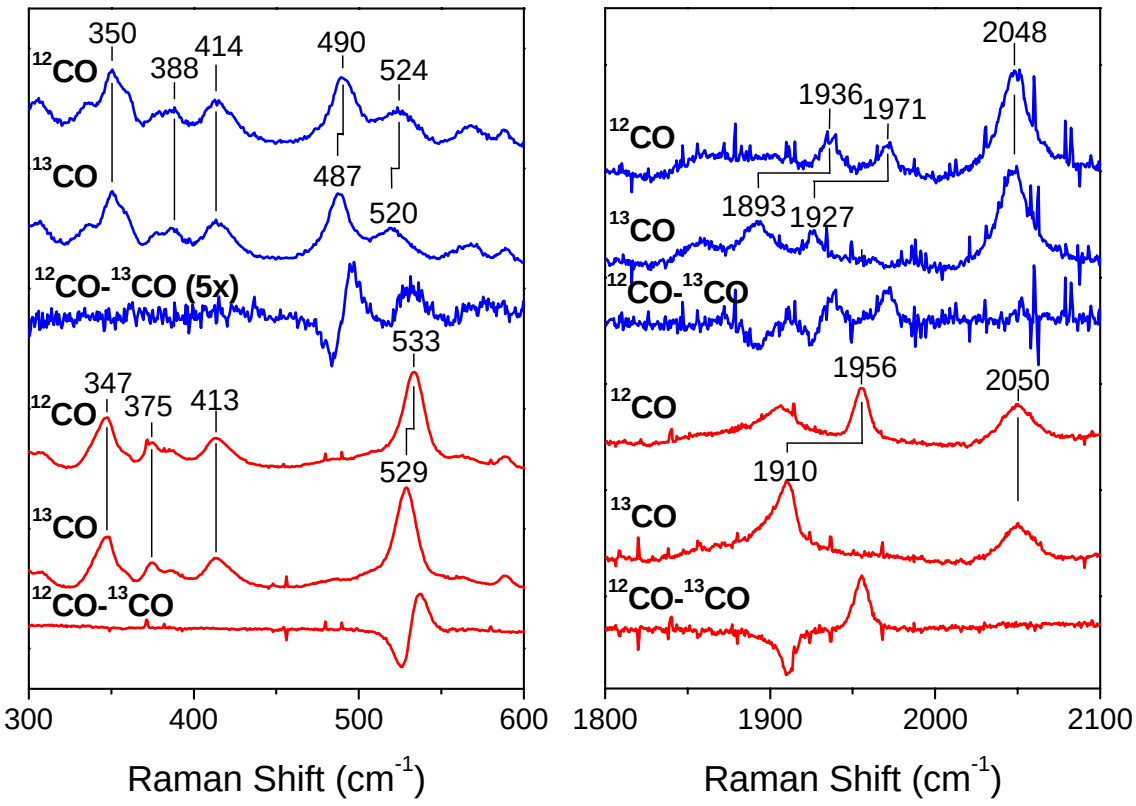

Fig. 3.4 Low-frequency (left) and high-frequency (right) RR spectra of wt (blue) and H149A (red) GAF-A DevS ^{12}CO and ^{13}CO adducts along and ^{12}CO - ^{13}CO difference spectra room temperature (λ_{exc} = 413 nm, 0.5 mW).

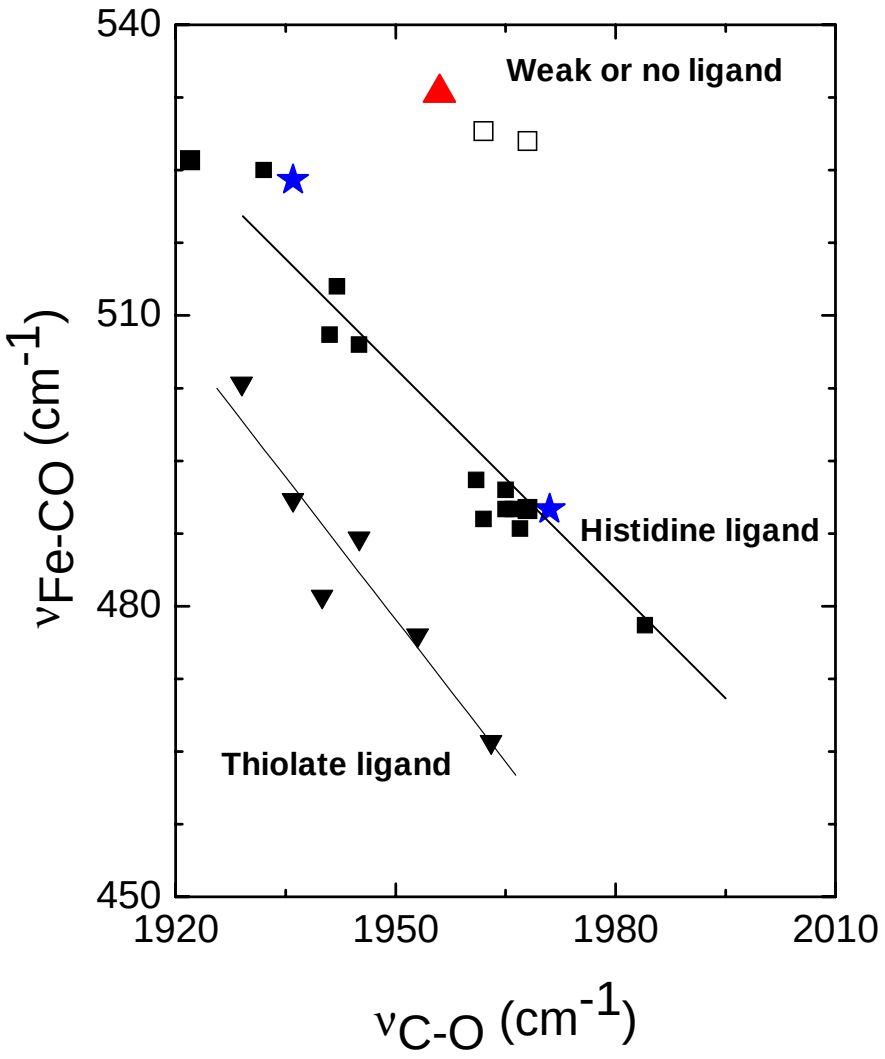

Fig. 3.5 ν(C-O) versus ν(Fe-CO) plots of hemoprotein-CO complexes. Data points for wt DevS (★) and H149A (▲) are compared with values for wt and distal mutants of Mb (Ray *et al.*, 1994) (■), and from cytochrome P450 and NO synthase (▼) (Fan *et al.*, 1997; McLean *et al.*, 2002). Also shown are proximal histidine mutants of heme oxygenase (□) (Sun *et al.*, 1994; Wilks and Moenne-Loccoz, 2000).

3.5 Spectroscopic Comparison of Truncated and Full-length DevS

The electronic absorption and RR spectra of the Fe(III) and Fe(II) states of all three DevS constructs (Fig 3.1) are essentially identical to those of GAF-A DevS (see Table 3.1, Fig. 3.2 and 3.3) and suggest a conserved heme pocket structure and coordination. Addition of CO, NO, or O_2 to dithionite-reduced DevS constructs results in the formation of stable, 6-coordinate adducts in all cases as determined by the position of Soret absorbance in the UV-vis spectra (Table 3.1). The near identity of the high-frequency RR spectra of the truncated and full-length DevS constructs bound to these ligands reinforces results seen in the Fe(III) and Fe(II) states, indicating that truncation does not significantly perturb the structure or coordination of the bound heme (data not shown).

Carbonyl Complexes

Despite the overall similarity of the CO complexes in truncated and full-length DevS, analysis of isotope-sensitive modes illustrates important differences in the organization of the distal pockets of DevS constructs. Section 3.4 reports on the observation of two CO conformers in GAF-A DevS (Fig. 3.4 and 3.5). In GAF-A/B DevS, the relative populations of the heme-CO conformers have changed significantly from those observed in GAF-A DevS to favor the conformation lacking the distal interaction (Fig 3.6). Control experiments at minimal laser power confirm that photolysis of heme-carbonyl complexes does not play a role in the differences observed between DevS constructs (data not shown). Peak fitting analysis comparing GAF-A DevS and GAF-A/B DevS indicates that introduction of the GAF-B domain alone is sufficient to decrease the intensity of the ν(C-O) at 1936 cm^{-1} by more than half. The low- and high-frequency RR spectra of FL DevS bound to CO are similar to those of GAF-A/B DevS-CO. Although the inclusion of the kinase and ATPase domains may lead to further reduction in the population of this CO conformer, the effect is too subtle to be reliably observed in the RR data. Thus, it seems that the conformational flexibility that allows GAF-A DevS to stabilize two CO conformers in the distal pocket is restricted upon the introduction of the GAF-B domain. This suggests an interaction between GAF-A and

GAF-B that increases the specificity of the interaction between bound CO and the distal heme pocket.

Nitrosyl Complexes

The ν(N-O) modes of heme-nitrosyl complexes are also sensitive to the electrostatics of the distal environment (Tomita *et al.*, 1999). These modes reside in a spectral region that is dominated by intense porphyrin ring modes, making their assignment from primary spectra extremely difficult. Difference spectra of $^{14}N^{16}O$ and $^{15}N^{18}O$ DevS adducts are therefore used for their identification. Analogous to the carbonyl complex data, the $^{14}N^{16}O$-$^{15}N^{18}O$ difference spectrum for the GAF-A DevS nitrosyl complex (Fig. 3.7) shows two isotope sensitive bands at 1638 and 1604 cm^{-1} that downshift approximately 72 and 73 cm^{-1}, respectively, upon $^{15}N^{18}O$ substitution. These shifts are in good agreement with the calculated $^{14}N^{16}O$–$^{15}N^{18}O$ shift values of -73 and -72 cm^{-1} for these two bands, respectively. Reproducible spectral features at 1627 and 1577 cm^{-1} are attributed to vibrational mixing between the ν(^{15}N-^{18}O) and the vinyl stretch and the ν_2 mode, respectively, as has been observed in other systems (Tomita *et al.*, 1999). A positive feature at 1502 cm^{-1} is systematically observed in the $^{14}N^{16}O$-$^{15}N^{18}O$ difference spectrum but it is absent from the $^{14}N^{16}O$-$^{15}N^{16}O$ difference spectrum (data not shown). The origin of this signal is unclear; it may reflect differences in intensity borrowing and combination bands involving ν(Fe-NO) and/or δ(Fe-N-O). Despite these complications, the assignment of two distinct ν(^{14}N-^{16}O) modes can be made with confidence given the excellent agreement between experimental and calculated shift values and the close correlation between ν(N-O) and ν(C-O) modes as has been observed with hemoprotein sharing the same proximal ligation (Fig. 3.7) (Coyle *et al.*, 2003). Again, the difference between the nitrosyl conformers can be attributed to the presence of a hydrogen bond in one conformer, giving rise to the low-frequency N-O stretch through enhanced backbonding. These spectra also show a decrease in the relative intensity of the low-frequency ν(N-O) upon addition of the second GAF domain. The spectrum of the full-length protein is similar to that of GAF-A/B DevS, potentially showing even greater attenuation of the hydrogen bonded NO conformer. This observation would again seem to indicate that GAF-B interacts with GAF-A, leading to a

more specific interaction between bound NO and the distal heme pocket. In contrast to the ν(N-O) mode, the ν(Fe-NO)s of heme-nitrosyl complexes are not particularly sensitive to the electrostatic environment of the bound NO (Tomita *et al.*, 2002). Consequently, the positions of ν(Fe-NO) are not significantly different between the DevS constructs (data not shown).

Oxy Complexes

In contrast to the trends seen for the DevS adducts of other exogenous ligands, there seems to be no difference in how the DevS constructs bind oxygen, based on their $^{16}O_2$-$^{18}O_2$ difference spectra (Fig. 3.8). Each construct presents a ν(Fe-O_2) at 563 cm^{-1} that downshifts 22 cm^{-1} upon $^{18}O_2$ substitution, a value that is in good agreement with the calculated shift of -25 cm^{-1}, assuming a diatomic Fe-O oscillator. Although the presence of multiple Fe-O_2 stretching modes cannot be ruled out, the conserved width and shape of the derivative feature in the difference spectra of all constructs suggest that, if multiple conformations of O_2 are present, their relative populations remain unchanged in truncated and full-length proteins. Although this mode is not as sensitive a probe for the distal environment as the ν(N-O) or ν(C-O) modes, the lack of any observable difference between the oxy complexes of different constructs strongly suggests that, unlike CO and NO, O_2 binds to DevS in the same conformation(s) regardless of the presence or absence of the GAF-B and kinase domains.

The ν(Fe-O_2) frequencies observed in the different DevS constructs are at the lower end of heme-O_2 adducts with neutral histidine trans ligand (Vogel *et al.*, 1999) and are suggestive of strong distal hydrogen bonding to the proximal oxygen atom of the bound O_2 as in heme oxygenases (ν(Fe-O_2) = 565 cm^{-1}) (Takahashi *et al.*, 1995; Unno *et al.*, 2004) and Hbs from *Mycobacterium* (ν(Fe-O_2) = 560 cm^{-1}) (Couture *et al.*, 1999) and *Paramecium* (ν(Fe-O_2) = 563 cm^{-1}) (Das *et al.*, 2000). To test this hypothesis, the D_2O sensitivity of the ν(Fe-O_2) mode in DevS was also examined. When a hydrogen bond exists between the bound oxygen molecule and a distal protein residue, the frequency of ν(Fe-O_2) upshifts due to the longer O_2 to DO-X or DN-X (where X is the protein residue) distance (Ohta *et al.*, 2004). However, if this hydrogen bond is donated

by a water molecule, the position of the water is sufficiently flexible to allow it to maintain the same D-bond strength and the $\nu(Fe\text{-}O_2)$ is unchanged (Ohta *et al.*, 2004). The $H_2O - D_2O$ difference spectra of the $^{16}O_2$ adducts of all DevS constructs illustrate the effect of H/D exchange, showing maxima and minima at 563 and 575 cm^{-1}, respectively (Fig. 3.8). The effect of H/D exchange is more easily quantified by comparing the $^{16}O_2$-$^{18}O_2$ difference spectra in H_2O and D_2O. Indeed, the derivative signal in the $^{16}O_2$-$^{18}O_2$ difference spectra of GAF-A DevS and FL DevS in D_2O is upshifted 4 to 5 cm^{-1} relative to that in H_2O (see Fig. 4.9). The discrepancy in shift values obtained by each method suggests Fermi coupling between the $\nu(Fe\text{-}O_2)$ and porphyrin ring modes. Despite this added complexity, both methods show that H/D exchange perturbs the $\nu(Fe\text{-}O_2)$ and further support the presence of hydrogen bonding from a distal residue to bound O_2 in truncated and full-length DevS constructs.

3.6 Discussion

RR Analysis of the wt truncated GAF-A DevS shows that this protein binds Fe(III) heme in a 6-coordinate geometry which is predominantly high spin. Reduction of the heme with dithionite leads to a 5-coordinate high spin geometry (Fig 3.2). Excitation of this species with 442 nm (Fig. 3.3) allows for the observation of an intense mode at 214 cm^{-1} which is consistent with coordination of the Fe(II) by a neutral proximal histidine residue lacking significant hydrogen bond interactions (Kitagawa, 1988). This conclusion is supported by the positions of ν(C-O) and ν(Fe-CO) along the correlation line for proteins having proximal histidine ligation (Fig. 3.5). A previous report had suggested that His149 was the proximal heme ligand in DevS (Sardiwal *et al.*, 2005). We investigated the H149A variant of DevS in order to confirm this suggestion. Although heme is still capable of binding to this variant, RR analysis of the Fe(III) and Fe(II) forms show that the coordination of the heme is clearly perturbed relative to wt (Fig 3.2). Further, the reduced protein shows no $\nu(Fe\text{-}N_{His})$ on 442 nm excitation (Fig. 3.3) and the frequencies of ν(C-O) and ν(Fe-CO) are consistent with a 5-coordinate CO complex (Fig. 3.5). Given these observations, we can confidently assign His149 as the proximal heme ligand in wt DevS.

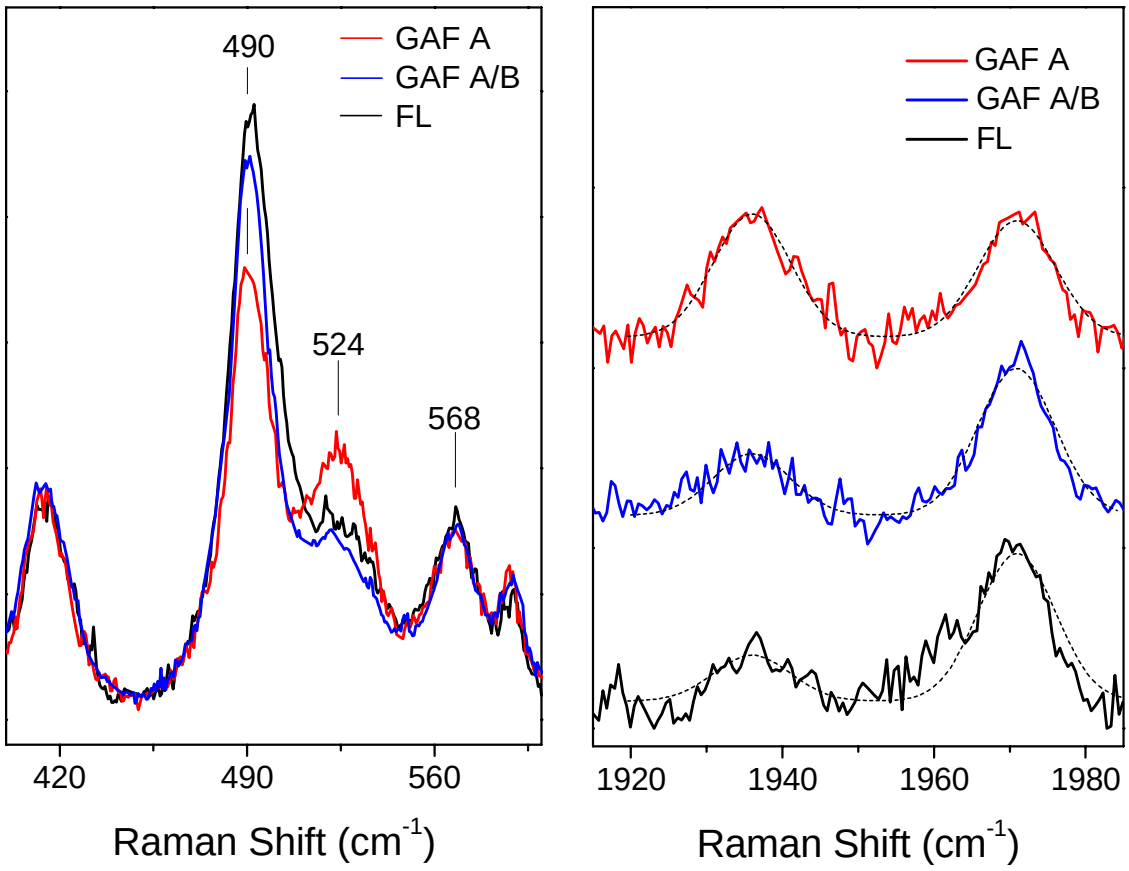

Fig. 3.6 Low-frequency (left) and high-frequency (right) RR spectra of GAF-A DevS-CO (red), GAF-A/B DevS-CO (blue), and FL DevS-CO (black) at room temperature (λ_{exc} = 413 nm, < 0.5 mW). Dotted lines show peak fitting results.

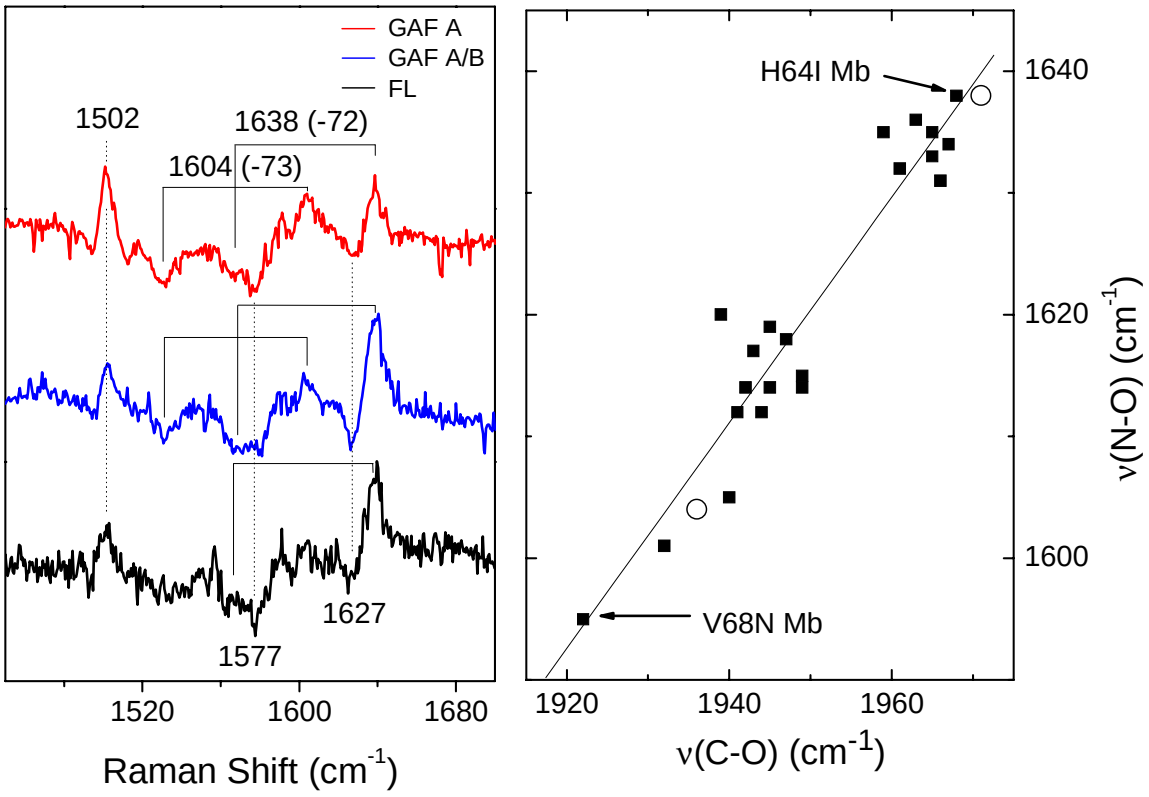

Fig. 3.7 High-frequency $^{14}N^{16}O$–$^{15}N^{18}O$ RR difference spectra for GAF-A DevS (red), GAF-A/B DevS (blue), and FL DevS (black) at room temperature (left) (λ_{exc} = 413 nm, 0.5 mW). ν(N-O) versus ν(C-O) plots of hemoprotein-NO and -CO complexes (right) points for wt DevS constructs (O) are compared with values for wt and distal mutants of Mb (Coyle *et al.*, 2003)

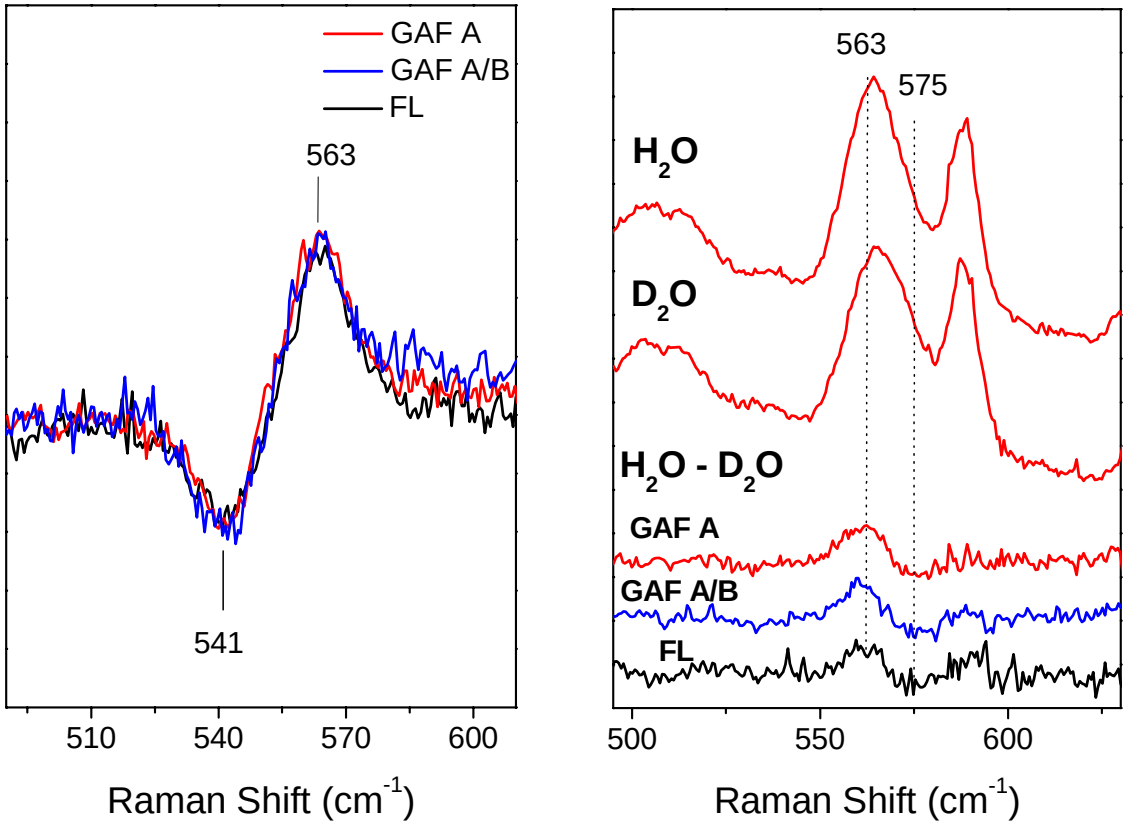

Fig. 3.8 Low-frequency RR spectra of $^{16}O_2$–$^{18}O_2$ difference spectra of GAF-A DevS (red), GAF-A/B DevS (blue), and FL DevS (black) (left) and GAF-A DevS-$^{16}O_2$ in H_2O buffer and D_2O buffer (top two traces, red) and H_2O–D_2O difference of GAF-A DevS-$^{16}O_2$ (red), GAF-A/B DevS-$^{16}O_2$ (blue), and FL DevS (black) (λ_{exc} = 413 nm, 1.0 mW).

The observation of two distinct CO conformations in the distal pocket of GAF-A DevS prompted us to investigate whether the presence of the other domains of DevS may affect their relative populations. The comparison of the RR spectra of full-length and truncated constructs of DevS led us to conclude that interdomain interactions impact the heme environment. The essentially identical UV-vis spectra, porphyrin core marker RR frequencies, propionate and vinyl peripheral group vibrations, and Fe-His stretching vibrations in all DevS constructs (data not shown) demonstrate that truncation of the GAF-B and kinase domains does not alter the proximal environment or the anchoring of the heme group in the GAF-A domain. However, analysis of the isotope sensitive modes of the CO (Fig. 3.6) and NO (Fig. 3.7) adducts of these constructs shows that the distal environment is influenced by the presence of the GAF-B domain. Specifically, the presence of this domain causes a significant perturbation in the relative populations of the two CO and NO conformers present in GAF-A DevS, causing a preference for the conformation lacking a strong hydrogen bond to the CO and NO ligands. Therefore, interactions between the two GAF domains of DevS limit the conformational flexibility of the heme distal pocket and destabilize the hydrogen-bonded conformers of the CO and NO heme adducts.

Although the direct observation of interdomain interactions by RR spectroscopy is unusual, similar observations have been made when comparing truncations of *R. meliloti* FixL, another modular heme-based sensor kinase (Lukat-Rodgers and Rodgers, 1997). In this case, two 5-coordinate ν(N-O) modes were detected in the low temperature RR spectrum of the isolated heme domain of FixL-NO. In the construct that included the kinase domain, only one of these modes was observed. This difference was interpreted as arising from contact between the kinase and heme domains, which caused a more specific interaction between the bound NO and the heme distal pocket. The kinase domain of FixL also modulates interactions between the heme distal pocket and bound CO. Although only one ν(C-O) mode was detected in both truncated FixL-CO and functional kinase FixL-CO, its frequency was found to be 6 cm^{-1} higher in the functional kinase than in the truncated heme domain (Miyatake *et al.*, 1999). Thus, interaction between the kinase and heme domains of *Rm*FixL modulates the interaction of the distal pocket with both CO and NO ligands.

The nature of the change that occurs in the distal pocket of FixL in the presence of the kinase domain remains uncertain. Miyatake *et al.* suggest that the relatively small shift in the ν(C-O) frequency of functional kinase FixL-CO, relative to truncated FixL-CO, reflects a change in the geometry of the bound CO caused by increased steric constraint in the distal pocket imposed by the presence of the kinase domain (Miyatake *et al.*, 1999). This explanation is favored over the alternative hypothesis that an electrostatic perturbation of the distal environment causes the observed frequency shift. The steric view is supported by EXAFS measurements showing a decrease in the Fe-C-O angle from 171° in truncated FixL-CO to 157° in functional kinase FixL-CO (Miyatake *et al.*, 1999). The more linear CO coordination by truncated FixL-CO is thought to result in a more efficient overlap of CO and porphyrin π* orbitals, leading to enhanced backbonding and, consequently, higher ν(Fe-CO) and lower ν(C-O) frequencies than are observed in the functional kinase FixL-CO (Miyatake *et al.*, 1999).

The DevS system is different from FixL in several respects: a) both conformations of GAF-A DevS-NO are six-coordinate complexes observable at room temperature, b) the two distinct CO conformers observed in GAF-A DevS are observed simultaneously rather than in different constructs as in FixL, c) the 35 cm^{-1} difference between the two ν(C-O) frequencies observed in GAF-A DevS is more than 5-fold greater than the 6 cm^{-1} difference in ν(C-O) frequencies observed in truncated and functional kinase FixL. It seems unlikely that steric factors alone could account for such a significant difference in ν(C-O) frequencies in DevS. RR characterization of the CO adducts of a variety of Mb mutants shows that mutations affecting only steric crowding in the distal pocket have relatively little effect on Fe-C-O vibrational frequencies when compared to those which alter the electrostatic environment of the bound CO (Li *et al.*, 1994). Therefore, we favor a model where the two conformations of CO and NO observed in GAF-A differ by the hydrogen bond interactions these groups engage in the distal pocket, and only occur to any significant extent in the absence of interdomain interactions.

In contrast to the carbonyl and nitrosyl complexes, oxygen binding in DevS seems impervious to the effects of truncation, yielding the same ν(Fe-O_2) at 563 cm^{-1} for all constructs. This frequency is low among hemoproteins with neutral proximal histidines but compares well with those of other proposed O_2-sensors such as *Bs*HemAT (560 cm^{-1})

(Aono *et al.*, 2002) and *Ec*DosH (562 cm^{-1}) (Tomita *et al.*, 2002) (Table 3.2). In these systems, the low $\nu(Fe\text{-}O_2)$ is thought to arise from the presence of a specific hydrogen bond to the bound O_2 (Aono *et al.*, 2002; Park *et al.*, 2004). Indeed, the crystal structure of O_2-bound EcDosH reveals two hydrogen bond interactions between the guanidinium group of an arginine residue and bound oxygen, one to each atom of the oxy group at 2.70 and 2.94 Å (Park *et al.*, 2004). In the case of HemAT, RR characterization of a T95A variant ($\nu(Fe\text{-}O_2)$ = 569 cm^{-1}) confirmed that this threonine residue is critical for the low-frequency of the $\nu(Fe\text{-}O_2)$ and led to the suggestion that it forms a hydrogen bond to bound O_2 (Ohta *et al.*, 2004). The unusually low $\nu(Fe\text{-}O_2)$ and the sensitivity of this mode to H/D exchange strongly suggest that the O_2 group is engaged in a strong hydrogen-bond interaction in the distal pocket of DevS as well. The identity and specific role of the hydrogen bond donor is discussed in detail in the following chapter.

Table 3.2 RR frequencies (cm^{-1}) of O_2, NO, and CO bound to Fe(II) heme sensor proteins. [a] (Aono *et al.*, 2002; Yoshimura *et al.*, 2006); [b] (Tomita *et al.*, 2002); [c] (Lukat-Rodgers and Rodgers, 1997; Miyatake *et al.*, 1999; Tamura *et al.*, 1996); [d] (Tomita *et al.*, 1999; Tsubaki *et al.*, 1982; Van Wart and Zimmer, 1985); [e] Observed in the truncated heme domain (DevS GAF-A); [f] Observed only in the truncated heme domain at low temperature

Protein	$\nu(Fe\text{-}O_2)$	$\nu(Fe\text{-}NO)$	$\nu(N\text{-}O)$	$\nu(Fe\text{-}CO)$	$\nu(C\text{-}O)$
FL DevS	563	561	1638	490, 524[e]	1971, 1936[e]
***Bs*HemAT**[a]	560	545	1636	494	1964
***Ec*DosH**[b]	562	563	1632/1576	487	1969
***Rm*FixL**[c]	571	525/558	1676/1664[f]	502	1956
SW Mb[d]	570	560	1613	512	1944

The similarities in exogenous ligand vibration modes in full-length DevS and HemAT extend to the CO- and NO-complexes, as the Fe-C-O and Fe-N-O frequencies of these proteins are quite similar, and consistent with these ligands residing in a purely hydrophobic environment (Table 3.2). Therefore, it seems likely that specific hydrogen

bonding networks are responsible for selective oxygen sensing in these proteins, as has been suggested for HemAT (Aono *et al.*, 2002; Ohta *et al.*, 2004; Yoshimura *et al.*, 2006). This view is supported by the apparent insensitivity of the $\nu(Fe\text{-}O_2)$ frequency of DevS to truncation, suggesting that the distal pocket of this protein is optimized to interact with oxygen and does so even when conformational rigidity is not imposed by the presence of the GAF-B domain.

Based on the evidence acquired on the full-length and truncated constructs of DevS, we propose a model for ligand discrimination and signal transduction based on electrostatic interactions in the heme distal pocket of the GAF-A domain. Oxygen bound to the heme is engaged in a direct hydrogen bond to a protein residue in the distal pocket. The kinase domain is inactive in this conformation. Dissociation of O_2 from the heme under hypoxic conditions and/or displacement by NO or CO disrupts this hydrogen bond. The accompanying structural change at the heme domain is communicated to the kinase domains via the GAF-B domain, leading to kinase activity and induction of the dormancy regulon. This model is consistent with the observation that hypoxia and NO each lead to induction of the dormancy regulon and that O_2 competitively inhibits NO-mediated induction (Voskuil *et al.*, 2003). The presence of the GAF-B domain is essential in restricting the structure of the GAF-A domain so that only the O_2-complex can stabilize the inhibitory hydrogen bond network which presumably propagates to the kinase domain, modulating its activity. In this view, it is tempting to propose that the GAF-B acts as a transducer in the sensory process and is also crucial to the discriminatory power of the GAF-A domain. In the following chapter, we identify the hydrogen bond donor and make use of a variant protein to establish its role in ligand discrimination.

CHAPTER 4
LIGAND DISCRIMINATION IN THE HEME-BASED SENSOR PROTEIN DevS

4.1 The Distal Hydrogen Bond Donor in DevS

In the previous chapter, we reported the RR characterization of truncated and full-length wt DevS constructs. The results suggested that a specific hydrogen bond exists between a distal residue and the proximal oxygen atom of bound O_2. This hydrogen bond was absent from CO and NO adducts as well as the Fe(II) unligated state. Based on this evidence and the apparent function of DevS *in vivo*, we proposed that this hydrogen bond was responsible for differentiating exogenous ligands.

Subsequent to that work, the crystal structure of the GAF-A domain of the DevS paralog DosT (76% similarity) was solved (Podust *et al.*, 2008). Fortuitously, an oxygen molecule was bound to the heme group of one of the monomers in the asymmetric unit (the other appeared to be in the 5-coordinate Fe(II) form) (Fig. 4.1). The distal and proximal oxygen atoms were within 2.50 and 2.94 Å, respectively, of the phenol group of a distal tyrosine residue, Y169, suggesting a strong hydrogen bond interaction. This residue is conserved in DevS at position 171. Therefore, it seemed likely that it was responsible for differentiating between exogenous ligands by virtue of this hydrogen bond interaction as postulated in the previous chapter.

---

*Material in this chapter has been published in this or similar form in *Biochemistry*, and is used here with permission of the American Chemical Society.

Yukl, E. T., Ioanoviciu, A., Nakano, M. M., Ortiz de Montellano, P. R., Moënne-Loccoz , P. (2008) A Distal Tyrosine Residue Is Required for Ligand Discrimination in DevS from *Mycobacterium tuberculosis.* *Biochemistry* **47**, 12532-12539.

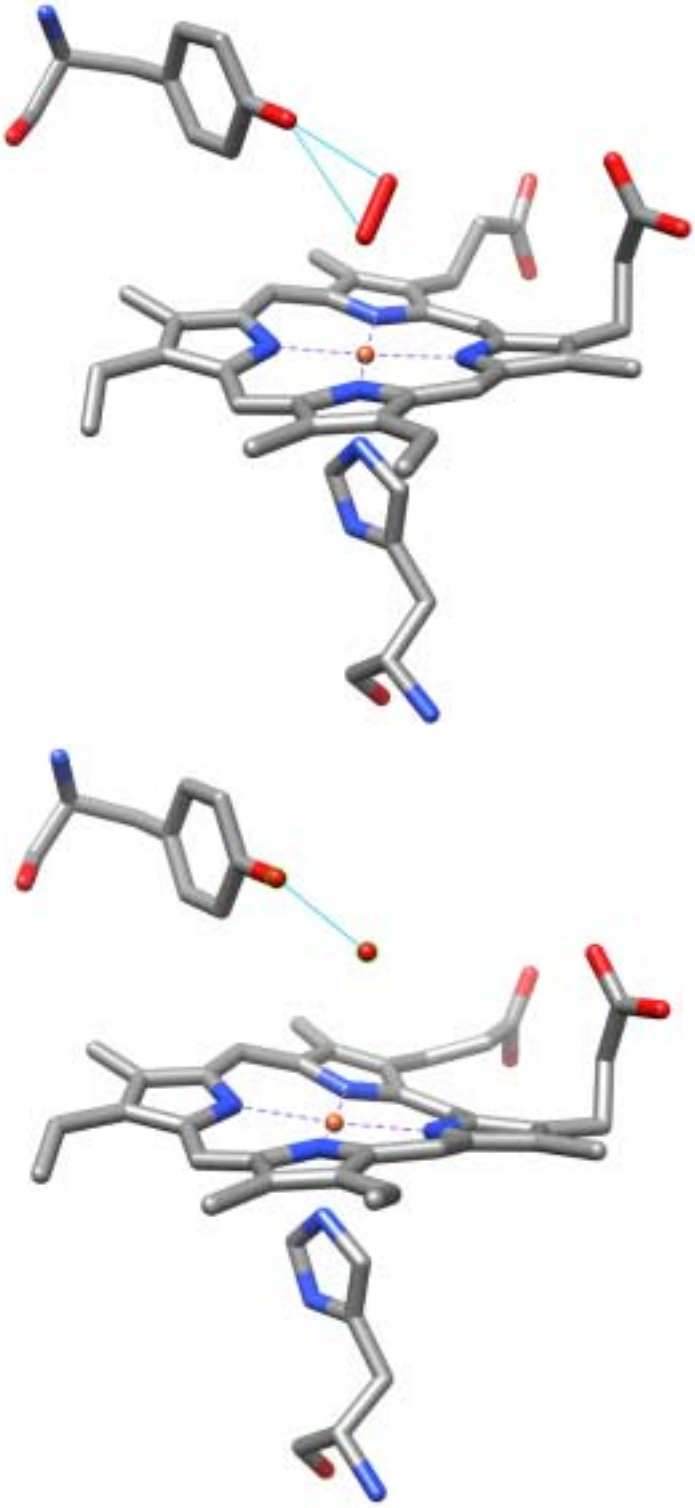

Fig. 4.1 Structures of the two heme sites present in DosT GAF-A crystals (2VZW) Fe(II)-O_2 (top) and Fe(II) (bottom). Adapted from (Podust *et al.*, 2008).

Here we report on the RR characterization and autokinase activity of the Y171F mutant of full-length DevS in the Fe(III), Fe(II), Fe-CO, Fe-NO, and Fe-O_2 states and compare the results to wt DevS. Because the wt Fe(II)-O_2 complex is inactive, and Tyr171 interacts with the bound O_2, the Y171F mutation might have been expected to release inhibitory constraints to produce a Y171F variant equally active in the O_2, NO, and CO complexes. However, our results show that the Y171F variant lacks autokinase activity in all three states where the distal pocket is occupied by an exogenous ligand and retains activity only in the deoxy form. These activity measurements are discussed in conjunction with the RR analysis to propose mechanistic models of regulation in DevS.

4.2 Materials and Methods

Expression and Purification

The mutant protein was expressed following the same protocol used in the case of wt DevS (see section 3.3). The purification procedures were also identical except that Y171F DevS was eluted from the His trap column using 250 mM imidazole. The protein was then applied to a DEAE column. The purified protein was obtained after gradient elution from 0 to 0.5 M NaCl in 50 mM Tris buffer containing 5% glycerol and 1 mM EDTA at pH 8.

Autophosphorylation Assays

Wt or Y171F DevS protein solutions in 50 mM potassium phosphate buffer at pH 7.5 with 100 mM NaCl were purged with Ar and reduced with sodium dithionite. Excess dithionite was removed using desalting columns and CO, NO, or O_2 gas was added to appropriate samples. The Fe(III) proteins were incubated in 2 mM potassium ferricyanide and desalted using spin columns. These operations were performed in the anaerobic glove box. All samples, except the oxy and Fe(III) proteins, were loaded into septum-sealed microcentrifuge tubes. All 50 μL assay samples contained final concentrations of 5.0 μM DevS, 100 mM Tris-HCl pH 7.5, 50 mM KCl, 5 mM $MgCl_2$, and, with the exception of oxy and Fe(III) samples, 500 μM sodium dithionite, after ATP addition. Reactions were initiated by syringe addition of a few μL of a solution

containing γ^{32}P ATP (4500 Ci/mmol) (Pharmacia Biotech) and Ar-purged, unlabeled ATP (Sigma) to a final concentration of 200 μM and 10 μCi. 10 μL aliquots were removed at various time points and combined with 3.0 μL stop buffer (208 mM Tris-HCl pH 6.8, 8.3% SDS, 42% glycerol, 167 mM DTT, and 0.08% bromophenol blue). These samples were run through a 12% polyacrylamide gel, which was vacuum-dried at 80 °C for 1.5 h, and exposed in a PhosphorImager cassette (Molecular Dynamics) for approximately 24 to 48 h. Levels of phosphorylated protein were imaged on a Typhoon Trio+ PhosphorImager (Amersham Biosciences) and quantified according to Nakamura et al. (Nakamura *et al.*, 2001) except that the 1.65 correction factor was eliminated since gels were completely dried. After exposure, dried gels were rehydrated in 20% methanol 5% acetic acid solution and Coomassie stained to confirm consistency in amount of protein loaded and integrity of full-length proteins. Control experiments using the oxy, Fe(II), Fe(II)-NO, and Fe(II)-CO proteins were conducted using identical conditions to the autophosphorylation assays except for the absence of γ^{32}P ATP. The UV-vis spectra of these controls were taken after 1 h incubation to confirm that the redox and coordination state of the heme iron was stable in the assay conditions.

Electronic Absorption and RR Spectroscopy

A 50 mM potassium phosphate buffer at pH 7.5 with 100 mM NaCl was used for all protein samples. Sample treatment and UV-vis and RR spectroscopy were performed as described in section 2.1.

4.3 Activity of WT and Y171F DevS

Autophosphorylation assays were performed by monitoring γ^{32}P-labeling of DevS for 10 min at room temperature (Fig. 4.2). Different states of wt DevS showed autokinase activities consistent with a previous report by Gilles-Gonzalez and coworkers (Sousa *et al.*, 2007). However, in our hands, the Fe(II) protein is systematically less active than the nitrosyl complex while equivalent activities are reported for these two states in Sousa et al. (Sousa *et al.*, 2007). Indeed, multiple experiments with two

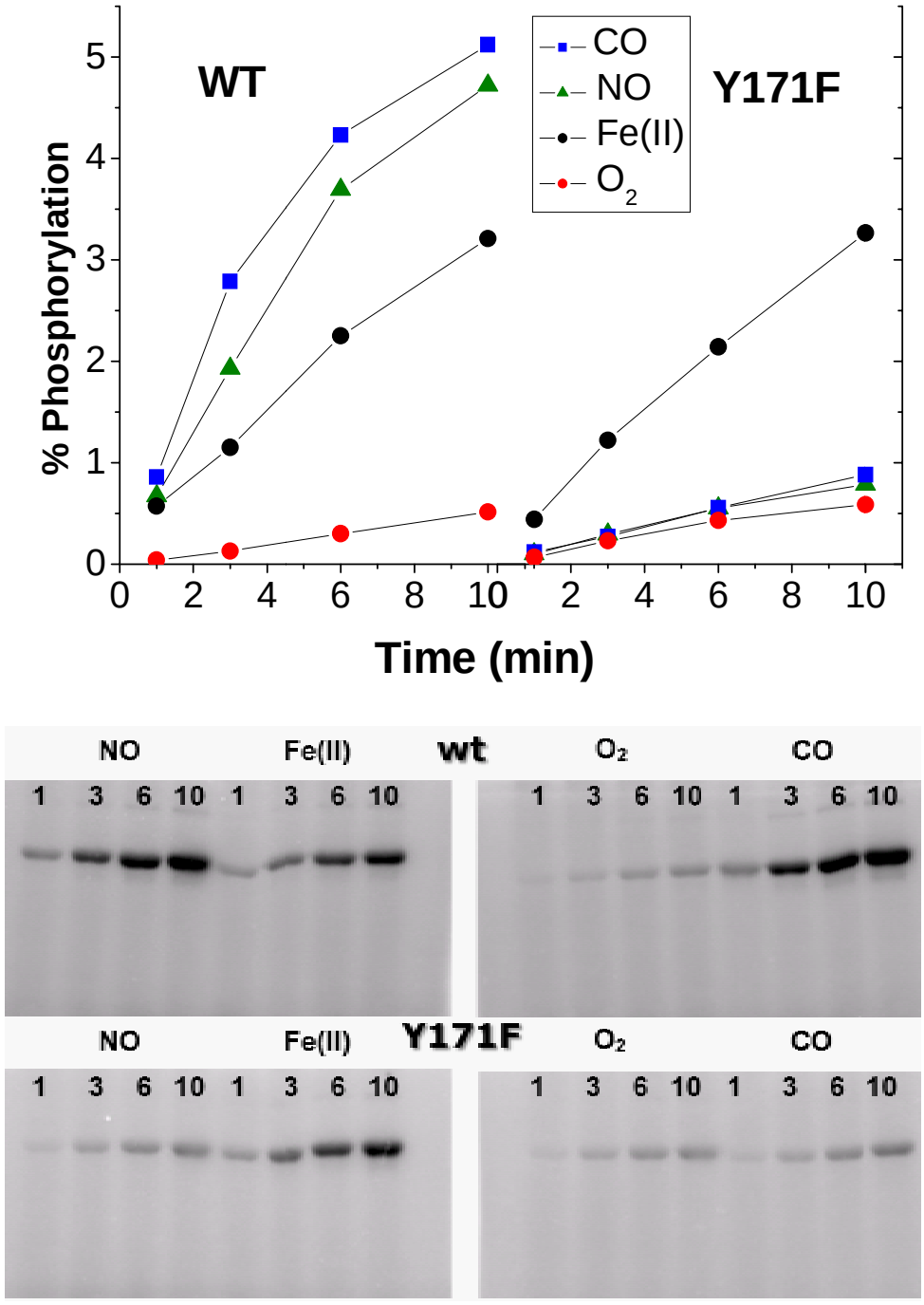

Fig. 4.2 Autophosphorylation of wt and Y171F DevS in various states. Reaction progress (top) as determined by quantifying autoradiographs of the dried gels (bottom)

different wt DevS constructs yielded the same pattern of activity for the various states of DevS (data not shown). Mutation of Tyr 171 to Phe has no apparent impact on the autophosphorylation level observed in the Fe(II) state, but the mutation disrupts the discriminatory power of DevS toward exogenous ligands with the CO, NO, and O_2-bound states all lacking activity (Fig. 4.2). As reported earlier for wt DevS (Kumar *et al.*, 2007), the met Fe(III) state of Y171F is inactive (data not shown). These data are consistent with a determining role for the hydroxyl group of Tyr171 in distinguishing between distal exogenous ligands in DevS. The maintenance of autophosphorylation activity in the deoxy form of Y171F DevS demonstrates that the point mutation does not result in a major protein conformational change. In the deoxy form, the heme is pentacoordinate (see below) and the lack of a distal ligand results in a lack of sensitivity to the Tyr171 to Phe mutation.

4.4 Spectroscopic Comparison of WT and Y171F DevS

UV-vis spectroscopic data for wt and Y171F DevS at pH 7.5 are summarized in Table 4.1. Distinctive absorption features were obtained for the Fe(II), Fe(II)-CO, and Fe(II)-NO forms, with both proteins displaying nearly identical spectra. The Fe(III) form of Y171F shows significant red shifts in the α/β region, a decrease in intensity of the charge transfer band near 630 nm, as well as a red shift and significant decrease in the extinction coefficient of the Soret band (Table 4.1, Fig. 4.3). These observations suggest an increase in the proportion of low-spin Fe(III) heme in the mutant relative to wt protein (Makinen and Churg, 1983).

This interpretation of the UV-vis changes is consistent with the high-frequency RR spectra obtained with Soret excitation (Fig. 4.4) where the frequencies of the porphyrin skeletal mode ν_4 correlates with the oxidation state of the iron, and the ν_3, ν_2, and ν_{10} modes report the coordination and spin state of the iron (Spiro and Li, 1988). Specifically, in the wt protein, the ν_3, ν_2, and ν_{10} observed at 1479, 1557, and 1609 cm^{-1}, respectively, are indicative of a 6-coordinate high-spin (6cHS) heme while those at 1507, 1579, and 1639 cm^{-1} correspond to a 6-coordinate low-spin (6cLS) population. Equivalent sets of frequencies are also observed in the RR spectrum of the Y171F variant

(Fig. 4.4 and Table 4.2), but the relative intensities of these bands suggest a shift of the 6cHS/6cLS distribution, from predominantly 6cHS in the wt protein to predominantly 6cLS in the variant protein.

Table 4.1. UV-Vis spectroscopic data for wt and Y171F DevS

DevS Proteins		Soret and visible λ_{max} (nm)
Fe(III)	wt	406, 500, 630
	Y171F	409, 540, 633
Fe(II)	wt	428, 562
	Y171F	429, 561
Fe(II)-CO	wt	422, 570, 540
	Y171F	421, 569, 540
Fe(II)-NO	wt	419, 577, 547
	Y171F	419, 573, 544
Fe(II)-O_2	wt	414, 578, 543
	Y171F	420, 573, 542

RR spectra of Fe(III) wt and Y171F DevS at different pH show that conversion from high-spin to low-spin Fe(III) heme occurs at a much lower pH in Y171F (pH ~ 7) than it does in wt DevS (pH ~ 10) (Fig. 4.5). These observations suggest that the removal of the hydroxyl group of Tyr171 alters the ligand-field strength of the distal ligand. At pH 10, the Tyr171 side chain may coordinate the wt heme Fe(III) as a phenolate ligand. Alternatively, a solvent molecule coordinates the heme Fe(III) with a bond strength that is governed by its interaction with Tyr171. In the Y171F DevS variant, the sixth ligation to the Fe(III) is most likely occupied by a solvent molecule with a pK_a near 7. Attempts to gather direct evidence identifying the sixth ligand in Fe(III) wt and Y171F DevS were unsuccessful. Specifically, low-frequency RR spectra in $^{18}OH_2$ and D_2O did not reveal isotope-sensitive modes that could be assigned to a ν(Fe-OH) mode, as previously observed with hydroxy-complexes in heme oxygenases and Hb at high pH (Asher *et al.*, 1977; Kim *et al.*, 2006; Takahashi *et al.*, 1994; Wilks *et al.*, 1995) nor a ν(Fe-O_{Tyr}) as previously observed in the 6cLS alkaline Fe(III) *Chlamydomonas* Hb (Das *et al.*, 2000) (data not shown).

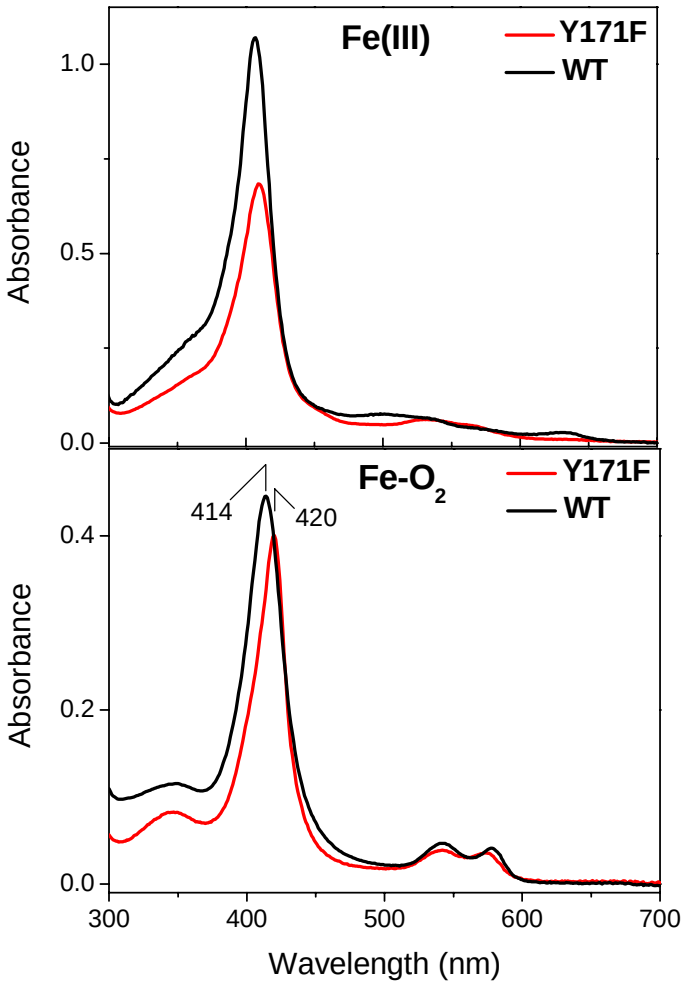

Fig. 4.3 UV-vis spectra of Fe(III) (top) and oxy (bottom) wt and Y171F DevS at pH 7.5. The two spectra in each group are normalized based on a conserved extinction coefficient at 421 nm of 177 cm^{-1} mM^{-1} for both wt and Y171F DevS-CO complexes.

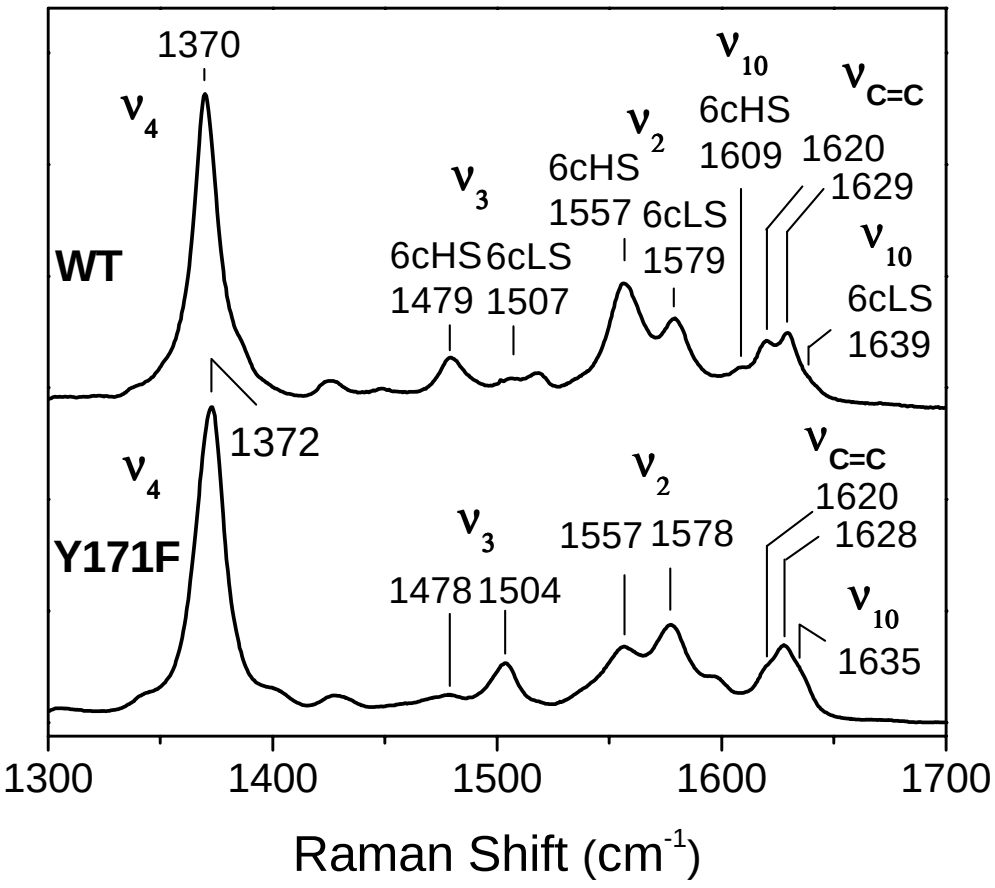

Fig 4.4 High-frequency RR spectra of Fe(III) wt DevS and Y171F DevS at room temperature (λ_{exc} = 413 nm; 5 mW).

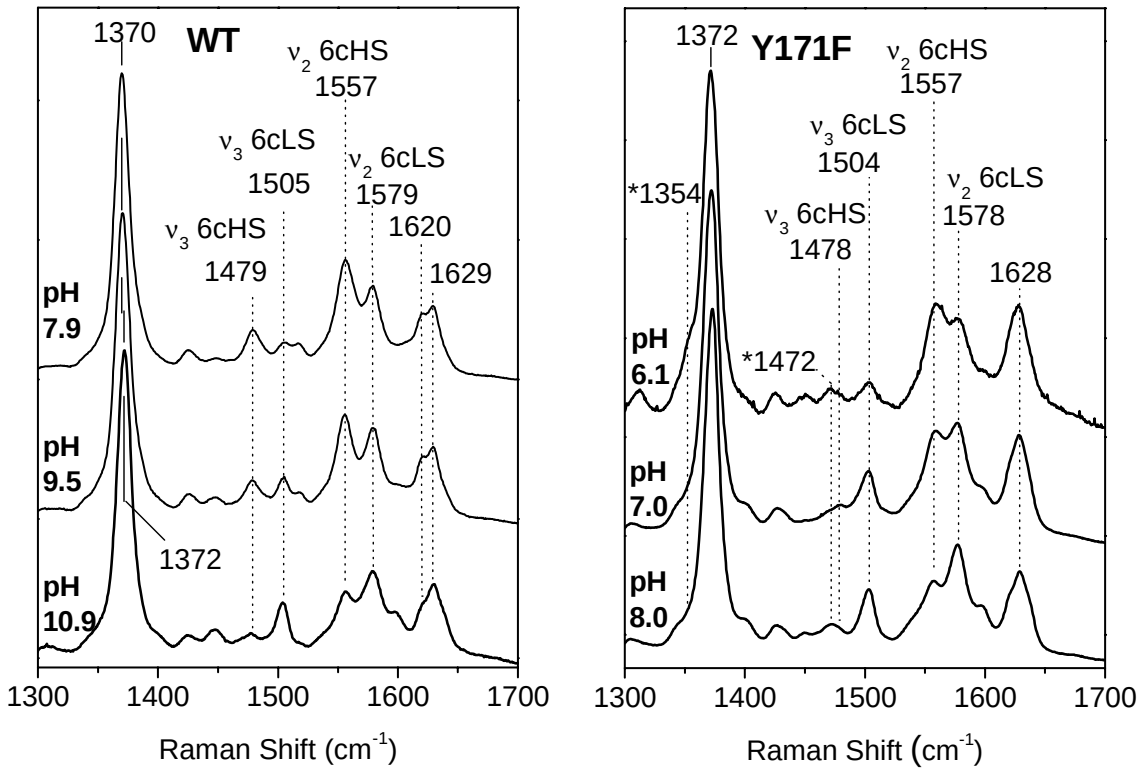

Fig. 4.5 High-frequency RR spectra of Fe(III) wt (left) and Y171F (right) DevS at varying pH (λ_{exc} = 413 nm; 5 mW; asterisks indicate peaks arising from photoreduction of the Fe(III) heme).

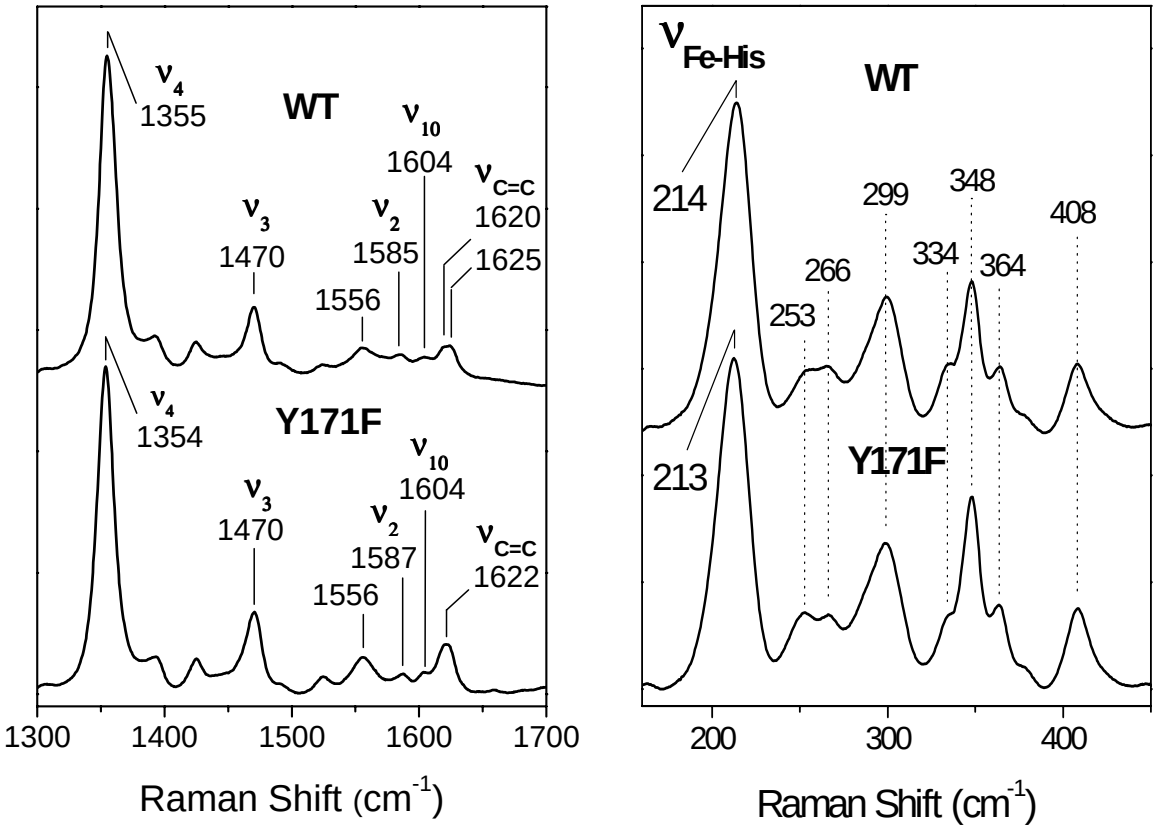

Fig. 4.6 High-frequency (left) (λ_{exc} = 413 nm; 5 mW) and low-frequency (right) (λ_{exc} = 442 nm; 10 mW) RR spectra of Fe(II) deoxy wt and Y171F DevS

The high-frequency RR spectra of Fe(II) wt and Y171F DevS are both indicative of a pure 5-coordinate high-spin (5cHS) heme (Fig. 4.6 and Table 4.2). Two ν(C=C) vinyl stretches are observed in wt DevS at 1620 and 1625 cm^{-1}, but a single broad ν(C=C) is observed at 1622 cm^{-1} in Y171F DevS. A similar perturbation is seen in the Fe(III) state, where two well-resolved ν(C=C) vibrations are observed at 1620 and 1629 cm^{-1} in the wt protein, while the Y171F variant shows a dominant ν(C=C) at 1628 cm^{-1} and a shoulder at 1620 cm^{-1} (Fig. 4.4). Although these data indicate a slight difference in the vinyl groups in the wt and variant proteins, the equivalent activity of the Fe(II) state in these two proteins suggests that the vinyl perturbations have no impact on function. Low-frequency RR spectra obtained with 442-nm excitation (Fig. 4.6) exhibit a strong band at 214 cm^{-1} for the wt protein previously assigned to the ν(Fe-N_{His}) mode. This mode shifts -1 cm^{-1} in the RR spectrum of Y171F DevS, while other low-frequency heme peripheral deformation modes are nearly identical in both proteins. These results indicate that the effect of the Y171F mutation is limited to the distal environment and does not significantly perturb the proximal heme pocket of DevS.

In the previous chapter, we identified a major CO conformer in wt DevS with ν(C-O) and ν(Fe-CO) frequencies at 1971 and 490 cm^{-1}, respectively, as well as a second, very minor, CO conformer with ν(C-O) and ν(Fe-CO) bands at 1936 and 524 cm^{-1}, respectively. This second conformer is likely engaged in electrostatic and/or hydrogen bond interactions within the distal pocket. The RR spectra of the CO complex of Y171F DevS exhibit a ν(C-O) at 1965 cm^{-1} and a ν(Fe-CO) at 497 cm^{-1} (Fig. 4.7). The variations in ν(C-O) and ν(Fe-CO) frequencies in the two proteins suggest only a modest change in the degree of back-bonding from filled Fe *d* orbital to the empty π^* orbital of the bound CO in the variant compared to the wt protein. A δ(Fe-C-O) near 568 cm^{-1} is observed with equivalent intensity and ^{13}C-shift (- 12 cm^{-1}) in both proteins. Finally, the Y171F mutation does not appear to affect interactions engaged by the heme propionate groups since the 350 to 450 cm^{-1} region of the RR spectra is equivalent in wt and Y171F DevS. The δ($C_\beta C_c C_d$) propionate deformation modes are sensitive to electrostatic interactions at the heme propionate groups (Uchida and Kitagawa, 2005), and are tentatively assigned to bands at 379 and 387 cm^{-1} (Table 4.2).

Comparison of the high-frequency $^{14}N^{16}O - {}^{15}N^{18}O$ difference spectra of wt and Y171F DevS lead to a similar analysis to that of the CO data (Fig. 4.8). As discussed previously, vibrational mixing between $\nu(^{15}N\text{-}^{18}O)$ and vinyl ν(C=C) and ν_2 modes (Tomita *et al.*, 1999) increases the number of differential signals contributing to these traces. Despite these perturbations, the strongest positive band in the $^{14}N^{16}O - {}^{15}N^{18}O$ difference spectra is readily assigned to the $\nu(^{14}N\text{-}^{16}O)$, and it is observed at 1638 and 1635 cm^{-1} in wt and Y171F DevS, respectively. Moreover, the values for the major ν(N-O) and ν(C-O) bands in wt and Y171F DevS closely follow the linear correlation observed for other hemoproteins sharing proximal histidine ligation (Coyle *et al.*, 2003) (Fig. 4.8). The minor conformer evidenced by a ν(N-O) at 1604 cm^{-1} in the wt protein, is not observed in the Y171F variant. Overall, both NO and CO complexes show a modest increase in back-bonding in Y171F DevS relative to the major conformer of the wt protein. As with the carbonyl complex, the low-frequency RR spectra of the nitrosyl adduct show very little difference between wt and Y171F (see ν(Fe-NO) and $\delta(C_\beta C_c C_d)$ frequencies in Table 4.2).

The oxy complexes of wt and Y171F DevS show greater divergence than do any other state of these proteins, which was anticipated based on the crystal structure of DosT, which shows Tyr169 (DosT numbering) directly interacting with the heme-bound oxygen group (Podust *et al.*, 2008). The Soret absorbance of the variant is red-shifted 6 nm relative to the wt protein (Fig. 4.3). Porphyrin skeletal modes ν_4 and ν_3 in the RR spectra show 1 and 3 cm^{-1} downshifts, respectively, in the variant protein relative to the wt protein (Table 4.2). The $\nu(Fe\text{-}O_2)$ mode is isolated from porphyrin modes in the low-frequency RR spectra using $^{16}O_2\text{-}^{18}O_2$ difference spectra (Fig. 4.9), and was previously observed in wt DevS at 563 cm^{-1} with a 22-cm^{-1} ^{18}O-downshift (Yukl *et al.*, 2007) (see section 3.5). In Y171F, the $\nu(Fe\text{-}O_2)$ mode is observed at 567 cm^{-1}, i.e., 4-cm^{-1} higher than in the wt oxy complex. H/D exchange affects the $\nu(Fe\text{-}O_2)$ mode of wt DevS with a ~ 4 cm^{-1} upshift of the $^{16}O_2 - {}^{18}O_2$ differential signal in D_2O (Fig. 4.9). No such effect is observed in Y171F, reflecting a perturbation of hydrogen bonding to the proximal oxygen atom of bound O_2 in this mutant (Ohta *et al.*, 2004). The origin of the H/D effect is described in section 3.5. As seen with the carbonyl and nitrosyl complexes, mutation of

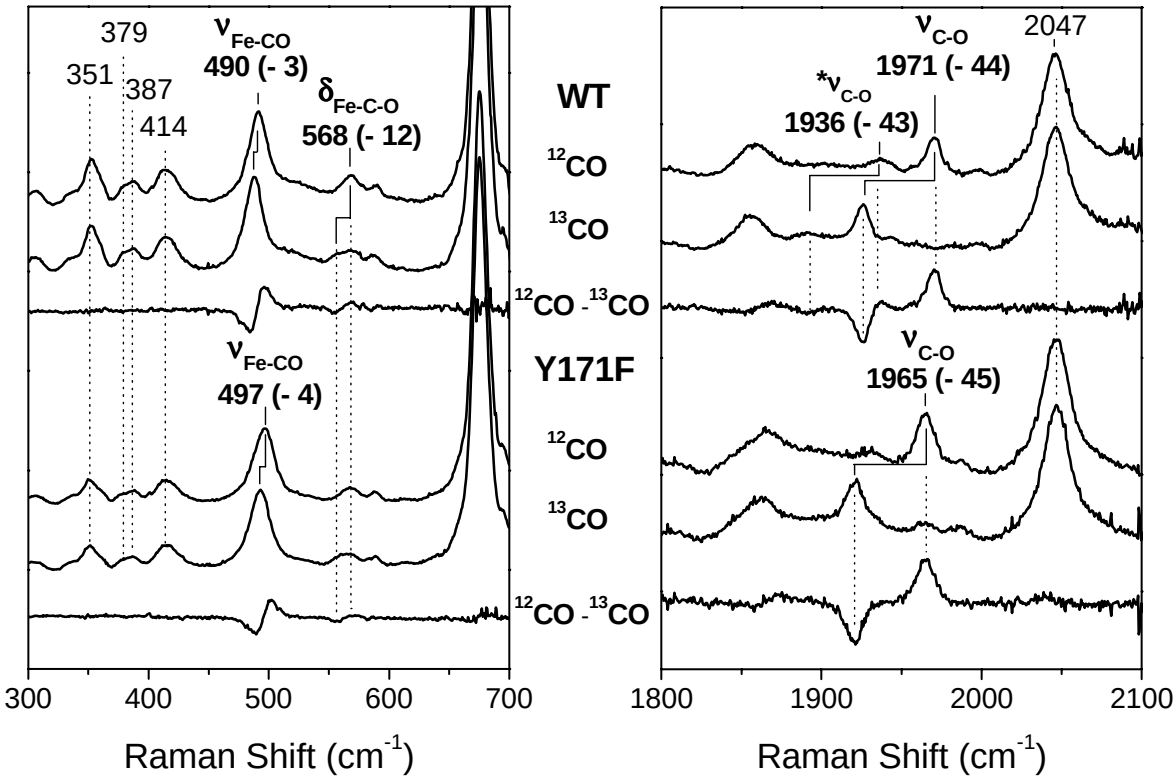

Fig. 4.7 Low-frequency (left) and high-frequency (right) RR spectra of wt and Y171F ^{12}CO and ^{13}CO complexes at room temperature. ^{12}CO – ^{13}CO difference spectra are also shown (λ_{exc} = 413 nm, <0.5 mW).

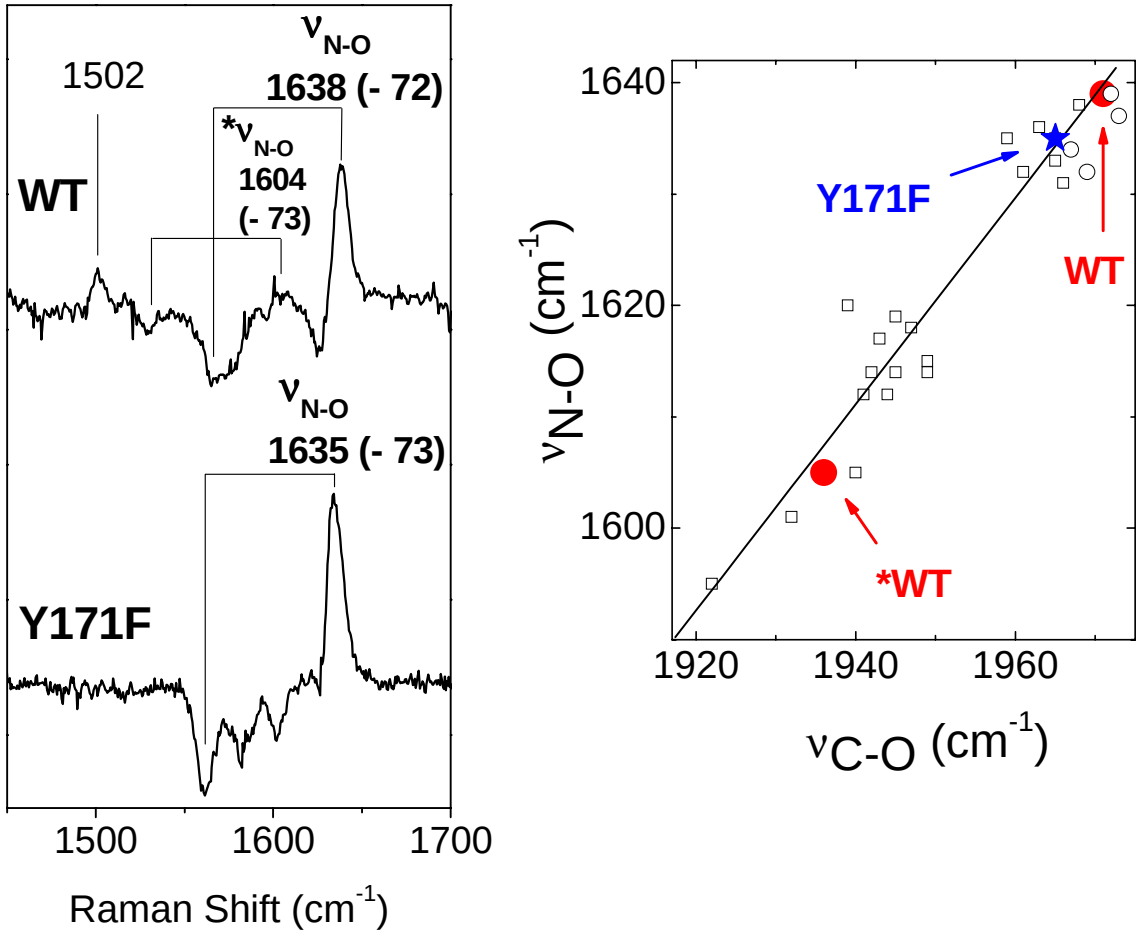

Fig. 4.8 High-frequency RR difference spectra of $^{14}N^{16}O$ – $^{15}N^{18}O$ for wt and Y171F DevS (λ_{exc} = 413 nm; 0.5 mW). The asterisk indicates contributions from a minor NO conformer. ν(N-O) versus ν(C-O) plot (right) of heme nitrosyl and carbonyl complexes with proximal His ligation for wt DevS (filled circles), Y171F DevS (filled star), wt and distal variants of Mb (open squares), and other heme sensor proteins (open circles) (See (Tomita *et al.*, 2002; Yukl *et al.*, 2007) and references therein). The asterisk indicates contributions from a minor CO/NO conformer.

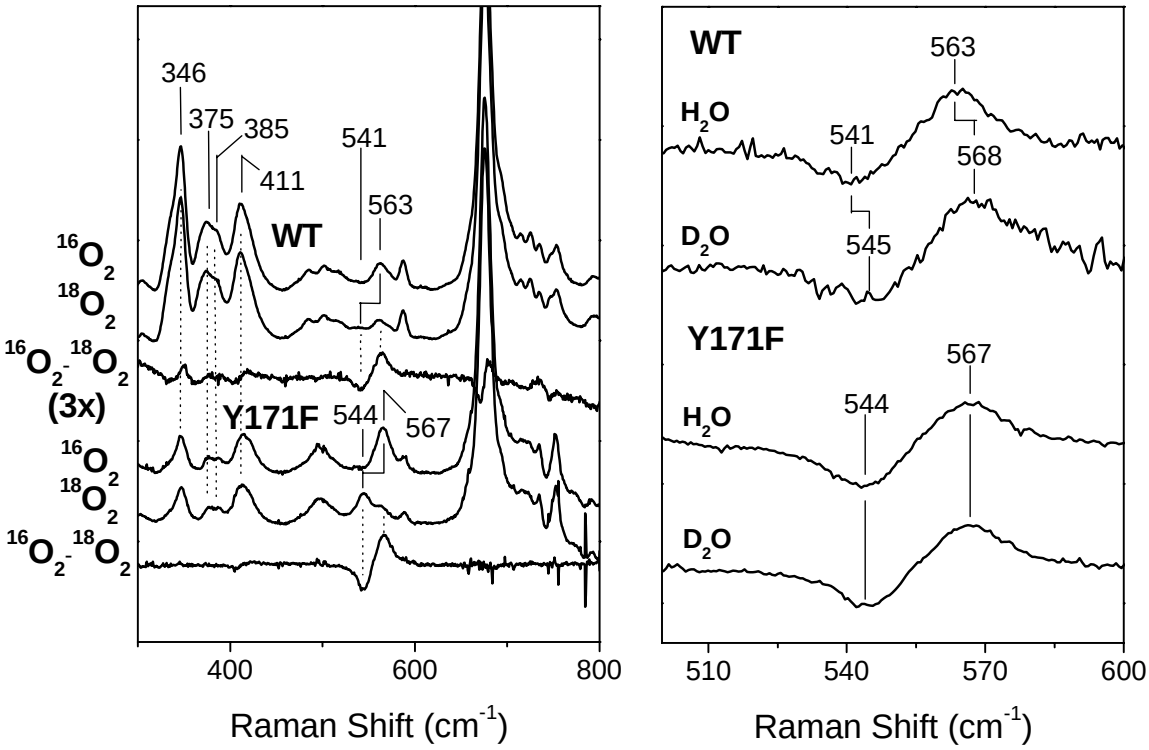

Fig. 4.9 Low-frequency RR spectra of wt and Y171F DevS $^{16}O_2$ and $^{18}O_2$ complexes at room temperature (left) The $^{16}O_2 - {}^{18}O_2$ difference spectra in H_2O and D_2O are also shown (right) (λ_{exc} = 413 nm; 0.5 mW).

Table 4.2 RR frequencies (cm^{-1}) for wt and Y171F DevS in various heme states (minor spectral components are in parentheses)

DevS protein	heme state	ν_4, ν_3, ν_2, ν_{10}	$\nu_{C=C}$	δ_{CCC}	ν_{Fe-L}	$\nu_{(X-O)}$
Fe(III) wt	6cHS	1370, 1479, 1557, 1609	1620, 1629	370, 385		
	(6cLS)	(1372, 1506, 1579, 1639)				
Y171F			1628, 1620sh.	375, 388		
	(6cHS)	(n.d., 1478, 1557, n.d.)				
	6cLS	1372, 1504, 1578, 1635				
Fe(II) wt	5cHS	1355, 1470, 1556, 1604	1620, 1625	348, 364	214 ν_{Fe-His}	
Y171F	5cHS	1354, 1470, 1556, 1604	1622broad	348, 364	213ν_{Fe-His}	
Fe(II)-CO wt	6cLS	1372, 1495, 1580, n.d.	1625	379, 387	490	1970 (1936)
Y171F	6cLS	1372, 1496, 1582, n.d.	1626	379, 387	497	1965
Fe(II)-O_2 wt	6cLS	1374, 1503, 1578, 1636	1629	375, 385	563	n.o.
Y171F	6cLS	1373, 1500, 1578, 1633	1627	378, 387	567	n.o.
Fe(II)-NO wt	6cLS	1374, 1498, 1576, n.d.	1626	378, 385	561	1638 (1604)
Y171F	6cLS	1375, 1499, 1579, n.d.	1627	378, 385	564	1635

Tyr171 had no significant impact on the frequency of the $\delta(C_\beta C_c C_d)$ propionate deformation modes in the oxy complexes (Fig. 4.9, Table 4.2).

4.5 Discussion

The crystal structure of GAF-A DosT identifies Tyr169 as the sole polar side chain in the distal pocket and as the hydrogen bond partner to the metal-bound O_2 in the oxy form of the protein (Podust *et al.*, 2008). A sequence alignment comparison of DosT and DevS predicts that, in DevS, the Tyr171 hydroxyl group is a hydrogen bond donor to the oxy group in the O_2-adduct, as well as in the minor population of hydrogen bonded CO and NO conformers identified in the RR spectra of the wt protein. The RR spectra of Y171F DevS reported here support this hypothesis since these hydrogen-bonded CO and NO conformers are not observed. In addition, the Y171F mutation significantly lowers the pH at which the Fe(III) heme is converted from high-spin to low-spin. In view of the crystal structure of GAF-A DosT (Podust *et al.*, 2008) (Fig. 4.1), it is tempting to propose that in Fe(III) DevS, the Tyr 171 OH group interacts with the Fe(III) heme distal ligation

site via the intermediate of a solvent molecule, and that the ionization of Tyr 171 at pH ~ 10 converts the Fe(III) heme to a 6-coordinate low-spin species. The absence of the hydroxyl group in the Y171F variant would allow for stabilization of a solvent molecule as a sixth ligand with a pK_a value similar to those observed in globin Fe(III)-aqua complexes such as Mbs (pK_a ~ 9.0) and heme oxygenases (pK_a ~ 8.0) (Asher *et al.*, 1977; George and Hanania, 1957; Sun *et al.*, 1993; Takahashi *et al.*, 1994; Wilks and Moenne-Loccoz, 2000). We could not confirm this hypothesis with the observation of a ν(Fe-OH) in the RR spectra of the Fe(III) Y171F variant at alkaline pH, presumably because of conformational disorder. However, coordination of the heme Fe(III) in Y171F by a solvent molecule is consistent with the overall data, including those obtained on the reduced protein. Indeed, stretching modes from the CO and NO adducts in Y171F DevS are only marginally changed from their dominant counterparts in the wt protein and rule out a purely hydrophobic distal environment in the Y171F variant. Electrostatic effects from a solvent molecule on the CO and NO groups would account for the slightly lower ν(C-O) and ν(N-O) frequencies observed in Y171F relative to the wt major conformers. In the oxy complex, the variant protein shows a ν(Fe-O) at 567 cm^{-1}, which suggests a polar environment. However, this feature is not sensitive to H/D exchange. This is consistent with a hydrogen bond interaction with a solvent molecule rather than the stronger Tyr 171 hydrogen bond donor present in the wt protein (Ohta *et al.*, 2004). As mentioned in the previous chapter, a water molecule can reorient itself slightly so that the D-bond strength to the oxygen is maintained.

Autophosphorylation assays of wt and Y171F variant DevS in different heme states demonstrate the crucial role of Tyr171 in ligand discrimination. Mutation of Tyr171 to a non-polar residue leads to the inability of DevS to distinguish between the exogenous ligands CO or NO and O_2, and leaves all Fe(II)XO (where X = O, N, or C) complexes inactive. In contrast, the Y171F mutation has no significant impact on the activity of the deoxy-Fe(II) protein. Because the Fe(II) hemes of wt and variant DevS are 5-coordinate species with a vacant Fe(II) distal ligation site, a conserved level of autophosphorylation activity in the distal variant Fe(II) protein is not unexpected. Our data also indicate that the autokinase activity in Fe(II) wt DevS is lower than that of the CO and NO complexes. From these observations, we propose that interactions between

Tyr171 and distal diatomic ligands turn the kinase activity ON or OFF, and that the absence of an exogenous distal ligand interacting with Tyr171 leads to a lower level of kinase activity, possibly corresponding to a rapid toggling between ON and OFF forms. Mutation of Tyr 171 to Phe disrupts the ON/OFF switch leading to an inactive kinase in all states with distal coordination, while the variant retains the lower level kinase activity associated with the empty distal pocket. Many molecular models can be envisioned within this context but we can delineate several important features:

1) The OFF state is dependent on a hydrogen bond interaction observed between the coordinating O-atom of the oxy group and the hydroxyl group of Tyr171. This specific hydrogen bond may lock the phenol side chain in an inhibitory conformation which cannot be achieved with NO or CO. In the Fe(III) protein, which is also inhibited (Kumar *et al.*, 2007), the Fe(III) sixth coordination site is occupied by a water molecule, and based on the crystal structure of GAF-A domain of DosT (Podust *et al.*, 2008), it is hydrogen bonded by Tyr 171 (Fig. 4.1). Thus, Tyr171 adopts equivalent conformation in the Fe(III) and the oxy forms of wt DevS.

2) The ON state in the CO and NO complexes requires a hydrogen bond network that involves Tyr171 and that is distinct from that in the oxy form. Although minor populations of NO and CO conformers interact with Tyr171 via a hydrogen bond, the majority of the CO and NO complexes do not, and as such, this larger population may release constraints on Tyr171 to allow its hydroxyl group to engage other hydrogen-bond partners in forming the ON state. Alternatively, the hydrogen-bonded NO and CO conformers may be the species responsible for the ON state, but the hydrogen bond acceptor is the non-coordinating oxygen atom of the XO group rather than the coordinating atom as in the oxy complex. In either case, the Y171F mutation prevents the formation of the hydrogen bond network necessary for stabilization of the ON state.

3) The intermediate-level kinase activity observed with the deoxy form of wt DevS is unaffected by the Tyr171 to Phe mutation. The lack of a distal ligand is expected to reduce steric constraints in the distal pocket and, whether the Tyr171 hydroxyl group is present or not, both ON and OFF states may be populated to produce an intermediate level autokinase activity.

Very recently, a crystal structure of the GAF-A domain of DevS has been solved (Cho *et al.*, 2009), and it identifies other residues potentially involved in the activating H-bond network mentioned above. We are currently analyzing mutants of these residues in the hope of more precisely delineating the activation pathway of full-length DevS. Also, we have observed that DevS possesses NO dioxygenase activity. We are in the process of determining the kinetics of this reaction as well as attempting to identify intermediates. A more detailed description of this work is found in chapter 7.

CHAPTER 5
SPECTROSCOPIC CHARACTERIZATION OF THE IRON SULFUR CLUSTER OF NsrR

5.1 Anaerobic Metabolism in *Bacillus subtilis*

In the absence of oxygen, *Bacillus subtilis* can grow by nitrate respiration (Nakano and Zuber, 1998). The ResDE two-component regulatory system is required for the induction of genes involved in nitrate respiration under anaerobic conditions (Geng *et al.*, 2004) (Fig. 5.1). These genes include *fnr*, (anaerobic transcription factor which, in turn, activates transcription of *narGHIJK*, the nitrate reductase operon) (Cruz-Ramos *et al.*, 1995), *nasDEF* (nitrite reductase operon) (Nakano *et al.*, 1998), and *hmp* (flavohemoglobin gene) (LaCelle *et al.*, 1996). However, anaerobic conditions alone are not sufficient for the full induction of the ResDE-controlled genes *hmp* and *nasDEF*. The presence of NO is required to attain the full induction of these genes (Nakano, 2002).

The necessity for such a regulatory mechanism emerges from the fact that *B. subtilis* endogenously produces NO during anaerobic nitrate respiration (Nakano *et al.*, 2006). The flavohemoglobin Hmp has emerged as the major route of NO detoxification among diverse bacteria, converting NO to nitrate (NO_3^-) using molecular oxygen (Gardner, 2005). Interestingly, it has been shown to protect certain bacteria from NO donors and GSNO (Crawford and Goldberg, 1998; Liu *et al.*, 2000) during anaerobic growth as well, despite the necessity of oxygen for the NOD reaction. This suggests the

---

*Material in this chapter has been published in this or similar form in *Biochemistry*, and is used here with permission of the American Chemical Society.

Yukl, E. T., Elbaz, M. A., Nakano, M. M., Moënne-Loccoz , P. (2008) Transcription Factor NsrR from *Bacillus subtilis* Senses Nitric Oxide with a 4Fe-4S Cluster. *Biochemistry* **47**, 13084-13092.

possibility that Hmp may have NO reductase activity under anaerobic conditions although this activity has been shown to be very weak in both cells (Gardner *et al.*, 2002) and *in vitro* (Gomes *et al.*, 2002) relative to an authentic NO reductase. Regardless of its protective mechanism, Hmp was found to be essential for long term survival during anaerobic nitrate respiration of *B. subtilis* (Nakano, 2006). However, Hmp is also capable of reducing molecular oxygen under aerobic conditions, generating superoxide radical which leads to oxidative stress (Membrillo-Hernandez *et al.*, 1996). Thus, tight control of *hmp* expression is essential. The effect of NO is abrogated in an *nsrR* mutant strain, indicating a role for NsrR in NO-mediated control of the ResDE regulon (Nakano *et al.*, 2006) shown schematically in figure 5.1.

NsrR belongs to the Rrf2 family of transcription regulators and is widely found in various bacteria (Rodionov *et al.*, 2005). Sequence analyses predict that NsrR contains a helix-turn-helix which likely binds to the promoter region of its target genes (Rodionov *et al.*, 2005). *In vivo* studies of *nsrR* mutants and the effect of NO on NsrR-controlled genes have shown that NsrR is an NO-responsive transcription repressor in *Escherichia coli* (Bodenmiller and Spiro, 2006), *B. subtilis* (Nakano *et al.*, 2006), *Salmonella enterica* serovar Typhimurium (Bang *et al.*, 2006), *Neisseria gonorrhoeae* (Overton *et al.*, 2006), and *Neisseria meningitides* (Rock *et al.*, 2007). In addition, NsrR was shown to repress ResDE-dependent *in vitro* transcription of *hmp* and *nasD* (Nakano *et al.*, 2006). The critical role of NsrR in modulating Hmp levels in both aerobic and anaerobic conditions and its impact on oxidative and nitrosative stress was recently exemplified in *Salmonella enterica* serovar Typhimurium (Gilberthorpe *et al.*, 2007). However, any sort of structural information on NsrR remains sparse.

5.2 NO Sensing by NsrR

Although NsrR plays a definite role in NO sensing, the specific feature which allows this protein to sense NO remains in question. NsrR bears significant homology (30% identity, 48% similarity) to IscR, a 2Fe-2S cluster-containing transcriptional regulator of Fe-S cluster synthesis genes in *E. coli* (Schwartz *et al.*, 2001). Notably, among the residues conserved between these proteins are three cysteine residues which

mutagenesis studies suggest coordinate the iron sulfur cluster in IscR (Yeo *et al.*, 2006), although the number of residues separating the first Cys from the CX_5C motif varies in IscR and NsrR orthologs. A transient brownish color in aerobically purified NsrR suggested that NsrR also contains an Fe-S cluster sensitive to O_2-mediated decomposition (Nakano *et al.*, 2006).

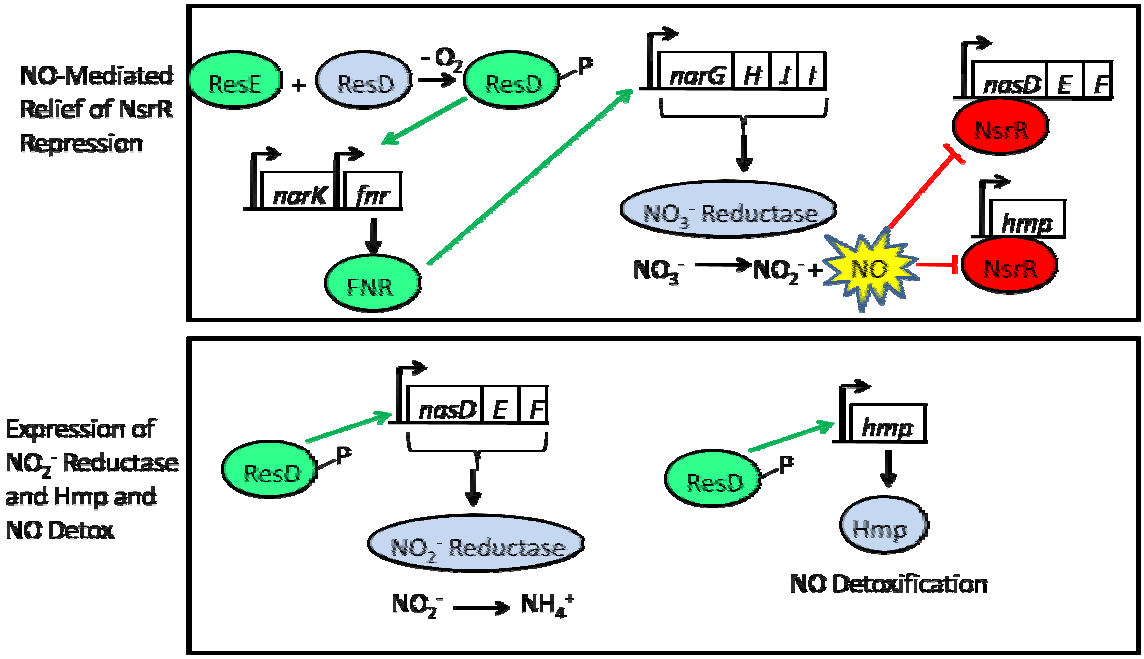

Fig. 5.1 Anaerobic regulation of genes involving nitrate respiration in *B. subtilis*. Ovals represent proteins while boxes represent genes. Green indicates an activating role, blue a neutral or catalytic role, and red indicates an inhibitory role. Anaerobic conditions activate kinase ResE to phosphorylate transcription factor ResD which activates transcription of FNR which activates the transcription of the nitrate reductase operon (Nakano and Zuber, 1998). NO is produced as a byproduct of nitrate reduction and derepresses transcription of *hmp* and *NasDEF* by NsrR (Nakano *et al.*, 2006). Hmp can then detoxify NO

Other transcriptional regulators bearing Fe-S clusters whose activities are modulated by NO have been reported. NO binds to the $[2Fe\text{-}2S]^+$ cluster of SoxR to form a dinitrosyl iron complex (DNIC) that activates transcription of *soxS* (Ding and Demple, 2000). Similarly, FNR contains a $[4Fe\text{-}4S]^{2+}$ that reacts with NO. However, in this case, NO-binding inhibits the transcriptional regulation activity of FNR (Cruz-Ramos

et al., 2002). Finally, NO has been shown to disassemble the 4Fe-4S cluster of aconitase to convert this enzyme into an iron regulatory protein, IRP-1, that controls mRNA translation and stability by interacting with iron responsive elements (Beinert *et al.*, 1996; Cairo *et al.*, 2002; Rouault, 2006). Thus, there are precedents for the utilization of Fe-S clusters as NO sensors to regulate the activity of Fe-S proteins involved in diverse cellular physiology.

Here we use UV-vis, RR, and EPR spectroscopies to demonstrate that anaerobically purified NsrR harbors a $[4Fe\text{-}4S]^{2+}$ cluster. Size exclusion chromatography and chemical crosslinking experiments were used to determine that NsrR is dimeric in both holo and apo forms. Exposure of this cluster to O_2 leads to its destruction via a $[3Fe\text{-}4S]^{+}$ intermediate. The $[4Fe\text{-}4S]^{2+}$ cluster of NsrR also reacts with NO to form at least two distinct forms of dinitrosyl-iron complexes. Other exogenous ligands such as dithiothreitol (DTT) and cyanide (CN^-) are also shown to bind to the Fe-S cluster. We conclude that the 4Fe-4S cluster of NsrR contains at least one labile ligand, either a hydroxide/aqua ligand or a non-Cys endogenous residue, e.g., an aspartate residue as in the 4Fe-4S cluster of *P. furiosis* ferredoxin (Conover *et al.*, 1990; Conover *et al.*, 1991; Hu *et al.*, 1999).

5.3 Materials and Methods

Expression and Purification

Expression and aerobic purification of NsrR were carried out in the Nakano laboratory. *E. coli* BL21 (DE3)/pLysS carrying pMMN648 or pMMN740 was grown at 37 °C in 1 to 2 L of M9-glucose medium (Miller, 1972) supplemented with 40 μM Fe(III) ammonium citrate, 50 μg/mL of ampicillin, and 5 μg/mL of chloramphenicol. At an OD_{600} of 0.4, isopropyl-β-D-thiogalactopyranoside (IPTG) was added to a final concentration of 0.5 mM. After incubating at 37 °C for 3 h, cells were collected by centrifugation at 5,000*g*, resuspended in culture medium, and transferred into a 1-L sealed bottle. The cell suspension was sparged with argon and kept overnight at 4 °C. Cells were broken by passing through a French press placed in a plastic anaerobic glovebag (Glas-Col, LLC) continuously flushed with argon. The cleared lysate was

recovered by centrifugation in a sealed tube at 15,000*g* for 20 min. Subsequent purification steps were performed in an anaerobic chamber containing less than 1 ppm O_2 (Omni-Laboratory System; Vacuum Atmospheres Co.). All buffers and solutions were purged with argon and kept in the anaerobic chamber before use.

Cleared lysate was mixed with 15 mL of Ni^{2+}-nitrilotriacetic acid (Ni-NTA) resin (QIAGEN or Sigma) in buffer A (50 mM Tris-HCl, pH 8.5, 100 mM NaCl, 30 mM imidazole). After 1 h of incubation, the column was washed with 10 volumes of buffer A followed by 2 volumes of buffer A containing 1.0 M KCl, 2 volumes of buffer A containing 60 mM imidazole, and 2 volumes of buffer A containing 100 mM imidazole. His_6-NsrR was eluted with buffer A containing 300 mM imidazole. Fractions containing His_6-NsrR were pooled and exchanged into an imidazole-free buffer containing 50 mM Tris-HCl and 100 mM KCl at pH 8.5 using HiTrap Desalting columns (GE Healthcare). The C-terminal His-tag protein was eluted from the Ni-NTA column in an identical fashion, but 5 mM dithiothreitol (DTT) was added to the exchange buffer to prevent protein precipitation likely due to the poor Fe−S incorporation observed in this construct.

Complementation of nsrR with His_6-NsrR

To examine whether CH-NsrR complements the *nsrR* null mutation in *B. subtilis*, two plasmids pMMN749 and pMMN750 were generated. pMMN749 was constructed by cloning the erythromycin-resistance gene isolated from pDG646 (Guérout-Fleury *et al.*, 1995) into pMMN740 digested with *Hin*cII and *Xba*I, and pMMN750 was constructed by cloning the tetracycline-resistance gene from pDG1515 (Guérout-Fleury *et al.*, 1995) into pMMN740 digested with *Hin*cII. pMMN749 and pMMN750 were used to transform a *B. subtilis* strain JH642 (*nsrR*$^+$) to generate ORB7270 and ORB7285, respectively. The transformants were obtained by a single crossover recombination at the *nsrR* locus, resulting in transcription of *ch-nsrR* from the native *nsrR* promoter. ORB7270 and ORB7285 were transduced with SPβ phage carrying a transcriptional *nasD-lacZ* fusion (Nakano *et al.*, 1998) to generate ORB7284 and ORB7287, respectively.

Complementation experiments were carried out in the Nakano laboratory by determining the expression of *nasD-lacZ* in ORB7284 and ORB7287 together with LAB2854 (wild type carrying *nasD-lacZ*) (Nakano *et al.*, 1998) and ORB6188 (*nsrR*

mutant carrying *nasD-lacZ*) (Nakano *et al.*, 2006). Cells were grown under anaerobic conditions in 2× YT (Nakano *et al.*, 1988) supplemented with 1% glucose and 0.2% KNO_3 or 2× YT supplemented with 0.5% glucose and 0.5% pyruvate with appropriate antibiotics. Cells were collected at 1-h intervals and β-galactosidase activity was measured as previously described (Nakano *et al.*, 1988) and was shown in Miller units (Miller, 1972).

Iron and protein determinations.

The iron content of NsrR was determined spectrophotometrically with the ferrene assay (Douglas *et al.*, 1984). Specifically, 30 μL samples of NsrR at two different concentrations were incubated at room temperature with 3 μL 38% HCl for 10 min. The sample was centrifuged at 15,000 x g for 15 min to remove denatured protein before addition of 50 μL 3 M sodium acetate and 5 μL of 1 M ascorbic acid pH 5.5. Finally, 5 μL of 3.0 mM 3-(2-pyridyl)-5,6-bis(5sulfo-2furyl)-1,2,4-triazine disodium salt hydrate (ferrene, Aldrich) was added. Absorbance was measured at 593 nm (ε_{593} = 35.5 mM^{-1} cm^{-1}) and compared to two blanks lacking either NsrR or ferrene. As expected the same procedure applied to apo-NsrR did not reveal any significant iron. Protein concentrations were determined by Bradford assay (Bradford, 1976) using bovine serum albumin (Sigma-Aldrich) as a standard. Total amino acid analyses of the holo- and apo-proteins (AAA Service Laboratory Inc, Damascus, Oregon) suggest that the Bradford assay overestimates NsrR concentration by ~ 25%. Because NsrR contains no tryptophan, calculated 280 nm molar extinction coefficient on the basis of the amino acid primary sequence is unreliable. Instead, concentrations of NsrR monomers are calculated using 280 nm molar extinction coefficients deduced from the total amino acid analyses of holo-NsrR (ε_{280} = 38 mM^{-1} cm^{-1}) and apo-NsrR (ε_{280} = 24.3 mM^{-1} cm^{-1}).

Size exclusion chromatography.

Size exclusion chromatography was performed using a BioSil® SEC 250 pre-packed size exclusion column (Bio-Rad) with a Varian HPLC system. Protein samples (60 to 100 μM) were loaded and eluted at 1.0 mL/min with argon-purged buffer containing 100 mM potassium phosphate pH 7.5, 150 mM KCl, and 2.5 mM DTT.

Elution profiles were monitored by absorbance at 280 nm. The column was calibrated using a gel filtration standard containing thyroglobulin, γ-globulin, ovalbumin, Mb, and vitamin B_{12} (Bio-Rad).

Chemical crosslinking.

Holo-NsrR was exchanged into the appropriate buffer using HiTrap™ Desalting columns (GE Healthcare). Apo-NsrR was acquired by extensive aerobic dialysis (~ 24 h) of holo protein against 50 mM Tris-HCl, 100 mM KCl, 5 mM DTT, and 10 mM EDTA pH 8.5 at room temperature, followed by dialysis into 50 mM potassium phosphate buffer pH 7.5, 100 mM KCl, and 5 mM DTT. Holo and apo-NsrR at 33 and 77 μM were anaerobically incubated with 1.0 mM dimethyl suberimidate dihydrochloride (Fluka) and 100 mM KCl in 50 mM potassium phosphate buffer pH 7.5. After 1 h incubation at room temperature, the reaction was quenched with the addition of a 4-fold volume of pure acetic acid (Sigma-Aldrich) and each sample was diluted to ~10 μM for analysis by SDS-PAGE (12% gel).

Spectroscopic characterization of NsrR.

All sample preparation steps were performed in the anaerobic chamber. When necessary, samples for spectroscopic analysis were concentrated using filtering devices (Microcon 10 kD cutoff, Biomax, Millipore). Reduced protein was generated by the addition of excess sodium dithionite in the presence or absence of DTT. Oxidized NsrR was generated either by the addition of excess potassium ferricyanide followed by its removal using desalting spin columns (Zeba™ 0.5 mL; Pierce) or by the addition of DTT to 4.0 mM followed by exposure to O_2 gas. Addition of NO to the headspace of an NsrR sample was performed with a gastight Hamilton syringe to reach a partial pressure of 0.5 atm. After ~5 min incubation, the samples were exposed to the inert atmosphere of the glove box to release the excess NO, and transferred to EPR tubes (Wilmad Lab Glass) sealed with rubber septa. Alternatively, NsrR samples were incubated with varying concentration of diethylamine NONOate (Sigma-Aldrich) for 1 h at room temperature or diluted 2.5 fold with NO-saturated buffer in a sealed tube and incubated 5 min. Cyanide complexes were generated by 15-min incubation of reduced NsrR with 20 mM NaCN.

All UV-vis and RR spectra were obtained as described in section 2.1. EPR spectra were obtained on a Bruker E500 X-band EPR spectrometer equipped with a superX microwave bridge and a dual mode cavity with a helium flow cryostat (ESR900, Oxford Instruments, Inc.) for measurements at 5 – 10 K and a super HiQ cavity resonator (ESR4122, Bruker) for measurements at 100 K. The experimental conditions, i.e., temperature, microwave power, and modulation amplitude, were varied to optimize the detection of all potential EPR active species and ensure nonsaturating conditions. Quantitation of the EPR signals was performed with Cu^{II}(EDTA) standards.

5.4 Spectroscopic Characterization of the Fe-S Cluster of NsrR

Several constructs of NsrR were used in order to avoid the possibility that a particular affinity tag could influence the nature of the Fe-S cluster. Specifically, we investigated NsrR with a 6-His tag appended to both the N- and C-termini as well as a Strep-Tag version. All but the N-terminal His tag construct, which was not produced in *B. subtilis*, were able to complement a Δ*nsrR* strain, indicating that they are functional *in vivo.* However, we did observe significant differences in the degree of Fe-S cluster loading between these constructs expressed in *E. coli*, with the N-terminal His-tagged protein exhibiting the greatest degree of cluster incorporation with ~ 2.8 iron atoms per protein. Nonetheless, spectroscopic results were qualitatively identical between the three constructs. Thus, further discussions of spectroscopic data and iron:protein ratios are based on data obtained with NsrR bearing an N-terminal 6-His tag.

Anaerobically purified NsrR is greenish-brown in color and displays a broad visible absorption feature around 412 nm (Fig. 5.2) characteristic of proteins containing $[4Fe\text{-}4S]^{2+}$ clusters (Orme-Johnson and Orme-Johnson, 1982). This assessment is confirmed by RR and EPR data discussed below. Assuming that all iron in NsrR is present as 4Fe-4S clusters the iron quantitation leads to a ε_{412} = 13.5 $mM^{-1}cm^{-1}$ per 4Fe-4S cluster which is in good agreement with values observed for other 4Fe-4S proteins (Duin *et al.*, 1997) such as FNR (ε_{420} = 13.3 $mM^{-1}cm^{-1}$) (Jordan *et al.*, 1997). However, this implies a 1:2 ratio of 4Fe-4S cluster per NsrR subunit. Two models can be envisioned given this data: a) NsrR is incompletely loaded with Fe-S clusters as has been

observed for other overexpressed Fe-S proteins, or b) The Fe-S cluster is bridging with Cys residues from different subunits recruited for the coordination of the 4Fe-4S cluster. Anaerobic gel filtration of holo-NsrR in the presence of 2.5 mM DTT suggests that, at ~65 μM, holo-NsrR exists exclusively as a dimer with an apparent molecular weight of 41 kDa (Fig. 5.3). This value is in good agreement with the theoretical molecular weight of 39 kDa for the dimer. Apo-NsrR under the same conditions also elutes as a dimer while a small shoulder at 24 kDa is likely to represent a minor monomeric population. The predominance of the dimeric form in both holo- and apo-NsrR is also confirmed by chemical crosslinking experiments (Fig. 5.4). Specifically, incubation of holo-NsrR and apo-NsrR at two different concentrations with the chemical cross-linker dimethyl suberimidate were analyzed by denaturing SDS-PAGE and showed the presence of the dimeric form, as indicated by a protein band approximately twice the size of the individual monomers (Fig. 5.4). As expected for this protein concentration range (Davies and Stark, 1970), no evidence of higher oligomer is observed. Thus, if the cluster is in a bridging conformation, it is not required for dimerization of NsrR.

The Labile [4Fe-4S] Cluster Ligand

The room temperature RR spectrum of anaerobically isolated NsrR obtained with a 488-nm excitation exhibits a strong ν(Fe-S) bridging mode at 338 cm^{-1} consistent with a $[4Fe\text{-}4S]^{2+}$ cluster, and lacks an equally intense band near 290 cm^{-1} which would support a $[2Fe\text{-}2S]^{2+}$ cluster (Fig. 5.5) (Duin *et al.*, 1997). The RR spectrum is similar to those obtained for oxidized *Clostridium pasteurianum* ferredoxin (*Cp* Fdx) and reduced *Chromatium vinosum* high potential iron-sulfur protein at the same excitation wavelength at 77 K (Spiro *et al.*, 1988). It has been suggested that the high-frequency of the totally symmetric ν(Fe-S) bridging mode is characteristic of $[4Fe\text{-}4S]^{2+}$ clusters with a non-Cys terminal ligand, as in *Pyrococcus furiosus* ferredoxin where the bridging ν(Fe-S) = 442 cm^{-1} in frozen solution (Conover *et al.*, 1990). Although the frequency at room temperature for this mode in NsrR is not unusually high, it is interesting to note a -3 cm^{-1} shift in the presence of DTT (Fig. 5.5). A change in the UV-vis spectrum is also observed upon DTT addition (Fig. 5.2). These observations suggest that DTT might bind to one of the Fe ions within the Fe-S cluster.

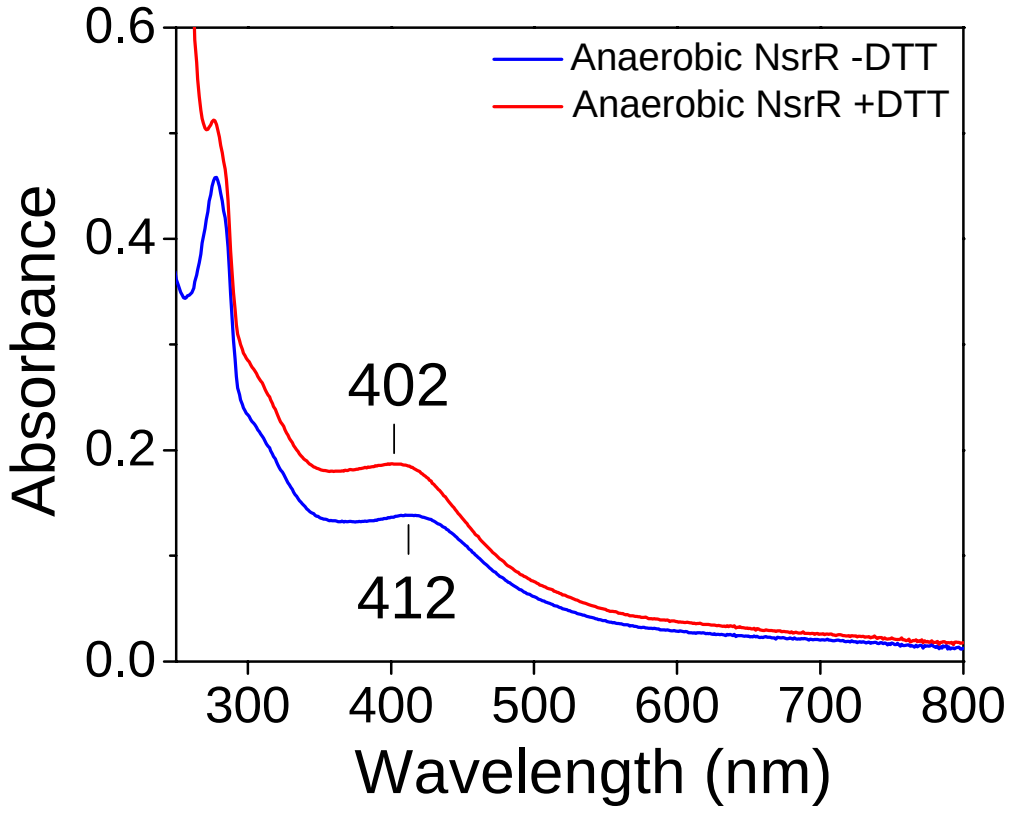

Fig. 5.2 Absorption spectra of anaerobically purified NsrR (30 μM) at pH 8.5 in the absence (blue) and presence (red) of 5 mM DTT

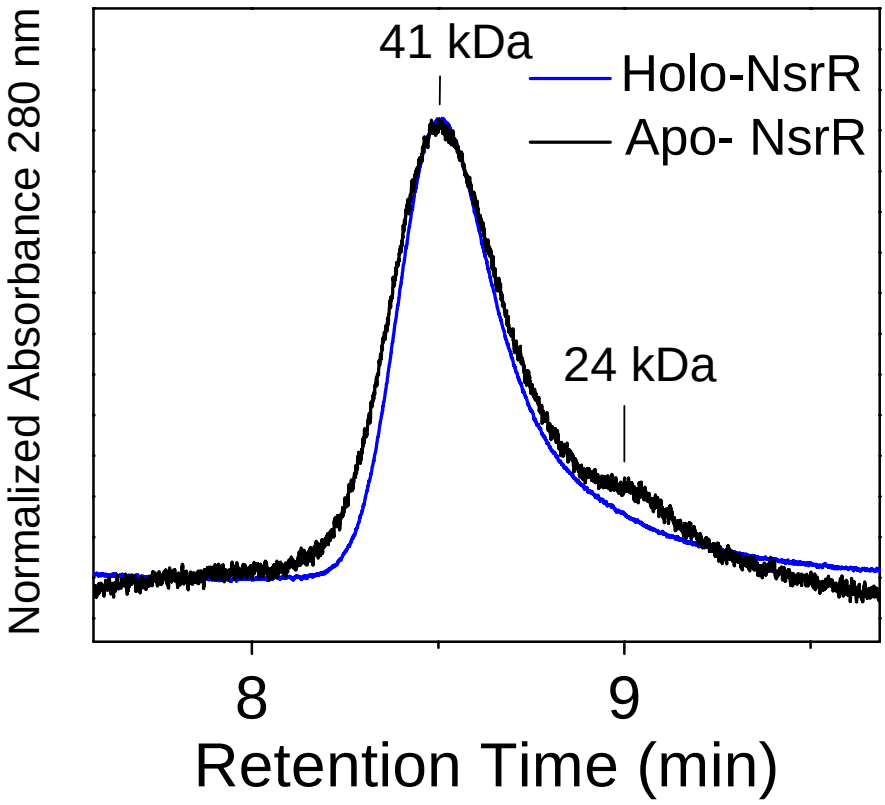

Fig. 5.3 Anaerobic size exclusion chromatography elution profile of anaerobically purified holo-NsrR (65 μM, blue) and apo-NsrR (92 μM, black) at pH 7.5 monitored at 280 nm.

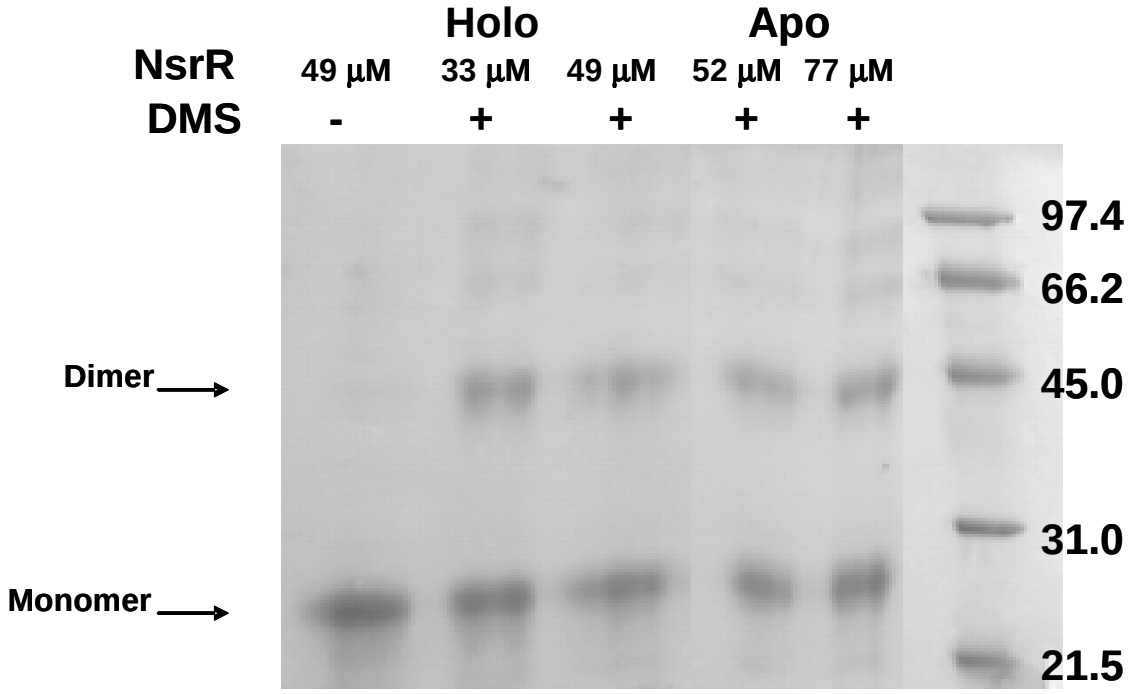

Fig. 5.4 Chemical crosslinking of holo and apo-NsrR. The noted protein concentrations were anaerobically incubated in the presence of 1.0 mM dimethyl suberimidate for 1 h before quenching the reaction with acetic acid and subject samples to 12% SDS-PAGE analysis.

The as-isolated sample is EPR-silent, as expected for an antiferromagnetically coupled $[4Fe\text{-}4S]^{2+}$ cluster (data not shown). Treatment with excess dithionite at pH 8.5 yields a fast-relaxing EPR signal at g = 2.04 and 1.93 observable only below 40 K, as is typical for reduced $[4Fe\text{-}4S]^{+}$ clusters (Fig. 5.6). Attempts at reduction at pH 7.5 were unsuccessful as deduced from a lack of EPR activity in these samples. This is likely due to the increased midpoint potential of dithionite at low pH, particularly where the stock solution may be contaminated with sulfite (Mayhew, 1978) and may be indicative of a fairly low reduction potential of the $[4Fe\text{-}4S]^{2+}$ cluster in NsrR.

Quantitation of the reduced NsrR signal against Cu^{II}-EDTA yields 0.18 - 0.22 spin per 4Fe-4S cluster (as deduced from the UV-vis spectrum of starting material). At microwave powers saturating the S = 1/2 signal, another resonance at g = 5.2 is observed (Fig. 5.6) which likely represents a population of S = 3/2 clusters (Lindahl *et al.*, 1985) and explains, at least in part, the weak intensity of the S = 1/2 signal. Incubation of reduced NsrR with CN^- results in a disappearance of the g = 5.2 signal and produces a new S = 1/2 signal (Fig. 5.6) which now accounts for 0.64 spin per cluster. These observations are consistent with coordination of exogenous CN^- to convert the $[4Fe\text{-}4S]^{+}$ to a pure S = 1/2 species as observed for *Pyrococcus furiosus* ferredoxin (Conover *et al.*, 1991). The remaining spin count missing in the EPR spectra may be due to chelation by the high concentration of CN^- (20 mM), incomplete reduction of the 4Fe-4S cluster, and/or an overestimation of the cluster concentration caused by adventitious iron in the preparation. In any case, the CN^- binding clearly demonstrates the presence of a labile Fe coordination site in NsrR.

The weak binding of an Fe ligand in NsrR is further illustrated by its reactivity toward O_2. Exposure of anaerobically isolated NsrR to O_2 leads to a bleaching of the $[4Fe\text{-}4S]^{2+}$ absorption features (Fig. 5.7). Difference spectra of the oxygen-exposed samples minus anaerobic NsrR indicate a relative increase in absorbance around 500 nm and relative decrease at 410 nm, even as the overall absorbance decreases. These changes suggest the formation of a population of $[2Fe\text{-}2S]^{2+}$ clusters as previously observed upon exposure of FNR to O_2 (Jordan *et al.*, 1997). However, in our case the net decrease in absorbance around 500 nm over time suggests that neither the initial 4Fe-4S cluster nor the 2Fe-2S cluster is aerobically stable in these conditions.

Interestingly, the presence of 4-5 mM DTT stabilizes the Fe-S cluster and allows the acquisition of transient UV-vis absorption after exposure to O_2 (Fig. 5.7). Although absorption features from DTT/Fe(III) complexes may form if Fe(III) is released by NsrR and would contribute to these spectra, the initial absorption increases observed between 450 and 600 nm are similar to those obtained in the absence of DTT. An EPR analysis of the resulting species yields a narrow spectrum with g = 2.01 and 1.96 observable up to 70 K (Fig. 5.6). This spectrum bears strong resemblance to a $[3Fe\text{-}4S]^{+}$ cluster as in oxidized *Desulfovibrio fructosovorans* [NiFe] hydrogenase, where the Ni atom is quantitatively lost from the $NiFe_3\text{-}S_4$ cluster upon oxidation (Rousset *et al.*, 1998). The same species is formed by anaerobic exposure of NsrR to excess ferricyanide (data not shown), but both methods yield only 0.04-0.05 spin per cluster. Again, these data are very similar to those obtained with FNR where only 5 - 8% of air or ferricyanide-oxidized samples could be accounted for by the [3Fe-4S] EPR signal (Khoroshilova *et al.*, 1997). The remainder may be accounted for by varying populations of EPR-silent $[4Fe\text{-}4S]^{2+}$and $[2Fe\text{-}2S]^{2+}$ clusters and free iron for samples with longer incubation times. Our UV-vis data show no significant loss of absorbance at 410 nm after 30 min incubation with O_2 in the presence of 5 mM DTT and suggest that the majority of iron is present as $[4Fe\text{-}4S]^{2+}$ and $[2Fe\text{-}2S]^{2+}$ clusters.

There are reports of homologues of NsrR from *N. gonorrhoeae* (Isabella *et al.*, 2009) and *Streptomyces coelicolor* (Tucker *et al.*, 2008) containing 2Fe-2S clusters. These assessments were made on the basis of mass spectroscopic and UV-vis data, respectively, on proteins purified aerobically in the presence of DTT. Thus, we investigated whether NsrR from *B. subtilis* could likewise stabilize a 2Fe-2S cluster. Indeed, we found that we could stabilize proteins with UV-vis spectra consistent with a $[2Fe\text{-}2S]^{2+}$ cluster either by aerobic purification in the presence of DTT or by low temperature, aerobic dialysis of the anaerobically purified protein in buffer containing DTT (Fig. 5.8). Attempts to characterize this form of the protein by RR spectroscopy were met with limited success due to apparent instability of this form at high concentration. This is consistent with the reports of 2Fe-2S cluster NsrR where only low concentrations of NsrR were used (Isabella *et al.*, 2009; Tucker *et al.*, 2008). Interestingly, we found that, regardless of whether the cells were grown in the presence

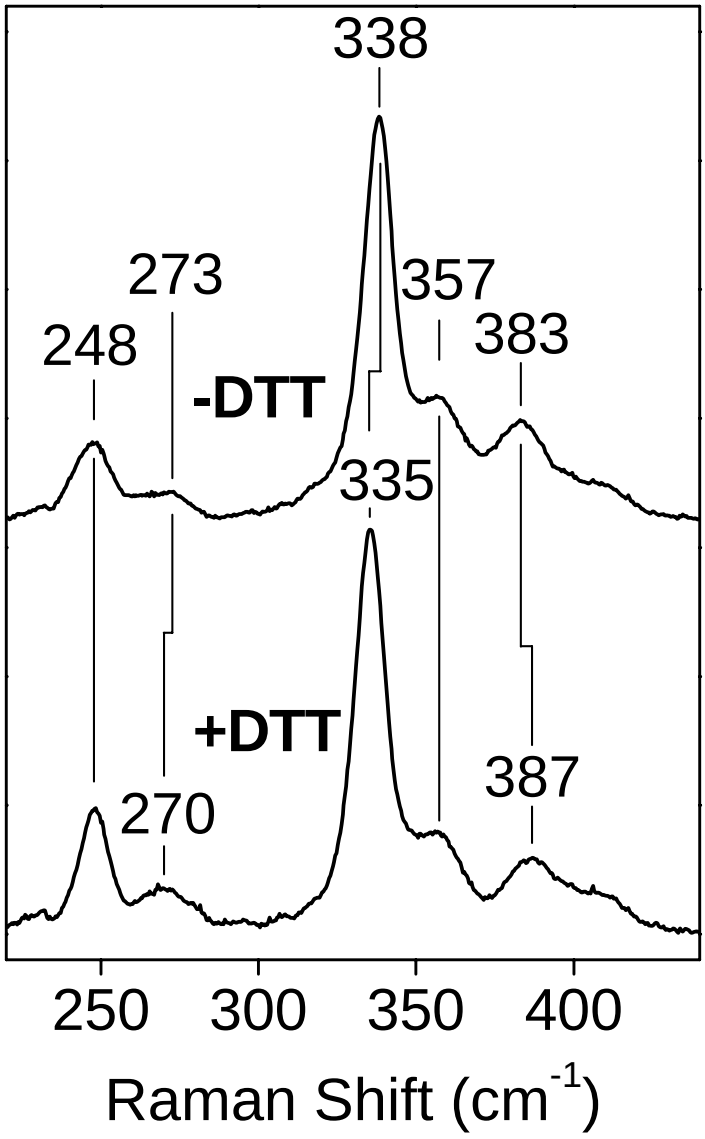

Fig. 5.5 Room temperature RR spectra of anaerobically purified NsrR (750 μM) and anaerobically purified NsrR (750 μM) + 5.0 mM DTT (λ_{exc} = 488 nm, 100 mW).

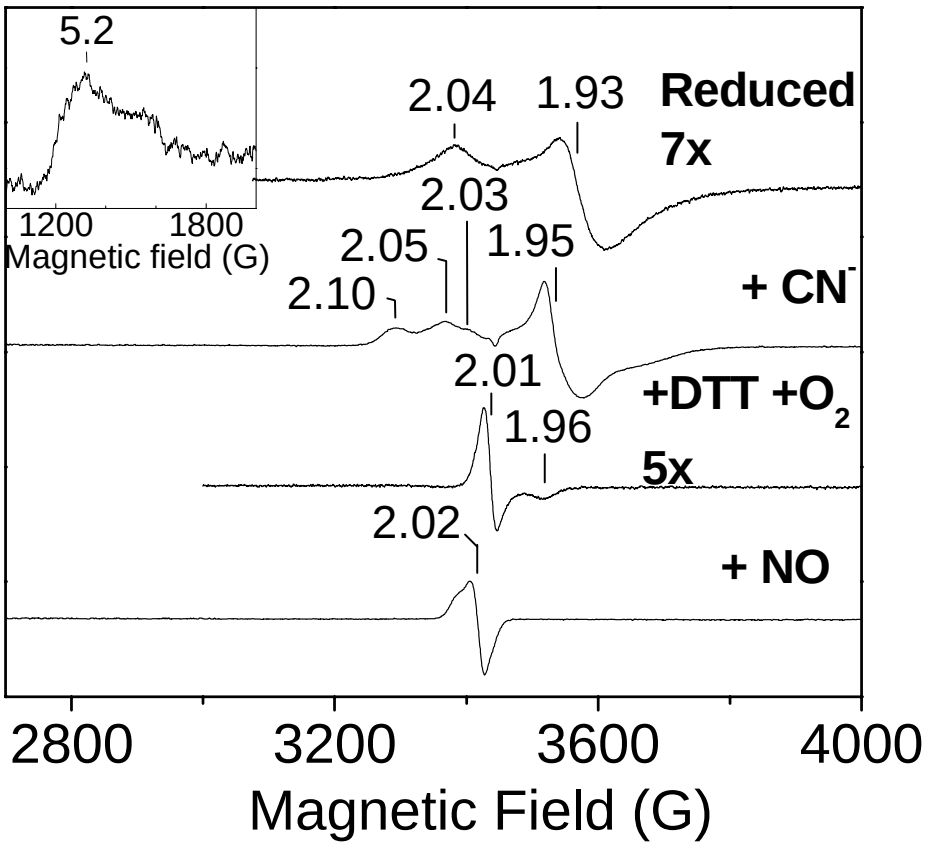

Fig. 5.6 EPR spectra of anaerobically isolated NsrR chemically reduced with dithionite, reduced NsrR incubated with 20 mM NaCN, anaerobically isolated NsrR exposed to O_2 in the presence of 4 mM DTT, and NsrR in the presence of 1.5 molar equivalents of NO from NONOate. EPR spectrum of reduced NsrR highlighting S = 3/2 population (inset). All spectra have been normalized according to microwave power and sample concentration.

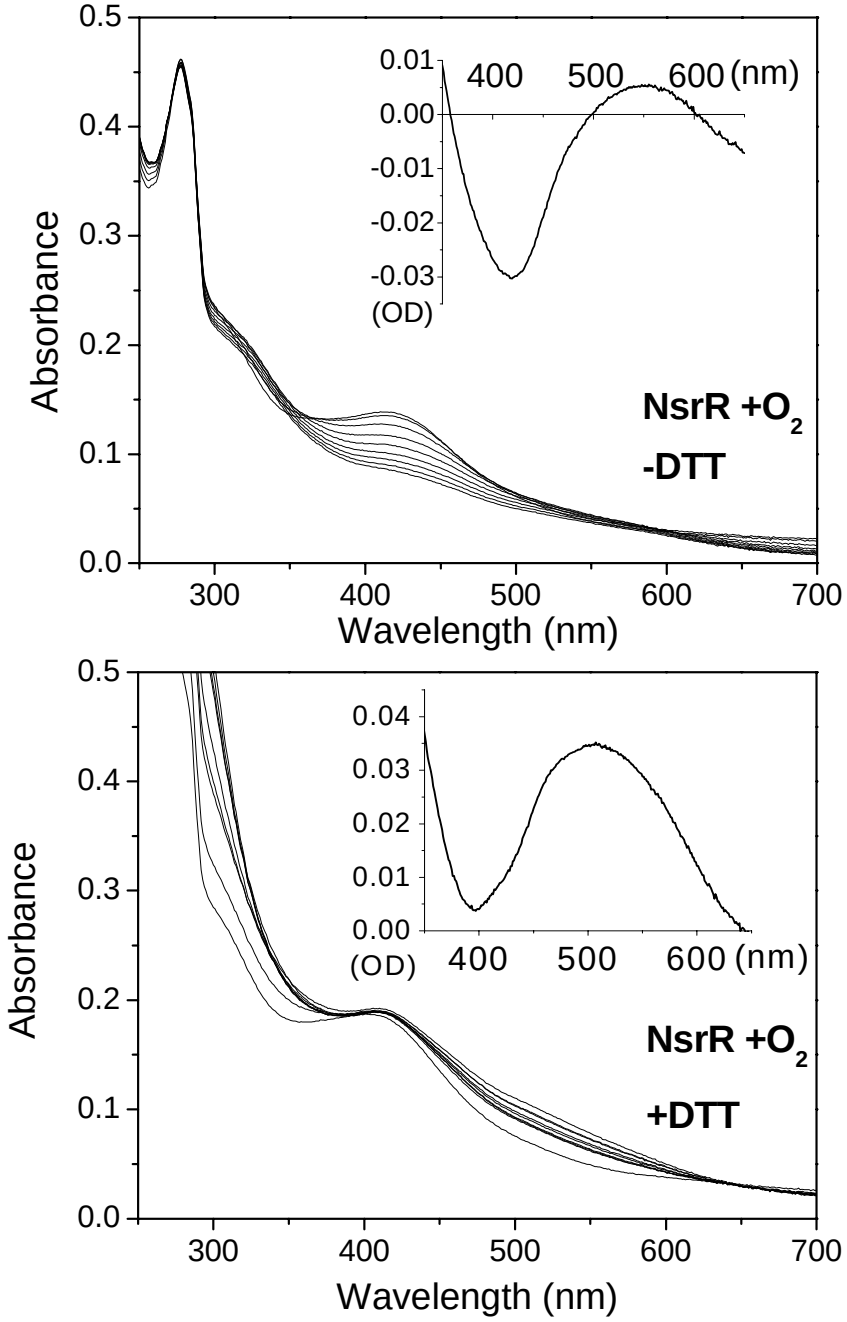

Fig. 5.7 Absorption spectra of NsrR (30 μM) exposed to O_2 in the absence (top) or presence (bottom) of 5 mM DTT, scans taken every 4 min. Difference spectrum of O_2- exposed NsrR at 14 min. minus anaerobic NsrR (top inset). Difference spectrum of O_2-exposed NsrR at 6 min minus anaerobic NsrR (bottom inset).

of oxygen, anaerobically purified NsrR was always observed to contain a $[4Fe\text{-}4S]^{2+}$ cluster, suggesting that mechanisms exist within the cell to prevent conversion to the 2Fe-2S form even in the presence of oxygen.

Anaerobic exposure of NsrR to excess NO gas or dilution in NO-saturated buffer result in the formation of a new chromophoric species with a broad and intense near-UV absorption band at 363 nm (Fig. 5.9). This optical spectrum is consistent with those of dinitrosyl-iron complexes (DNIC) with extinction coefficients in the order of ~ 4 $mM^{-1}cm^{-1}$ (Costanzo *et al.*, 2001), and it suggests that the conversion of the 4Fe4S cluster into $[Fe(NO)_2]$ species is efficient. The EPR spectrum displays a g_{av} = 2.03 (2.041, 2.034, 2.015) axial signal characteristic of $[L_2Fe(NO)_2]^-$ d^7 dinitrosyl-Fe(I) complex (Fig. 5.9) (Foster and Cowan, 1999; Lee *et al.*, 1994; McDonald *et al.*, 1965; Vanin *et al.*, 1998). Exposure of NsrR to lower concentrations of NO reveal mixtures of DNIC species with g_{av} = 2.02 (Figs. 5.6 and 5.9) which are gradually replaced with the more typical 2.033 DNIC signal at high NO concentration. Quantitation of these EPR spectra range from 0.06 to 0.22 spin per 4Fe-4S cluster for the lowest and saturating NO concentrations, respectively. Thus, only a fraction of the DNIC clusters detected by UV−vis absorption is EPR-active, presumably because of antiferromagnetic coupling between $Fe(NO)_2$ species in DNIC dimers. Similar observations have been reported on DNIC complexes in FNR, another NO sensing transcription factor (Cruz-Ramos *et al.*, 2002; Wu *et al.*, 2000). The UV-vis spectra of NO-treated NsrR samples were unaffected by extensive degassing (data not shown) and suggest that, at least *in vitro*, the DNIC formed in NsrR are irreversible complexes.

5.5 Discussion

Fe-S proteins function as versatile regulators by directly sensing O_2, NO, and iron (reviewed in (Kiley and Beinert, 2003)). Previous studies in various bacteria have shown that NsrR is an NO-sensitive repressor but how NsrR responds to NO remained to be elucidated. The data presented here demonstrates for the first time that anaerobically isolated NsrR is a dimeric protein containing a $[4Fe\text{-}4S]^{2+}$ cluster. RR characterization of this species yields a spectrum quite similar to those seen for other $[4Fe\text{-}4S]^{2+}$ clusters in

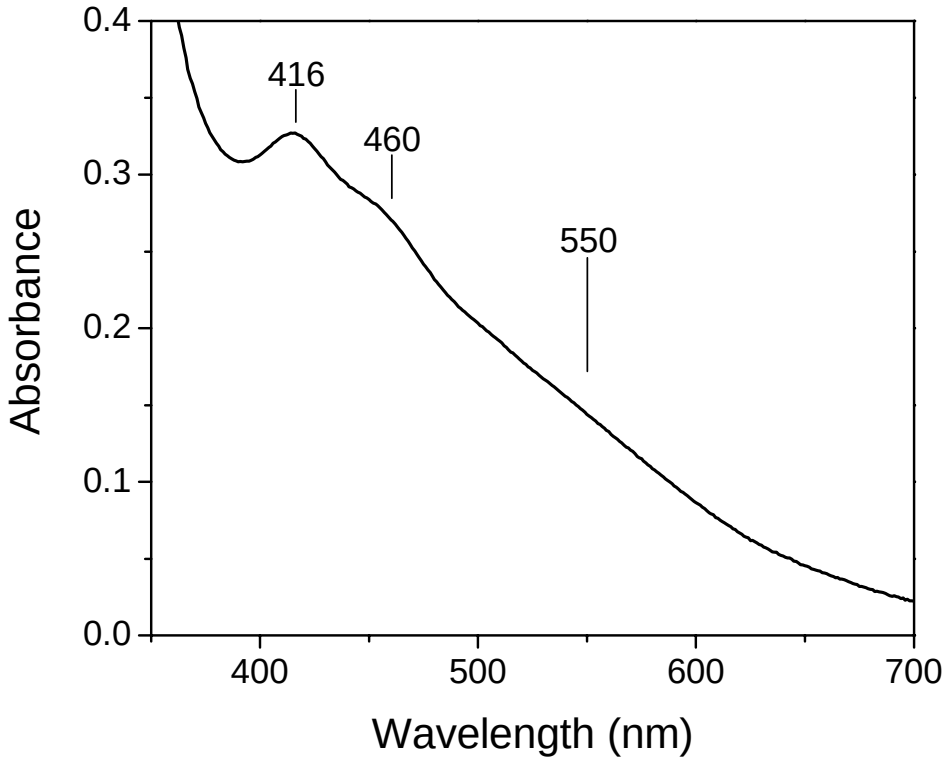

Fig. 5.8 Absorption spectra of Strep-Tag NsrR purified under aerobic conditions in the presence of 5 mM DTT

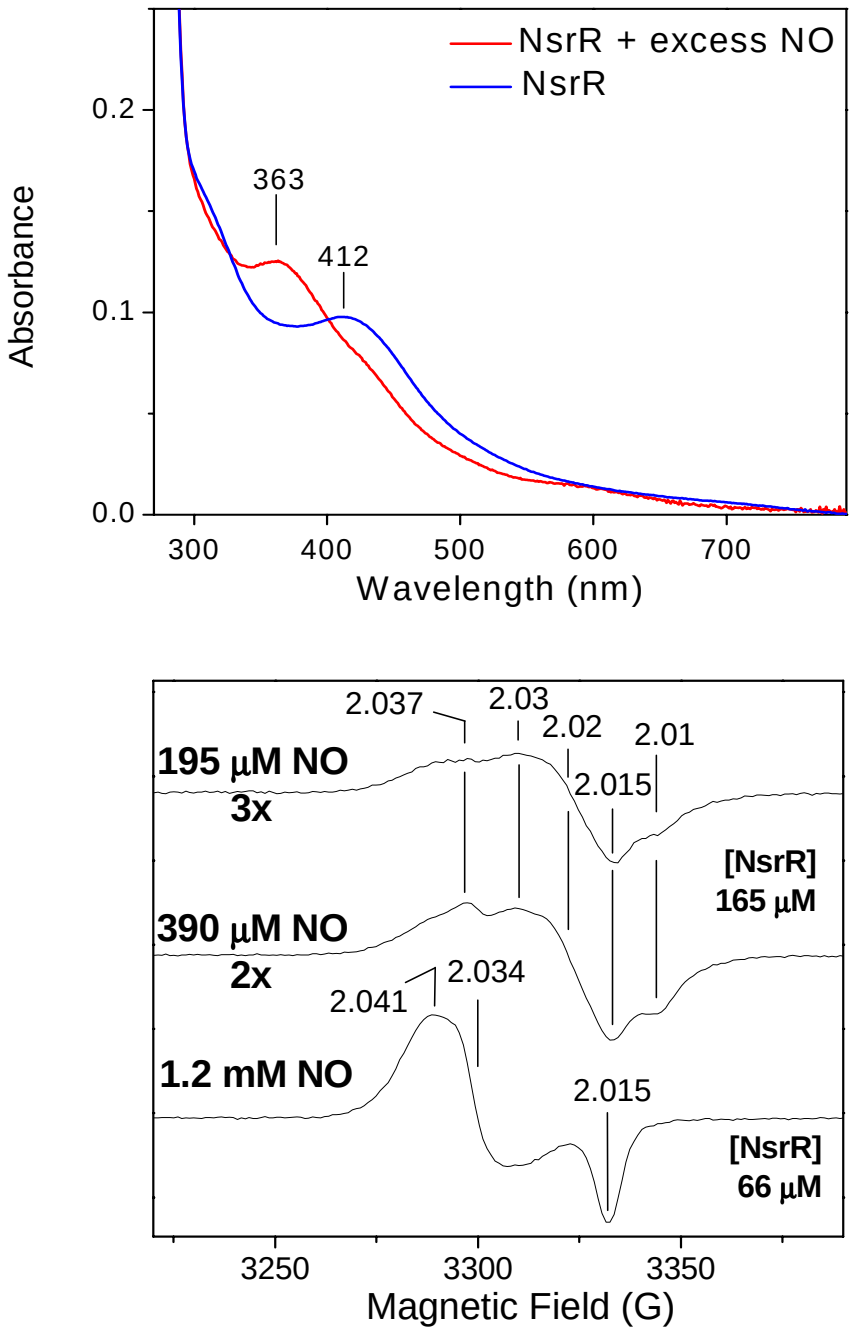

Fig. 5.9 Absorption spectra of anaerobically isolated NsrR before (blue) and after (red) addition of NO gas (top). EPR spectra of anaerobically isolated NsrR treated with either saturated NO solution or the indicated concentrations of NO (bottom)

proteins such as certain bacterial ferredoxins and reduced high potential iron proteins (Spiro *et al.*, 1988). Reduction of NsrR with excess dithionite yields an EPR active species with relaxation properties consistent with those of a $[4Fe\text{-}4S]^{+}$ cluster. The $[4Fe\text{-}4S]^{2+}$ cluster of NsrR shows remarkable reactivity with exogenous ligands such as DTT and CN^{-}, O_2 and NO. Cyanide binding to native Fe-S clusters has been observed only in *P. furiosus* ferredoxin (Conover *et al.*, 1990) where one of the Fe atoms of the 4Fe-4S cluster is ligated by an Asp residue (Sham *et al.*, 2002). Reports of ligation by exogenous thiols are also scarce but recruitment of β-mercaptoethanol as a sulfur ligand was observed in Cys/Ala and Cys/Gly mutants of the F_A and F_B clusters in photosystem I (Jung *et al.*, 1996). In the absence of DTT, the labile Fe coordination site in NsrR is likely to be occupied by a non-Cys endogenous residue or an exogenous aqua or hydroxide ligand.

Exposure of NsrR to O_2 results in a gradual degradation of the 4Fe-4S cluster and formation of 3Fe-4S and 2Fe-2S clusters before complete loss of the Fe-S clusters. The addition of DTT stabilizes the $[4Fe\text{-}4S]^{2+}$ cluster although O_2-mediated decay and conversion to $[2Fe\text{-}2S]^{2+}$ continue to occur. The presence of DTT in the aerobic purification procedures is likely responsible for the observation of a 2Fe-2S cluster in NsrR homologues (Isabella *et al.*, 2009; Tucker *et al.*, 2008). The reaction of NsrR with NO is also complex and results in the formation of multiple DNIC species. At saturating NO concentration, a typical EPR signal with $g_{av} = 2.03$ reveals the formation of one $(Cys)_2Fe(NO)_2$ per 4Fe-4S cluster. Examination of NO complexes formed at lower NO concentrations reveal more isotropic EPR signals with $g_{av} = 2.02$ that are also suggestive of DNIC species. These multiple EPR signatures for DNIC species in NsrR are in contrast with reports for FNR (Cruz-Ramos *et al.*, 2002), WhiB3 of *Mycobacterium tuberculosis* (Singh *et al.*, 2007) and SoxR of *E. coli* (Ding and Demple, 2000) where only a single EPR-active DNIC is observed regardless of NO concentration. While the DNIC species formation in NsrR appears irreversible *in vitro*, iron-sulfur repair systems may regenerate the 4Fe-4S cluster of holo-NsrR in *B. subtilis*.

The structural picture emerging from this spectroscopic study is that of a 4Fe-4S cluster anchored to a NsrR homodimer via three Cys ligands. Because there are three conserved Cys residues in NsrR, it is tempting to suggest that our construct is limited to

"half-site" cluster loading. However, models where Cys residues from different subunits are recruited for the coordination of the 4Fe-4S cluster cannot be ruled out. Characterizations of Cys variants of NsrR are underway in our laboratories.

This *in vitro* characterization of NsrR also provides insight into its function *in vivo*. It has been previously shown that NsrR plays a key role in NO signaling in *B. subtilis*, and that aerobically purified NsrR is still capable of repressing *hmp* and *nasD* expression *in vitro* (Nakano *et al.*, 2006). It was also shown that the *nsrR* mutation results in derepression of the ResDE-independent expression of *hmp* under aerobic conditions. Thus, apo-NsrR might retain its role as a transcription repressor under aerobic conditions. Possibly, all that is required for DNA binding and gene regulation is for NsrR to adopt a dimeric form, and our size-exclusion chromatography data demonstrate that the presence of Fe-S clusters is not required to stabilize the dimer. In this regard it is interesting that holo-IscR acts as a transcription repressor (Overton *et al.*, 2008), whereas apo-IscR serves as a transcription activator (Fontecave and Ollagnier-de-Choudens, 2008), and DNA sequences recognized by the two forms of IscR are largely dissimilar. Alternatively, it is possible that within the cell the 4Fe-4S cluster is stabilized against O_2-mediated decay and that the holo enzyme is responsible for aerobic repression *in vivo*. The *in vitro* stabilization of the 4Fe-4S cluster by DTT suggests that cysteine or other thiol donors may be able to play the same role within the cell; this labile ligand may even provide opportunities for other levels of regulation. Sensing of NO by NsrR occurs via conversion of the Fe-S cluster into a DNIC species. The presence of a labile Fe coordination site in NsrR may provide a simple mechanism to increase the cluster sensitivity to low NO concentration.

The Fe-S cluster of NsrR shows chemical characteristics similar to those of FNR. Both proteins contain a $[4Fe\text{-}4S]^{2+}$ cluster, which upon exposure to O_2 converts to $[2Fe\text{-}2S]^{2+}$. However, the $[2Fe\text{-}2S]^{2+}$ cluster appears much less stable in NsrR than in FNR. *E. coli* FNR requires the $[4Fe\text{-}4S]^{2+}$ cluster to form a dimer, the form active as a transcription activator (Johnson *et al.*, 2005). In contrast, our gel filtration and crosslinking experiments showed that NsrR is dimeric in both holo and apo forms. A recent work on *B. subtilis* FNR showed that holo- and apo-FNR are dimeric although a $[4Fe\text{-}4S]^{2+}$ cluster is essential for DNA binding and transcription activation (Giel *et al.*,

2006). Unlike *E. coli* FNR where four cysteine residues are essential for its activity {Yeo, 2006 #202}, only three cysteines of *B. subtilis* FNR are indispensable for transcription activation. It was also shown that the three cysteine residues, together with non-cysteine ligand, serve as the ligands for the $[4Fe\text{-}4S]^{2+}$ cluster. Therefore, *B. subtilis* NsrR shares more chemical features with the iron-sulfur cluster of *B. subtilis* FNR than that of *E. coli* FNR.

Our study showed that *B. subtilis* NsrR, like *E. coli* FNR, interacts with NO and forms DNIC (Cruz-Ramos *et al.*, 2002). DNA-binding activity of FNR is either decreased (Cruz-Ramos *et al.*, 2002) or impaired (Wu *et al.*, 2000) by nitrosylation. It remains to be examined whether NsrR-DNIC exhibits reduced DNA-binding activity, resulting in loss of the repressor activity. Alternatively, nitrosylation of NsrR might change specificity of DNA binding or affect formation of transcription initiation complex. Moreover, since different DNIC species are observed depending on the concentration of NO, NsrR may exhibit different responses to different levels of NO concentration.

CHAPTER 6
CHARACTERIZATION OF AN INTERMEDIATE IN THE NO DIOXYGENASE REACTION OF MYOGLOBIN

6.1 Function of Myoglobin and Hemoglobin in NO Metabolism

As discussed in section 1.4, members of the globin family possess rapid NO dioxygenase (NOD) activity and thus have an important role in both detoxification of NO and regulation of NO signaling. Given the high concentrations of Hb and Mb in blood and muscle cells, respectively, a role for these proteins in modulating NO signaling, and consequently vasodilation, seems likely. The physiological relevance of the NOD reaction of Hb in intact erythrocytes to NO signaling is controversial as diffusion of NO across the erythrocyte membrane is too slow for it to have a significant impact on NO concentrations in the blood (Liao *et al.*, 1999; Liu *et al.*, 2002; Thomas *et al.*, 2001). However, there is no such barrier for free oxy-Hb which can react rapidly with NO. This property is likely responsible for the hypertensive effect of Hb-based blood substitutes (Olson *et al.*, 2004) and likely contributes to vasoconstriction upon hemolysis, an advantageous effect when hemolysis is caused by trauma but harmful when it is caused by a pathological condition such as sickle cell anemia (Reiter *et al.*, 2002).

---

*Material in this chapter has been published in this or similar form in *Journal of the American Chemical Society*, and is used here with permission of the American Chemical Society.

Yukl, E. T., de Vries, S., Moënne-Loccoz , P. (2009) The Millisecond Intermediate in the Reaction of Nitric Oxide with Oxymyoglobin Is an Fe(III)-Nitrato Complex, not a Peroxynitrite. *J. Am. Chem. Soc.* **131**, 7234-7235.

There is also evidence or an important role for Mb in NO signaling. Infusion of NO into wt mouse hearts led to the rapid accumulation of metMb, suggesting NO-mediated conversion of oxy- to metMb (Flogel *et al.*, 2001). Further, hearts of mutants lacking Mb were found to be more sensitive to the vasodilatory effects of NO (Flogel *et al.*, 2001). A role for Mb in protecting terminal oxidases from transient increases in NO concentration was suggested (Flogel *et al.*, 2001). In addition to the physiological relevance of its own NOD activity, Mb is a convenient and practical system for studying the reactions that occur in flavohemoglobins like Hmp. The importance of flavohemoglobins for bacterial survival of nitrosative stress by virtue of their NOD activity was discussed in the previous chapter.

6.2 Proposed Mechanism and Kinetics of the NO Dioxygenase Reaction

In the NOD reaction, NO is converted to nitrate (NO_3^-) with complete retention of the isotopic constitution of the O_2 and NO reactants. The mechanism is presumed to proceed via a high-spin Fe(III) peroxynitrite intermediate before homolytic cleavage of the O-O bond and recombination of the NO_2 radical with the ferryl-oxo to form the nitrate product (Fig. 6.1). The same reaction mechanism is likely to be the source of the NO dioxygenase activity reported in bacterial flavohemoglobins where a flavin domain reduces the met-heme product, allowing for catalysis (Gardner and Gardner, 2002; Gardner *et al.*, 1998; Gardner, 2005) (see section 1.4 for a description of these enzymes).

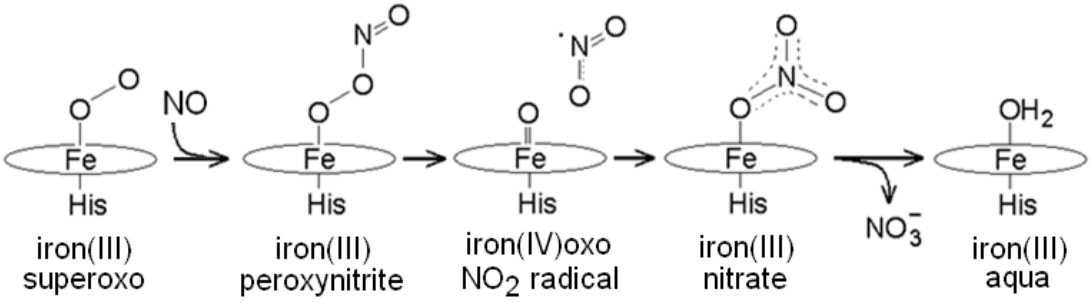

Fig. 6.1 Putative reaction mechanism of NO dioxygenation by oxy-heme (at alkaline pH, the Fe(III)aqua complex of Mb is resplaced by a Fe(III)hydroxo complex which adopts a low-spin configuration at cryogenic temperatures).

There are no observable intermediates in this reaction at neutral pH, but stopped-flow UV-vis experiments at alkaline pH show the rapid buildup and decay of a high-spin Fe(III) species (Herold, 1999; Herold *et al.*, 2001). Rapid-freeze quench (RFQ) samples of the reaction analyzed by EPR spectroscopy also support the formation of a Fe(III) high-spin transient species (Olson *et al.*, 2004). For Mb at pH 9.5 and 20° C, stopped-flow results indicate that the build-up in high-spin intermediate is maximal within the dead-time of the instrument (1 to 3 ms) and decays fully within 15 to 20 ms. On the basis of the UV-vis characteristics of the intermediate, the species was assigned to a Fe(III)-peroxynitrite complex (Herold, 1999; Herold *et al.*, 2001). Here, we report the characterization of this intermediate by RR spectroscopy of RFQ samples and identify the millisecond intermediate as an Fe(III)-nitrato complex.

6.3 Materials and Methods

NO and Mb-O_2 Solutions

Lyophilized horse heart Mb was purchased from Sigma. The protein was dissolved in 200 mM CHES pH 9.5 to a final concentration of 1 to 2 mM and purged with argon before being brought into a glovebox with a controlled atmosphere of less than 1 ppm O_2 (Omni-Lab System; Vacuum Atmospheres Co.). The protein was reduced by addition of a 5-fold excess of sodium dithionite followed by dialysis against 500 mL anaerobic buffer for 2 h or passage through a Sephadex G-25 column (GE Healthcare). Complete heme reduction and dithionite removal were confirmed by UV-vis spectroscopy with a Cary 50 spectrometer. Solutions were then transferred to sealed serum bottles and exposed to $^{16}O_2$ (Airgas) or $^{18}O_2$ (99% ^{18}O; ICON Stable Isotopes). Formation of Mb-O_2 was confirmed by UV-vis spectroscopy and the final Mb concentration was determined (typically 1.2 to 1.8 mM). Before drawing the solution in 2-mL RFQ syringes, the serum bottles were exposed to the glovebox to release excess O_2. Saturated $^{14}N^{16}O$ solutions were made either by bubbling $^{14}N^{16}O$ gas (Airgas) (scrubbed with 1 M KOH) into argon-purged buffer for a few minutes, or by serial additions of $^{14}N^{16}O$ (Airgas), $^{15}N^{16}O$ (98% ^{15}N, Aldrich), or $^{15}N^{18}O$ (98% ^{15}N, 95% ^{18}O, Aldrich) gas into a sealed vial of anaerobic buffer. Solutions in sealed serum bottles were drawn into

RFQ syringes using a needle attachment. To rule out any concerns with contaminant gases, experiments were also carried out using an NO donor and produced identical results and conclusions. Specifically, a concentrated solution of diethylamine NONOate (Cayman Chemical) (25 mM) was diluted to 1.4 mM in anaerobic phosphate buffer (20mM, pH 7.0), and incubating for 1 h at room temperature in the RFQ syringes. Concentration of NO solutions was determined by titration with deoxy-Mb. Contamination of NO solutions with nitrite was determined using an $\varepsilon_{354} = 22.5\ M^{-1}cm^{-1}$ (Strickler and Kasha, 1963)

RFQ Experiments

RFQ syringes were mounted in the System 1000 Chemical / Freeze Quench Apparatus (Update Instruments, Inc.) equipped with a water bath maintained at 3° C. Reaction times were controlled by varying either the ejection speed or the volume of the reactor hose. 5 ms are added to the calculated reaction time to account for time of flight and freezing in liquid ethane. Samples of 125 – 250 μL were ejected into a glass funnel attached to an NMR tube and containing liquid ethane at < -120° C. The frozen sample was packed into the tube as the assembly sat within a Teflon block cooled with liquid nitrogen to -100° C. Once packed the frozen samples were stored in liquid nitrogen before analysis by RR. Successful mixing and NO dioxygenation reaction was confirmed by UV-vis analysis of samples ejected into a microcentrifuge tube, and by RR analysis of samples shot into a room temperature NMR tube and frozen manually.

RR and UV-vis Spectroscopy

UV-vis and low temperature RR spectroscopy (~105 K) were performed as described in section 2.2.

6.4 Spectroscopic Characterization of a High-Spin Intermediate in the NO Dioxygenase Reaction

RR spectra obtained with Soret excitation are highly sensitive to the oxidation, spin, and coordination states of the heme iron (Spiro and Li, 1988). This technique is an

ideal analytical tool for studying the NO dioxygenation reaction since both starting Mb−O_2 and final metMb are six-coordinate low-spin species at low temperature and alkaline pH, while the putative intermediate is a six-coordinate high-spin species. Figure 6.2 shows the high-frequency RR spectra of RFQ samples taken at different time points during the reaction of Mb−O_2 with NO at pH 9.5 and 3 °C. The RFQ sample with the shortest reaction time is trapped within 6 ms. Its high-frequency RR spectrum exhibits strong ν_2 and ν_3 porphyrin skeletal modes at 1566 and 1482 cm^{-1}, characteristic of six-coordinate high-spin vibrations, while their low-spin counterparts (Feis *et al.*, 1994) at 1585 and 1505 cm^{-1} are weak. In contrast, the RR spectra of RFQ samples with longer reaction times show weak high-spin features, and the gradual conversion of high-spin to low-spin species is essentially complete by 55 ms (Fig. 6.2).

RFQ samples of the reaction of Mb−$^{16}O_2$ and Mb−$^{18}O_2$ with ^{14}NO, ^{15}NO, or $^{15}N^{18}O$ were used to isolate vibrational modes involving the exogenous ligand. RR spectra of the 6-ms RFQ samples of these reactions reveal a mode at 1282 cm^{-1} that downshifts with Mb−$^{18}O_2$ and is observed at 1260 cm^{-1} in Mb−$^{16}O_2$ + ^{15}NO (Fig. 6.3). This RR band is not observed in the RR spectra of samples trapped after longer reaction times, and accordingly, it is assigned to a ligand vibration from the high-spin Fe(III) millisecond intermediate species (Fig. 6.3). As expected, the low-frequency RR spectra of Mb−O_2 exhibit a ν(Fe−O_2) at 577 cm^{-1} that shifts −26 cm^{-1} with $^{18}O_2$, but no isotope sensitive modes could be detected in the low-frequency RR spectra of the 6-ms RFQ samples (Fig. 6.4). Additional testing of these samples with 351- and 458-nm laser excitations on either side of the Soret absorption did not enhance any new isotope sensitive vibrations (data not shown).

6.5 Discussion

The frequency and isotope sensitivity of the 1282-cm^{-1} signal are not readily matched with expectations for peroxynitrite vibrations (Lo *et al.*, 1995; Tsai *et al.*, 1994). Instead, the 1282-cm^{-1} Raman band is consistent with a $\nu_s(NO_2)$ from a Fe(III)-nitrato complex. For example, the six-coordinate high-spin Fe(TPP)(η^1-ONO_2)(THF) complex shows FTIR spectra with a strong $\nu_s(NO_2)$ at 1280 cm^{-1} that shifts −22 cm^{-1} with ^{15}N

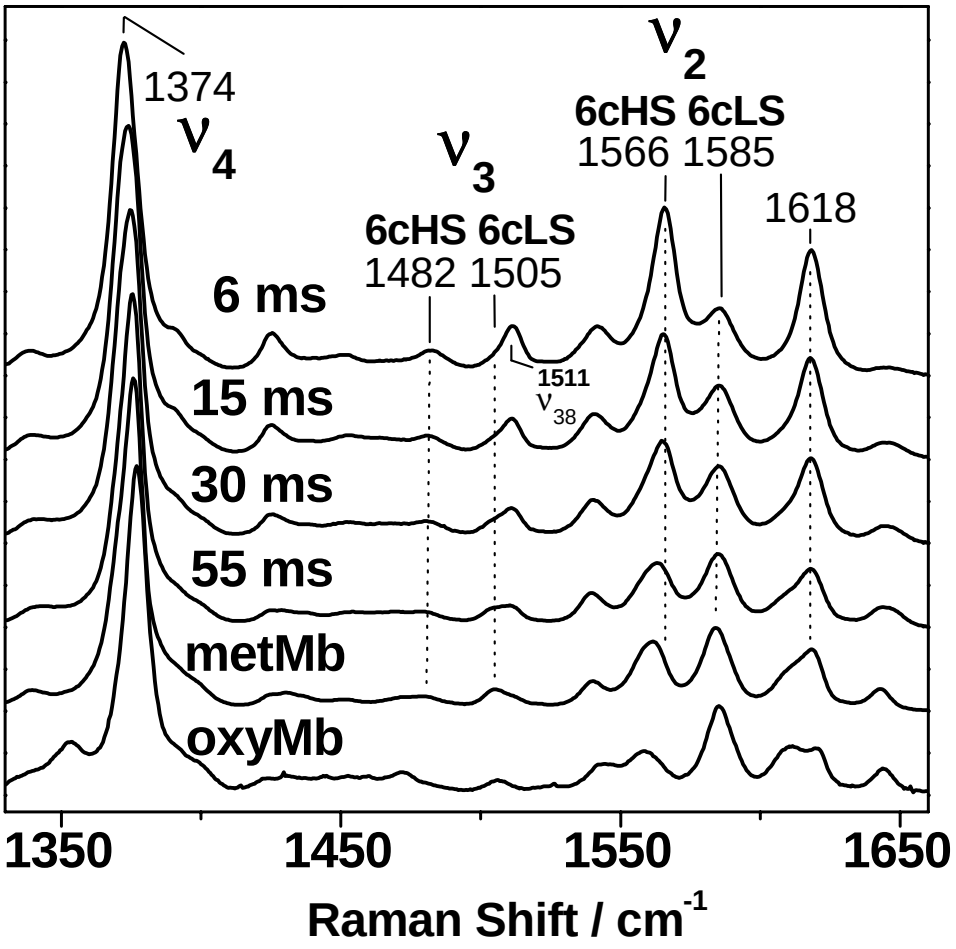

Fig. 6.2 High-frequency RR spectra of RFQ samples of the reaction of NO with oxyMb at 6 ms, 15 ms, 30 ms, and 55 ms. Also shown are the RR spectra of the product and starting material at pH 9.5, hydroxymetMb and oxy-Mb (λ_{exc} = 413 nm, 20 mW, T = 105 K).

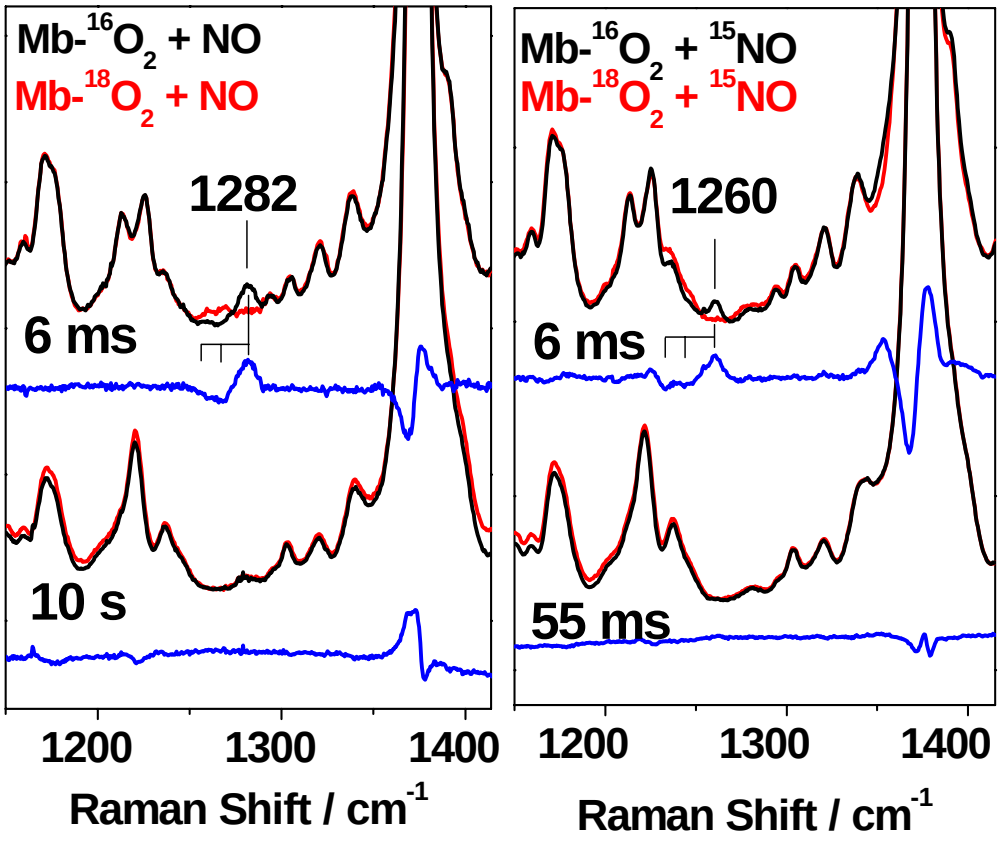

Fig. 6.3 Mid-frequency RR spectra of RFQ samples for the reaction of $^{14}N^{16}O$ (left) and $^{15}N^{16}O$ (right) with Mb-$^{16}O_2$ (black) versus Mb-$^{18}O_2$ (red). Difference spectra are shown in blue; the differential signals occurring at the intense ν_4 mode vary from independent experiments and represent less than 10% of the integrated ν_4 area (λ_{exc} = 413 nm, 20 mW, T = 105 K).

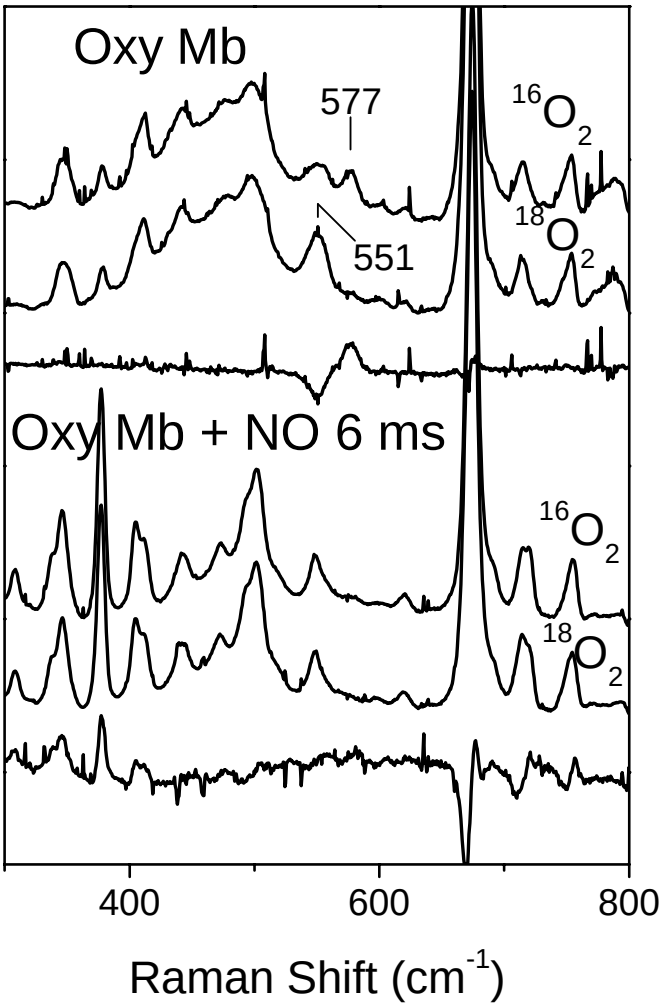

Fig. 6.4 Low-frequency RR spectra of Mb-$^{16}O_2$, Mb-$^{18}O_2$, Mb-$^{16}O_2$ + $^{14}N^{16}O$ at 6 ms and Mb-$^{18}O_2$ + $^{14}N^{16}O$ at 6 ms (λ_{exc} = 413 nm, 20 mW, T = 105K).

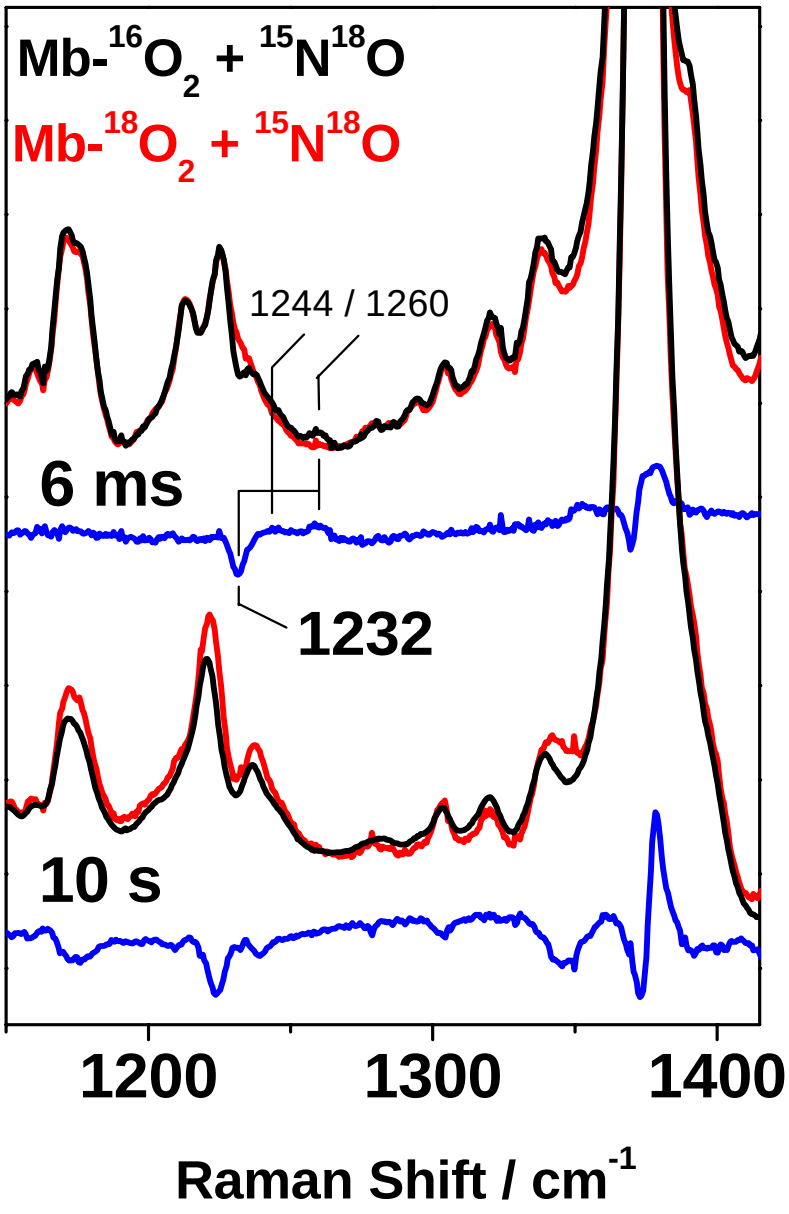

Fig. 6.5 Mid-frequency RR spectra of RFQ samples for the reaction of $^{15}N^{18}O$ with Mb-$^{16}O_2$ (black) versus Mb-$^{18}O_2$ (red). Difference spectra are shown in blue (λ_{exc} = 413 nm, 20 mW, T = 105K).

(Gulyan *et al.*, 2008). The assignment of the 1282-cm^{-1} signal to a nitrato $\nu_s(NO_2)$ in the RR spectra of the 6-ms intermediate is further supported by the impact of ^{18}O-labeling of Mb−O_2 and NO. Indeed, labeling of all three O-atoms produces the largest downshift of this mode to 1232 cm^{-1} (Fig. 6.5). In contrast, when Mb−$^{18}O_2$ is reacted with $N^{16}O$, two $\nu_s(NO_2)$ frequencies are observed (Fig. 6.3): the band with the largest downshift corresponds to Fe−$^{16}ON^{18}O_2$ and the other to Fe−$^{18}ON(^{16}O)^{18}O$. While the FTIR spectra of Fe(TPP)(η^1-ONO_2)(THF) show a weak $\nu_{as}(NO_2)$ at 1491 cm^{-1} and a very weak ν(N−O) near 1000 cm^{-1} (Gulyan *et al.*, 2008), these same modes are also expected to be weak in RR, and it is not surprising that they are not observed in the RR spectra of the 6-ms RFQ samples.

Although our results do not support the proposed peroxynitrite assignment by Herold and coworkers (Herold *et al.*, 2001), the trapping of an Fe(III)−nitrato complex is not inconsistent with a recent theoretical study by Blomberg and co-workers (Blomberg *et al.*, 2004). Using density functional theory, the decay of the peroxynitrite transient via homolytic cleavage of the O−O bond was predicted to occur with an energy barrier insufficient for accumulation of this species in the course of the reaction. Moreover, attempts to model the stabilization of a high-spin millisecond intermediate at alkaline pH as a peroxynitrite, via distal or proximal perturbations, were unsuccessful. In contrast, because anionic ligands show decreasing dissociation rate constants with increasing pH (Merryweather *et al.*, 1998; Wanat *et al.*, 2002), stabilization of the Fe(III)-nitrato complex is expected at alkaline pH, and is supported by our results. The assignment of the ms-intermediate to a Fe(III)−nitrato complex was rejected by Herold and co-workers on the basis of differences between the absorption spectrum of the ms-intermediate and resting metMb with nitrate (Herold *et al.*, 2001). However, a very large excess of nitrate (ca. 10^5 equiv) is required to affect the UV−vis spectrum of metMb and it is unclear whether the spectral changes reflect coordination of nitrate to the heme Fe(III) or less specific conformational changes. Control RFQ-RR experiments with metMb and high concentrations of nitrite or nitrate at pH 9.5 did not reveal formation of any high-spin heme species or vibrations involving exogenous ligands.

In conclusion, our RR analysis of RFQ samples of the reaction of oxyMb + NO at pH 9.5 identifies the ms-intermediate as a Fe(III)−nitrato complex. It is important to

stress that this species is not observed under equilibrium conditions, even with a high excess of nitrate, and thus corresponds to a transient Fe(III) complex. Assigning the ms-intermediate species to a nitrate rather than a peroxynitrite complex resolves the discrepancy between theoretical and experimental studies of the NO dioxygenation reaction in Mb. Our results do not invalidate the proposed reaction mechanism shown in Figure 6.1. Rather, they indicate that a greater time resolution will be required to determine whether a heme-peroxynitrite intermediate forms in the course of this reaction, and to structurally characterize this species. In the next chapter, we investigate the NOD reactivity of oxy-DevS and discuss its relevance to *M. tuberculosis* virulence.

CHAPTER 7
CONCLUSIONS AND FUTURE DIRECTIONS

7.1 DevS Signal Transduction

In our preliminary analysis of GAF-A DevS, we were able to identify the proximal ligand to the heme as His149 (Ioanoviciu *et al.,* 2007). Our work using full-length and truncated constructs of wt DevS showed that the GAF-B domain likely plays a role in the transduction of conformational changes that occur at the heme domain to change the activity of the kinase domain (Yukl *et al.,* 2007). We further showed that a distal tyrosine residue is required to differentiate between activating (CO and NO) and inhibitory (O_2) ligands by forming a hydrogen bond with the oxy ligand and, when CO or NO are bound, by stabilizing a hydrogen bond network that activates the kinase domain (Yukl *et al.,* 2008). A recent crystal structure of the GAF-A domain of DevS (Cho *et al.*, 2009) reveals a hydrogen bond network involving Tyr171, which is absent from the GAF-A domain of DosT (Podust *et al.*, 2008). This hydrogen bond network involves Glu87, His89, and a water molecule at the surface of GAF-A DevS (Fig 7.1) and could represent a pathway for communicating changes at the heme group to the surface of the GAF-A domain, changing the domain interactions between GAF-A and GAF-B to regulate the kinase domain (Fig. 7.1).

We are currently measuring the kinase activity and spectroscopic characteristics of mutants of these residues in an attempt to more clearly delineate the mechanisms of sensing in DevS. Preliminary results on a H89A mutant of full-length DevS indicate significantly lower levels of activity for all states investigated (Fig 7.2). The RR spectra of the CO complex indicate conformational heterogeneity very similar to that observed

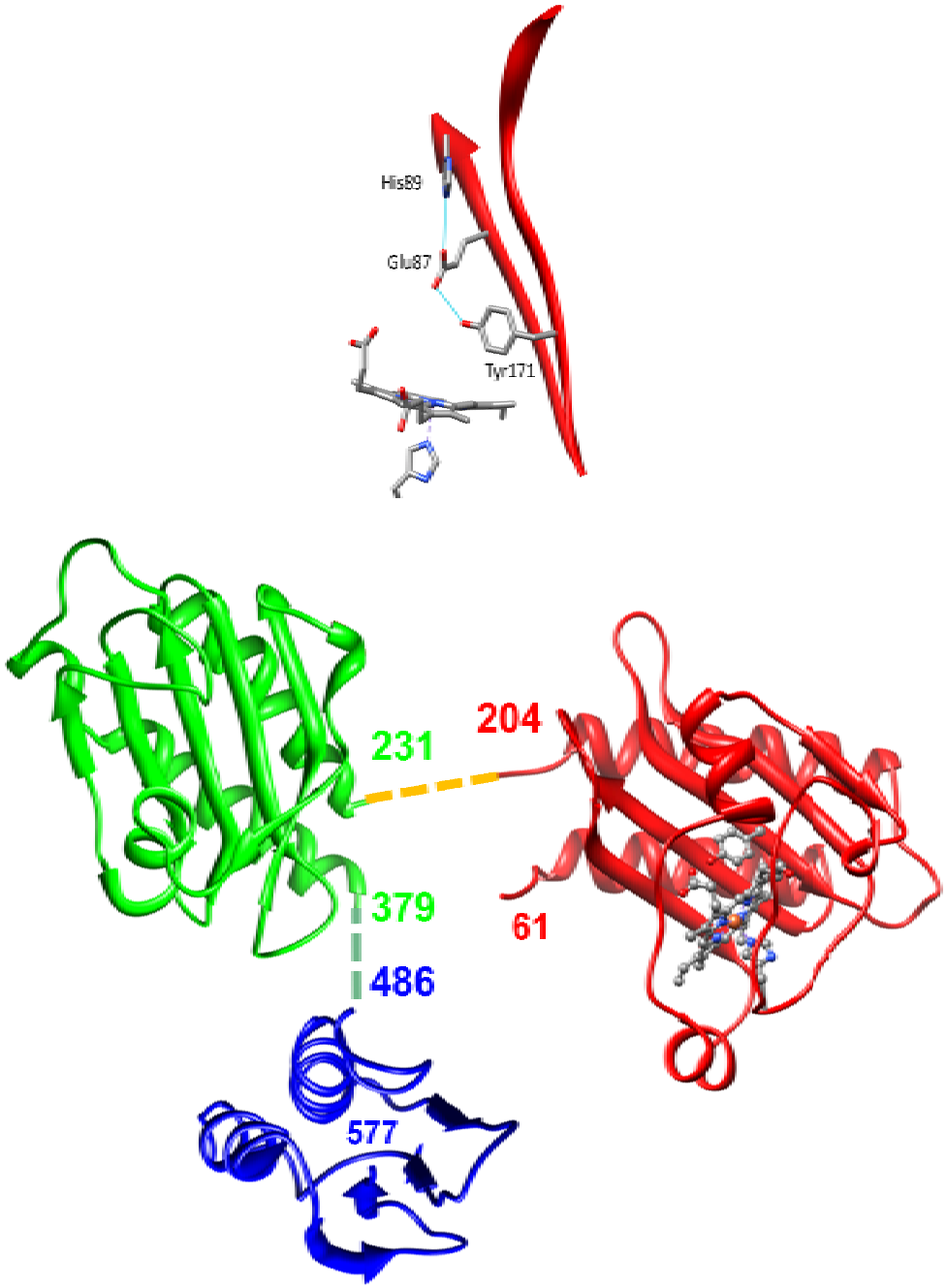

Fig. 7.1 Crystal structure of wt GAF-A DevS showing residues involved in a hydrogen bond network (top). Adapted from (Cho *et al.*, 2009). Structural model of DevS using crystal structures of the GAF-A domain (Red, 2W3F) (Cho *et al.*, 2009), the GAF-B domain (Green, 2VJW) (Cho *et al.*, 2008), and a homology based model (generated with 3-D Jigsaw server, http://bmm.cancerresearchuk.org/~3djigsaw/) of the histidine kinase domain (Blue).

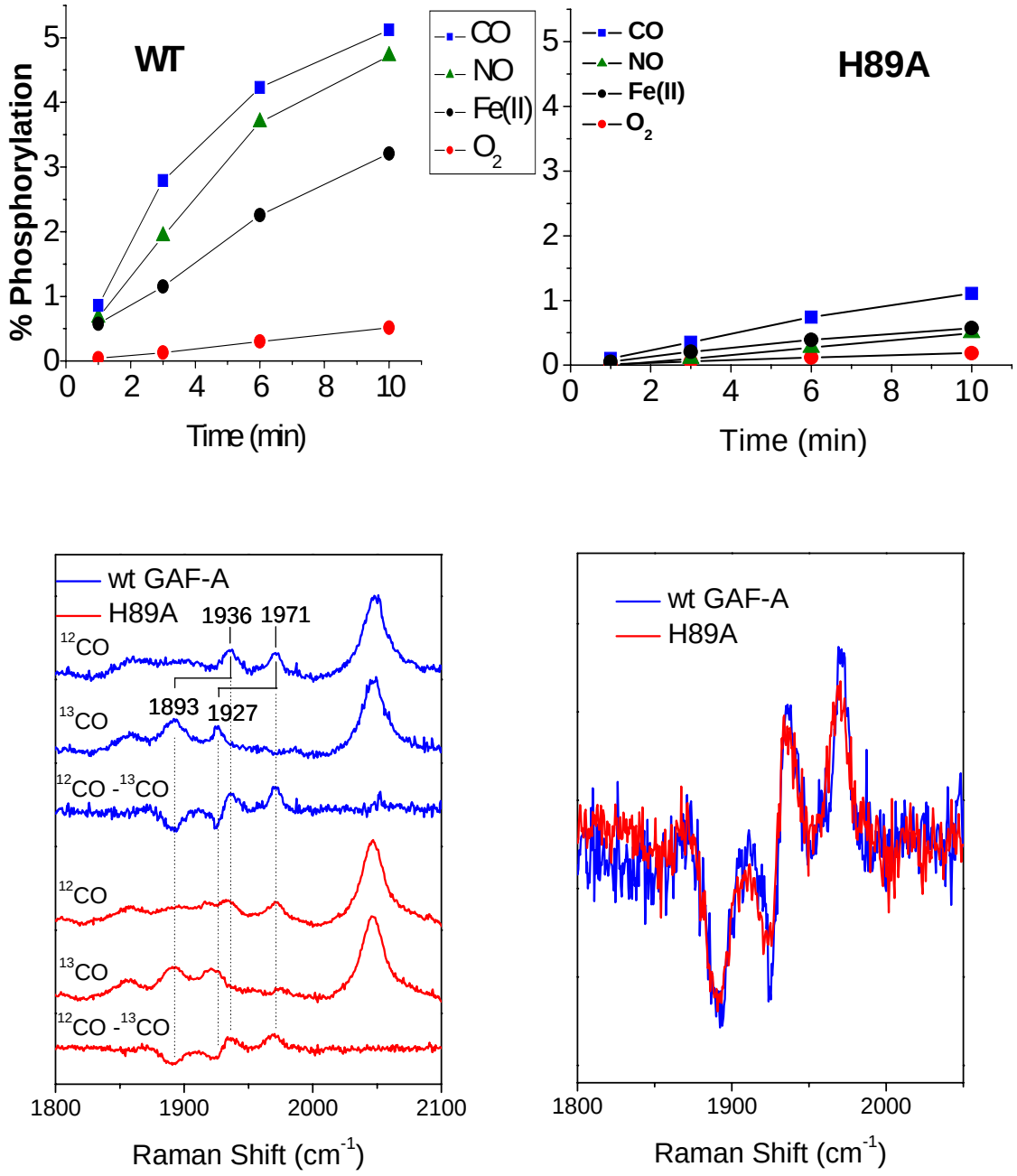

Fig. 7.2 Autophosphorylation of wt and H89A DevS (top). High-frequency RR spectra of wt GAF-A DevS and H89A DevS ^{12}CO and ^{13}CO complexes (bottom left). Comparison of wt and H89A DevS ^{12}CO - ^{13}CO difference spectra (right). (λ_{exc} = 413 nm, < 0.5 mW).

for the wt GAF-A DevS construct. These data suggest that when the His residue is mutated to a non-hydrogen bonding residue, the GAF-A domain can no longer interact efficiently with the GAF-B domain, preventing activation of the kinase regardless of the ligation state of the heme iron.

7.2 Detoxification of NO by Heme-Oxy Complexes

In the previous chapter, we characterized a Fe(III)-nitrato intermediate in the NOD mechanism of Mb (Yukl *et al.,* 2009). Recently, we also identified rapid NOD activity in wt GAF-A DevS and in a full-length variant of DevS, F98A DevS, which shows comparable kinase activity and specificity to that of the wt protein (data not shown). Stopped-flow spectroscopy of the reaction of NO with oxy-DevS at pH 7.5 and 9.5 at 3 °C show the rapid accumulation of Fe(III) DevS with apparent rate constants of 102 s^{-1} and 142 s^{-1}, respectively (Fig. 7.3). These rates are comparable to that obtained with Mb at pH 7.0 and 20 °C (Herold *et al.*, 2001). Given the rapid and efficient NOD activity exhibited by DevS, this protein could play an additional role in resistance of *M. tuberculosis* by directly oxidizing NO. The reaction would leave DevS in the Fe(III) state in which the kinase is inactive (Kumar *et al.*, 2007; Yukl *et al.*, 2008). However, it is likely that DevS is rapidly re-reduced in *M. tuberculosis*, leading to the active Fe(II)-deoxy form. Thus DevS would have a dual function as both a gas sensor and NO detoxifying protein.

We attempted to characterize an intermediate in the NOD reaction of DevS using RR of RFQ samples (Fig. 7.4). This method was successful in identifying the high-spin intermediate in the same reaction of Mb (Yukl *et al.,* 2009). However, these experiments showed no evidence of O_2 isotope sensitive vibrations that could be assigned to an intermediate Fe(III) species as all RR spectra are equivalent to that of the Fe(III) resting form. At this time, it is uncertain whether the reaction is simply too rapid to detect an intermediate or whether the intermediate adopts the same spin-configuration as the Fe(III) resting form at cryogenic temperatures.

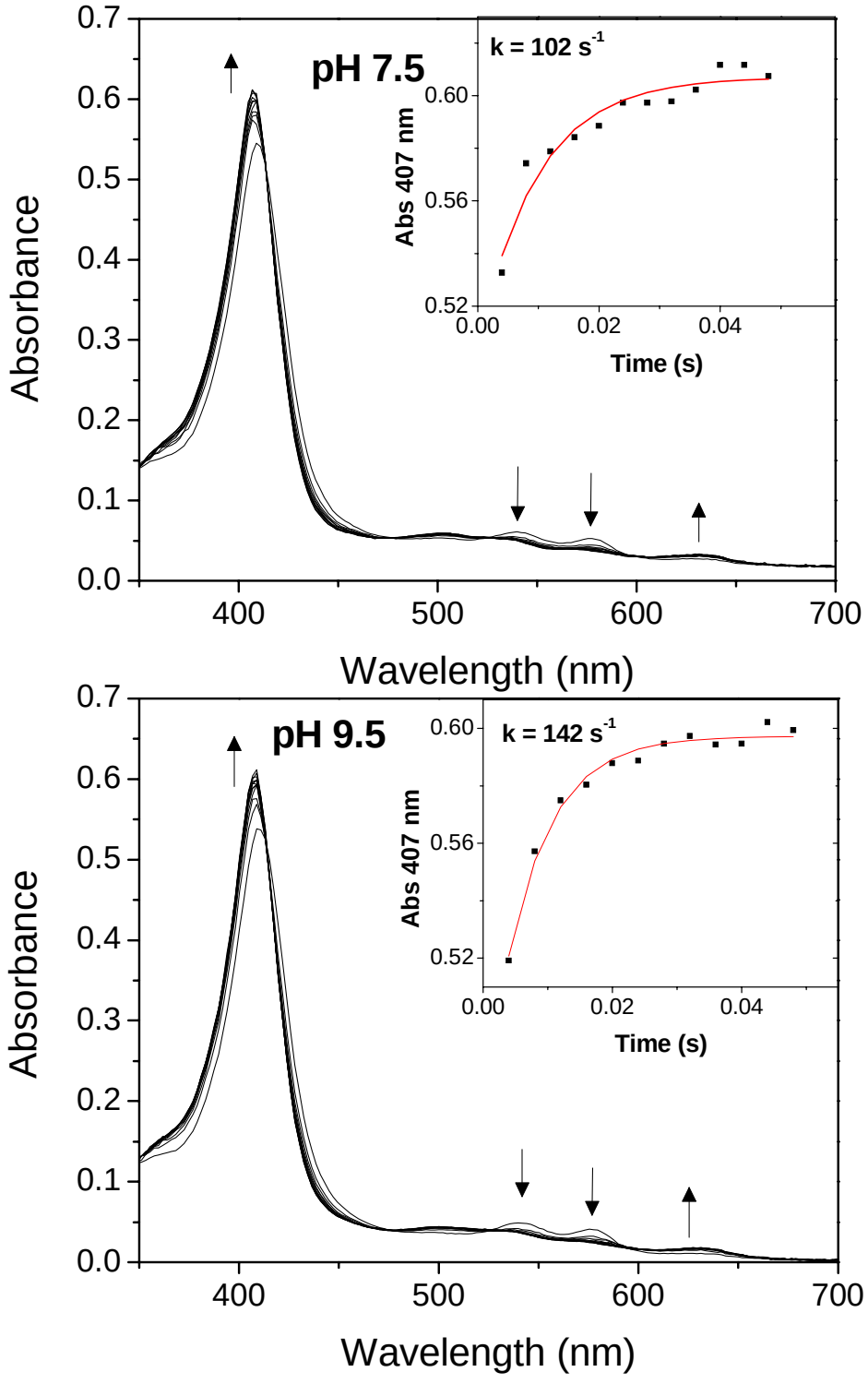

Fig. 7.3 Stopped-flow UV-vis spectroscopy of the reaction of oxy GAF-A DevS with NO at pH 7.5 (top) and 9.5 (bottom). Scans taken every 4 ms for 50 ms.

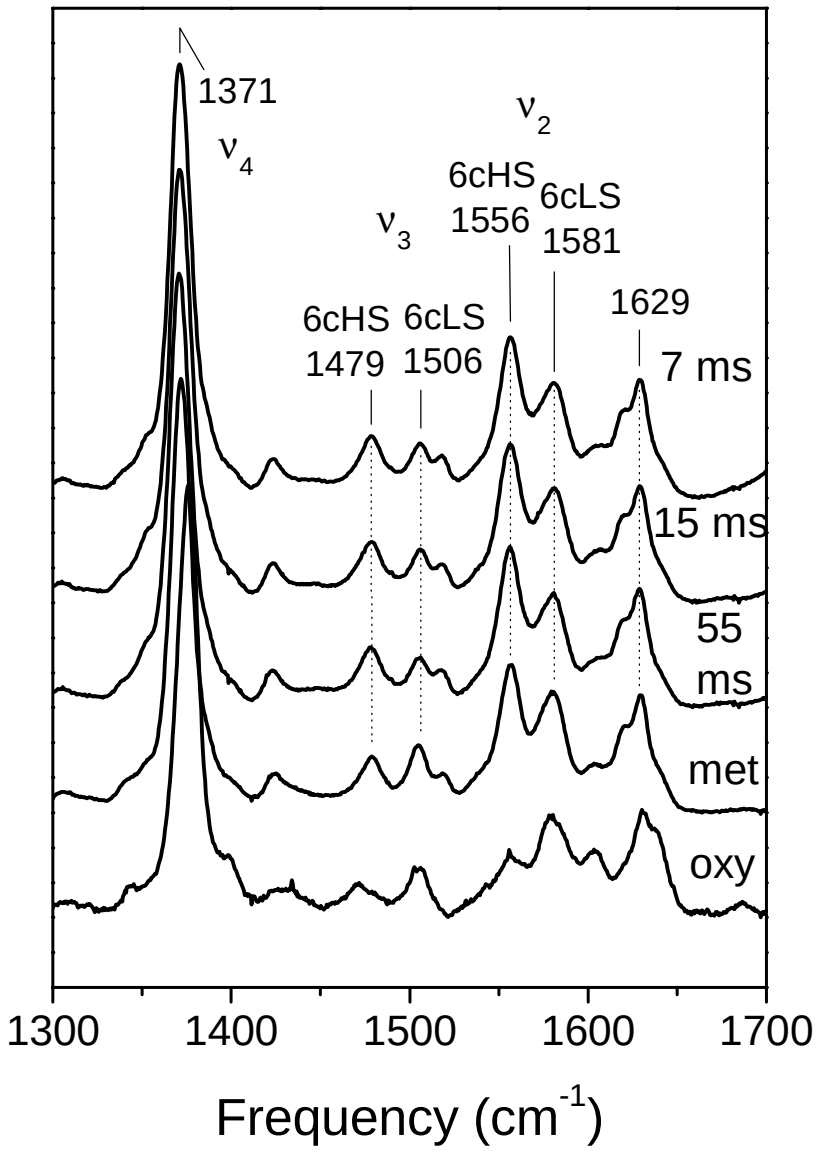

Fig 7.4 High-frequency RR spectra of RFQ samples of the reaction of NO with oxy GAF-A DevS at 7 ms, 15 ms, and 55 ms. Also shown are the RR spectra of the product and starting material at pH 9.5, met and oxy DevS, respectively. (λ_{exc} = 413 nm, 20 mW, T = 105 K).

To resolve this question, we are planning experiments using a microsecond hyper-freeze quench apparatus capable of freezing samples less than 100 μs after mixing (Cherepanov and de Vries, 2004). Using this approach, we should be able to detect an intermediate, if one exists, in the NOD reaction of DevS. Also, the sub-millisecond time resolution may allow us to observe the peroxynitrite intermediate proposed to form during the NOD reaction of Mb. These experiments should provide considerable insight into the mechanisms of NO oxidation by hemoproteins.

7.3 Roles of Various Forms of NsrR in Gene Regulation

We have shown that anaerobically purified NsrR binds a $[4Fe\text{-}4S]^{2+}$ cluster (Yukl *et al.,* 2008). However, in the presence of oxygen and DTT, NsrR can also anchor a $[2Fe\text{-}2S]^{2+}$ cluster. It is currently unknown whether the 2Fe-2S form is physiologically relevant, but it has been shown to bind target DNA and to lose that function upon exposure to NO (Isabella *et al.*, 2009; Tucker *et al.*, 2008). In order to assess this in *B. subtilis* NsrR, careful DNA-binding experiments need to be performed using anaerobically purified, aerobically purified, apo, and nitrosylated NsrR proteins in order to assess the potential of these various states in terms of gene regulation.

The observation that anaerobically purified NsrR contains a $[4Fe\text{-}4S]^{2+}$ cluster regardless of whether bacteria are grown aerobically brings up the question of how NsrR is stabilized within the cell. DNA binding may stabilize the 4Fe-4S cluster, but alternatively, an exogenous ligand to the 4Fe-4S cluster may dampen its reactivity. Recently, an antioxidant molecule known as bacillithiol has been isolated from *B. subtilis* (Newton *et al.*, 2009). This thiol could perform a similar function within the cell to that which DTT performs *in vitro*, perhaps coordinating the labile iron site in NsrR and shielding the cluster from oxygen-mediated degradation. Measuring the stability of the 4Fe-4S cluster by UV-vis in the presence of target DNA and bacillithiol could help to answer these questions.

7.4 Concluding Remarks

The importance of NO in biology has only recently been recognized. Its toxicity makes it a useful weapon of the immune system against invading pathogens, and avoidance of NO by these organisms, either by detoxification or entrance into a dormant state, is often critical for virulence. Bacteria can also encounter NO as a byproduct of nitrate respiration or denitirification. Finally, despite its toxicity, NO is used extensively as a signaling molecule in mammals. Thus, mechanisms for NO sensing and detoxification are essential to a tremendous variety of organisms for controlling myriad functions, and metalloproteins are often called upon to fill these roles.

Our work uses a variety of spectroscopic techniques to probe the metal centers of heme and iron-sulfur proteins in an attempt to understand the structural events taking place during NO sensing or detoxification. RR spectroscopy of resting samples has proven expecially useful in this vein for sensor proteins. Coupling this technique with RFQ protocols has allowed us to study intermediates in the NO dioxygenase reaction and promises to be a powerful method of determining mechanisms metalloenzyme reactions and binding events in general. Continued work and innovation in this field will lead to a greater understanding of the mechanisms by which organisms control and respond to NO, potentially having a significant impact upon human health.

LITERATURE CITED

Alontaga, A.Y., Rodriguez, J.C., Schonbrunn, E., Becker, A., Funke, T., Yukl, E.T., Hayashi, T., Stobaugh, J., Moënne-Loccoz, P., and Rivera, M. (2009) Structural characterization of the hemophore HasAp from *Pseudomonas aeruginosa*: NMR spectroscopy reveals protein-protein interactions between Holo-HasAp and hemoglobin. *Biochemistry* **48**: 96-109.

Andersson, L.A., Mylrajan, M., Sullivan, E.P., Jr., and Strauss, S.H. (1989) Modeling low-pH hemoproteins. *J. Biol. Chem.* **264**: 19099-19102.

Anderton, C.L., Hester, R.E., and Moore, J.N. (1997) A chemometric analysis of the resonance Raman spectra of mutant carbonmonoxy-myoglobins reveals the effects of polarity. *Biochim. Biophys. Acta* **1338**: 107-120.

Aono, S., Nakajima, H., Saito, K., and Okada, M. (1996) A novel heme protein that acts as a carbon monoxide-dependent transcriptional activator in *Rhodospirillum rubrum*. *Biochem. Biophys. Res. Commun.* **228**: 752-756.

Aono, S., Matsuo, T., Shimono, T., Ohkubo, K., Takasaki, H., and Nakajima, H. (1997) Signal transduction in the transcriptional activator CooA containing a heme-based CO sensor: Isolation of a dominant positive mutant which is active as the transcriptional activator even in the absence of CO. *Biochem. Biophys. Res. Commun.* **240**: 783-786.

Aono, S., Kato, T., Matsuki, M., Nakajima, H., Ohta, T., Uchida, T., and Kitagawa, T. (2002) Resonance Raman and ligand binding studies of the oxygen-sensing signal transducer protein HemAT from *Bacillus subtilis*. *J. Biol. Chem.* **277**: 13528-13538.

Arnold, W.P., Mittal, C.K., Katsuki, S., and Murad, F. (1977) Nitric oxide activates guanylate cyclase and increases guanosine 3',5'-cyclic monophosphate levels in various tissue preparations. *Proc. Natl. Acad. Sci. U. S. A.* **74**: 3203-3207.

Asher, S.A., Vickery, L.E., Schuster, T.M., and Sauer, K. (1977) Resonance Raman spectra of methemoglobin derivatives. Selective enhancement of axial ligand vibrations and lack of an effect of inositol hexaphosphate. *Biochemistry* **16**: 5849-5856.

Bang, I.S., Liu, L., Vazquez-Torres, A., Crouch, M.L., Stamler, J.S., and Fang, F.C. (2006) Maintenance of nitric oxide and redox homeostasis by the *Salmonella* flavohemoglobin *hmp*. *J. Biol. Chem.* **281**: 28039-28047.

Bates, D.M., Popescu, C.V., Khoroshilova, N., Vogt, K., Beinert, H., Münck, E., and Kiley, P.J. (2000) Substitution of leucine 28 with histidine in the *Escherichia coli* transcription factor FNR results in increased stability of the $[4Fe\text{-}4S]^{2+}$ cluster to oxygen. *J. Biol. Chem.* **275**: 6234-6240.

Beinert, H., Kennedy, M.C., and Stout, C.D. (1996) Aconitase as iron-sulfur protein, enzyme, and iron-regulatory protein. *Chem. Rev.* **96**: 2335-2373.

Blomberg, L.M., Blomberg, M.R.A., and Siegbahn, P.E.M. (2004) A theoretical study of myoglobin working as a nitric oxide scavenger. *J. Biol. Inorg. Chem.* **9**: 923-935.

Bodenmiller, D.M., and Spiro, S. (2006) The *yjeB* (*nsrR*) gene of *Escherichia coli* encodes a nitric oxide-sensitive transcriptional regulator. *J. Bacteriol.* **188**: 874-881.

Bradford, M.M. (1976) A rapid and sensitive method for the quantitation of microgram quantities of protein utilizing the principle of protein-dye binding. *Anal. Biochem.* **72**: 248-254.

Caignan, G.A., Deshmukh, R., Wilks, A., Zeng, Y., Huang, H.W., Moënne-Loccoz, P., Bunce, R.A., Eastman, M.A., and Rivera, M. (2002) Oxidation of heme to beta- and delta-biliverdin by *Pseudomonas aeruginosa* heme oxygenase as a consequence of an unusual seating of the heme. *J. Am. Chem. Soc.* **124**: 14879-14892.

Cairo, G., Ronchi, R., Recalcati, S., Campanella, A., and Minotti, G. (2002) Nitric oxide and peroxynitrite activate the iron regulatory protein-1 of J774A.1 macrophages by direct disassembly of the Fe-S cluster of cytoplasmic aconitase. *Biochemistry* **41**: 7435-7442.

Cary, S.P., Winger, J.A., and Marletta, M.A. (2005) Tonic and acute nitric oxide signaling through soluble guanylate cyclase is mediated by nonheme nitric oxide, ATP, and GTP. *Proc. Natl. Acad. Sc.i U. S. A.* **102**: 13064-13069.

Cescau, S., Cwerman, H., Létoffé, S., Deleplaire, P., Wandersman, C., and Biville, F. (2007) Heme acquisition by hemophores. *Biometals* **20**: 603-613.

Cherepanov, A.V., and de Vries, S. (2004) Microsecond freeze-hyperquenching: development of a new ultrafast micro-mixing and sampling technology and application to enzyme catalysis. *Biochim. Biophys. Acta* **1656**: 1-31.

Cho, H.Y., Cho, H.J., Kim, Y.M., Oh, J.I., and Kang, B.S. (2008) Crystallization and preliminary crystallographic analysis of the second GAF domain of DevS from *Mycobacterium smegmatis*. *Acta Crystall. F* **64**: 274-276.

Cho, H.Y., Cho, H.J., Kim, Y.M., Oh, J.I., and Kang, B.S. (2009) Structural insight into the heme-based redox sensing by DosS from *Mycobacterium tuberculosis* *J. Biol. Chem.* **284**: 13057-13067.

Choi, H.S., Rai, P.R., Chu, H.W., Cool, C., and Chan, E.D. (2002) Analysis of nitric oxide synthase and nitrotyrosine expression in human pulmonary tuberculosis. *Am. J. Respir. Crit. Care Med.* **166**: 178-186.

Colas, C., and Ortiz de Montellano, P.R. (2003) Autocatalytic radical reactions in physiological prosthetic heme modification. *Chem. Rev.* **103**: 2305-2332.

Conover, R.C., Kowal, A.T., Fu, W.G., Park, J.B., Aono, S., Adams, M.W., and Johnson, M.K. (1990) Spectroscopic characterization of the novel iron-sulfur cluster in *Pyrococcus furiosus* ferredoxin. *J. Biol. Chem.* **265**: 8533-8541.

Conover, R.C., Park, J.B., Adams, M.W.W., and Johnson, M.K. (1991) Exogenous ligand binding to the [Fe_4S_4] cluster in *Pyrococcus furiosus* ferredoxin. *J. Am. Chem. Soc.* **113**: 2799-2800.

Costanzo, S., Menage, S., Purrello, R., Bonomo, R.P., and Fontecave, M. (2001) Re-examination of the formation of dinitrosyl-iron complexes during reaction of S-nitrosothiols with Fe(II). *Inorg. Chim. Acta* **318**: 1-7.

Couture, M., Yeh, S.R., Wittenberg, B.A., Wittenberg, J.B., Ouellet, Y., Rousseau, D.L., and Guertin, M. (1999) A cooperative oxygen-binding hemoglobin from *Mycobacterium tuberculosis. Proc. Natl. Acad. Sci. U. S. A.* **96**: 11223-11228.

Coyle, C.M., Vogel, K.M., Rush, T.S., 3rd, Kozlowski, P.M., Williams, R., Spiro, T.G., Dou, Y., Ikeda-Saito, M., Olson, J.S., and Zgierski, M.Z. (2003) FeNO structure in distal pocket mutants of myoglobin based on resonance Raman spectroscopy. *Biochemistry* **42**: 4896-4903.

Crawford, M.J., and Goldberg, D.E. (1998) Role for the *Salmonella* flavohemoglobin in protection from nitric oxide. *J. Biol. Chem.* **273**: 12543-12547.

Cruz-Ramos, H., Boursier, L., Moszer, I., Kunst, F., Danchin, A., and Glaser, P. (1995) Anaerobic transcription activation in *Bacillus subtilis*: Identification of distinct FNR-dependent and -independent regulatory mechanisms. *EMBO J.* **14**: 5984-5994.

Cruz-Ramos, H., Crack, J., Wu, G., Hughes, M.N., Scott, C., Thomson, A.J., Green, J., and Poole, R.K. (2002) NO sensing by FNR: regulation of the *Escherichia coli* NO-detoxifying flavohaemoglobin, Hmp. *EMBO J.* **21**: 3235-3244.

Cunningham, A.F., and Spreadbury, C. L. (1998) Mycobacterial stationary phase induced by low oxygen tension: cell wall thickening and localization of the 16-kilodalton -crystallin homolog. *J. Bacteriol.* **180**: 801-808.

Das, T.K., Weber, R.E., Dewilde, S., Wittenberg, J.B., Wittenberg, B.A., Yamauchi, K., Van Hauwaert, M.L., Moens, L., and Rousseau, D.L. (2000) Ligand binding in the Fe(III) and Fe(II) states of *Paramecium* hemoglobin. *Biochemistry* **39**: 14330-14340.

Dasgupta, N., Kapur, V., Singh, K.K., Das, T.K., Sachdeva, S., Jyothisri, K., and Tyagi, J.S. (2000) Characterization of a two-component system, devR-devS, of *Mycobacterium tuberculosis*. *Tuber. Lung Dis.* **80**: 141-159.

D'Autreaux, B., Tucker, N., Spiro, S., and Dixon, R. (2008) Characterization of the nitric oxide-reactive transcriptional activator NorR. *Methods Enzymol.* **437**: 235-251.

Davies, G.E., and Stark, G.R. (1970) Use of dimethyl suberimidate, a cross-linking reagent, in studying the subunit structure of oligomeric proteins. *Proc. Natl. Acad. Sci. U. S. A.* **66**: 651-656.

Dawson, R.M.C., Elliott, D. C., Elliott, W. H., Jones, K. M. (1986) In *Data for Biochemical Research*. Oxford, England: Oxford University Press, pp. 230-231.

Deinum, G., Stone, J.R., Babcock, G.T., and Marletta, M.A. (1996) Binding of nitric oxide and carbon monoxide to soluble guanylate cyclase as observed with resonance Raman spectroscopy. *Biochemistry* **35**: 1540-1547.

Demple, B., Ding, H., and Jorgensen, M. (2002) *Escherichia coli* SoxR protein: sensor/transducer of oxidative stress and nitric oxide. *Methods Enzymol.* **348**: 355-364.

Desbois, A., Lutz, M., and Banerjee, R. (1979) Low-frequency vibrations in resonance Raman spectra of horse heart myoglobin. Iron-ligand and iron-nitrogen vibrational modes. *Biochemistry* **18**: 1510-1518.

Dick, T. (2001) Dormant tubercle bacilli: the key to more effective TB chemotherapy? *J. Antimicrob. Chemother.* **47**: 117-118.

Ding, H., and Demple, B. (2000) Direct nitric oxide signal transduction via nitrosylation of iron-sulfur centers in the SoxR transcription activator. *Proc. Natl. Acad. Sci. U. S. A.* **97**: 5146-5150.

Douglas, J.H., Reid, R.R., Smith, F.E., and Thompson, S.L. (1984) Ferene--a new spectrophotometric reagent for iron. *Can. J. Chem.* **62**: 721-724.

Duin, E.C., Lafferty, M.E., Crouse, B.R., Allen, R.M., Sanyal, I., Flint, D.H., and Johnson, M.K. (1997) [2Fe-2S] to [4Fe-4S] cluster conversion in *Escherichia coli* biotin synthase. *Biochemistry* **36**: 11811-11820.

Dunham, C.M., Dioum, E.M., Tuckerman, J.R., Gonzalez, G., Scott, W.G., and Gilles-Gonzalez, M.A. (2003) A distal arginine in oxygen-sensing heme-PAS domains is essential to ligand binding, signal transduction, and structure. *Biochemistry* **42**: 7701-7708.

Fan, B., Wang, J., Stuehr, D.J., and Rousseau, D.L. (1997) NO synthase isozymes have distinct substrate binding sites. *Biochemistry* **36**: 12660-12665.

Feis, A., Marzocchi, M.P., Paoli, M., and Smulevich, G. (1994) Spin state and axial ligand bonding in the hydroxide complexes of metmyoglobin, methemoglobin, and horseradish peroxidase at room and low temperatures. *Biochemistry* **33**: 4577-4583.

Flogel, U., Merx, M.W., Godecke, A., Decking, U.K., and Schrader, J. (2001) Myoglobin: A scavenger of bioactive NO. *Proc. Natl. Acad. Sci. U. S. A.* **98**: 735-740.

Fontecave, M., and Ollagnier-de-Choudens, S. (2008) Iron-sulfur cluster biosynthesis in bacteria: Mechanisms of cluster assembly and transfer. *Arch. Biochem. Biophys.* **474**: 226-237.

Foster, H.W., and Cowan, J.A. (1999) Chemistry of nitric oxide with protein-bound iron sulfur centers. Insights on physiological reactivity. *J. Am. Chem. Soc.* **121**: 4093-4100.

Foury, F., and Talibi, D. (2001) Mitochondrial control of iron homeostasis. A genome wide analysis of gene expression in a yeast frataxin-deficient strain. *J. Biol. Chem.* **276**: 7762-7768.

Gardner, A.M., and Gardner, P.R. (2002) Flavohemoglobin detoxifies nitric oxide in aerobic, but not anaerobic, *Escherichia coli*. Evidence for a novel inducible anaerobic nitric oxide-scavenging activity. *J. Biol. Chem.* **277**: 8166-8171.

Gardner, A.M., Helmick, R.A., and Gardner, P.R. (2002) Flavorubredoxin, an inducible catalyst for nitric oxide reduction and detoxification in *Escherichia coli*. *J. Biol. Chem.* **277**: 8172-8177.

Gardner, P.R., Gardner, A.M., Martin, L.A., and Salzman, A.L. (1998) Nitric oxide dioxygenase: an enzymic function for flavohemoglobin. *Proc. Natl. Acad. Sci. U. S. A.* **95**: 10378-10383.

Gardner, P.R. (2005) Nitric oxide dioxygenase function and mechanism of flavohemoglobin, hemoglobin, myoglobin and their associated reductases. *J. Inorg. Biochem.* **99**: 247-266.

Geng, H., Nakano, S., and Nakano, M.M. (2004) Transcriptional activation by *Bacillus subtilis* ResD: tandem binding to target elements and phosphorylation-dependent and -independent transcriptional activation. *J. Bacteriol.* **186**: 2028-2037.

George, P., and Hanania, G.I. (1957) The ionization of acidic metmyoglobin; ionic-strength charge effects. *Biochem. J.* **65**: 756-760.

Ghigo, J.M., Letoffe, S., and Wandersman, C. (1997) A new type of hemophore-dependent heme acquisition system of *Serratia marcescens* reconstituted in *Escherichia coli*. *J. Bacteriol.* **179**: 3572-3579.

Giel, J.L., Rodionov, D., Liu, M., Blattner, F.R., and Kiley, P.J. (2006) IscR-dependent gene expression links iron-sulphur cluster assembly to the control of O_2-regulated genes in *Escherichia coli*. *Mol. Microbiol.* **60**: 1058-1075.

Gilberthorpe, N.J., Lee, M.E., Stevanin, T.M., Read, R.C., and Poole, R.K. (2007) NsrR: a key regulator circumventing *Salmonella enterica* serovar Typhimurium oxidative and nitrosative stress *in vitro* and in IFN-gamma-stimulated J774.2 macrophages. *Microbiology* **153**: 1756-1771.

Gilles-Gonzalez, M.A., Gonzalez, G., Sousa, E.H., and Tuckerman, J. (2008) Oxygen-sensing histidine-protein kinases: assays of ligand binding and turnover of response-regulator substrates. *Methods Enzymol.* **437**: 173-189.

Gomes, C.M., Giuffre, A., Forte, E., Vicente, J.B., Saraiva, L.M., Brunori, M., and Teixeira, M. (2002) A novel type of nitric-oxide reductase. *Escherichia coli* flavorubredoxin. *J. Biol. Chem.* **277**: 25273-25276.

Green, J., Scott, C., and Guest, J.R. (2001) Functional versatility in the CRP-FNR superfamily of transcription factors: FNR and FLP. *Adv. Microb. Physiol.* **44**: 1-34.

Guérout-Fleury, A.M., Shazand, K., Frandsen, N., and Stragier, P. (1995) Antibiotic-resistance cassettes for *Bacillus subtilis*. *Gene* **167**: 335-336.

Gulyan, G.M., Kurtikyan, T.S., and Ford, P.C. (2008) Six-coordinate nitrato complexes of iron(III) porphyrins. *Inorg. Chem.* **47**: 787-789.

Han, Y. (2005) Utilization of ferroproteins by *Candida albicans* during candidastasis by apotransferrin. *Arch. Pharm. Res.* **28**: 963-969.

Hao, B., Isaza, C., Arndt, J., Soltis, M., and Chan, M.K. (2002) Structure-based mechanism of O_2 sensing and ligand discrimination by the FixL heme domain of *Bradyrhizobium japonicum*. *Biochemistry* **41**: 12952-12958.

Hargrove, M.S., Whitaker, T., Olson, J.S., Vali, R.J., and Mathews, A.J. (1997) Quaternary structure regulates hemin dissociation from human hemoglobin. *J. Biol. Chem.* **272**: 17385-17389.

Herold, S. (1999) Kinetic and spectroscopic characterization of an intermediate peroxynitrite complex in the nitrogen monoxide induced oxidation of oxyhemoglobin. *FEBS Lett.* **443**: 81-84.

Herold, S., Exner, M., and Nauser, T. (2001) Kinetic and mechanistic studies of the NO-mediated oxidation of oxymyoglobin and oxyhemoglobin. *Biochemistry* **40**: 3385-3395.

Hoard, J.L., and Scheidt, W.R. (1973) Stereochemical trigger for initiating cooperative interaction of the subunits during the oxygenation of cobaltohemoglobin *Proc. Natl. Acad. Sci. U. S. A.* **70**: 3919-3922.

Hou, S., Larsen, R.W., Boudko, D., Riley, C.W., Karatan, E., Zimmer, M., Ordal, G.W., and Alam, M. (2000) Myoglobin-like aerotaxis transducers in archaea and bacteria. *Nature* **403**: 540-544.

Hu, Y., Faham, S., Roy, R., Adams, M.W., and Rees, D.C. (1999) Formaldehyde ferredoxin oxidoreductase from *Pyrococcus furiosus*: the 1.85 Å resolution crystal structure and its mechanistic implications. *J. Mol. Biol.* **286**: 899-914.

Ioanoviciu, A., Yukl, E.T., Moënne-Loccoz, P., and Ortiz de Montellano, P.R. (2007) DevS, a heme-containing two-component oxygen sensor of *Mycobacterium tuberculosis*. *Biochemistry* **46**: 4250-4260.

Isabella, V.M., Lapek, J.D., Jr., Kennedy, E.M., and Clark, V.L. (2009) Functional analysis of NsrR, a nitric oxide-sensing Rrf2 repressor in *Neisseria gonorrhoeae*. *Mol. Microbiol.* **71**: 227-239.

Johnson, D.C., Dean, D.R., Smith, A.D., and Johnson, M.K. (2005) Structure, function, and formation of biological iron-sulfur clusters. *Annu. Rev. Biochem.* **74**: 247-281.

Jordan, P.A., Thomson, A.J., Ralph, E.T., Guest, J.R., and Green, J. (1997) FNR is a direct oxygen sensor having a biphasic response curve. *FEBS Lett.* **416**: 349-352.

Jung, Y.S., Vassiliev, I.R., Qiao, F., Yang, F., Bryant, D.A., and Golbeck, J.H. (1996) Modified ligands to F_A and F_B in photosystem I. Proposed chemical rescue of a [4Fe-4S] cluster with an external thiolate in alanine, glycine, and serine mutants of PsaC. *J. Biol. Chem.* **271**: 31135-31144.

Kerby, R.L., Hong, S.S., Ensign, S.A., Coppoc, L.J., Ludden, P.W., and Roberts, G.P. (1992) Genetic and physiological characterization of the *Rhodospirillum rubrum* carbon monoxide dehydrogenase system. *J. Bacteriol.* **174**: 5284-5294.

Kerby, R.L., Ludden, P.W., and Roberts, G.P. (1995) Carbon monoxide-dependent growth of *Rhodospirillum rubrum*. *J. Bacteriol.* **177**: 2241-2244.

Khoroshilova, N., Popescu, C., Munck, E., Beinert, H., and Kiley, P.J. (1997) Iron-sulfur cluster disassembly in the FNR protein of *Escherichia coli* by O_2: [4Fe-4S] to [2Fe-2S] conversion with loss of biological activity. *Proc. Natl. Acad. Sci. U. S. A.* **94**: 6087-6092.

Kiley, P.J., and Beinert, H. (1998) Oxygen sensing by the global regulator, FNR: the role of the iron-sulfur cluster. *FEMS Microbiol. Rev.* **22**: 341-352.

Kiley, P.J., and Beinert, H. (2003) The role of Fe-S proteins in sensing and regulation in bacteria. *Curr. Opin. Microbiol.* **6**: 181-185.

Kim, D., Yukl, E.T., Moënne-Loccoz, P., and Montellano, P.R. (2006) Fungal heme oxygenases: Functional expression and characterization of Hmx1 from *Saccharomyces cerevisiae* and CaHmx1 from *Candida albicans*. *Biochemistry* **45**: 14772-14780.

Kitagawa, T. (1988) Heme protein structure and the iron-histidine stretching mode. In *Biological Applications of Raman Spectroscopy. Vol. 3. Resonance Raman spectra of hemes and metalloproteins*. Vol. 3. Spiro, T.G. (ed). New York: John Wiley & Sons, pp. 97-131.

Kumar, A., Toledo, J.C., Patel, R.P., Lancaster, J.R., Jr., and Steyn, A.J.C. (2007) *Mycobacterium tuberculosis* DosS is a redox sensor and DosT is a hypoxia sensor. *Proc. Natl. Acad. Sci. U.S.A.* **104**: 11568-11573.

Kumar, A., Deshane, J.S., Crossman, D.K., Bolisetty, S., Yan, B.S., Kramnik, I., Agarwal, A., and Steyn, A.J. (2008) Heme oxygenase-1-derived carbon monoxide induces the *Mycobacterium tuberculosis* dormancy regulon. *J. Biol. Chem.* **283**: 18032-18039.

LaCelle, M., Kumano, M., Kurita, K., Yamane, K., Zuber, P., and Nakano, M.M. (1996) Oxygen-controlled regulation of the flavohemoglobin gene in *Bacillus subtilis*. *J. Bacteriol.* **178**: 3803-3808.

Lanzilotta, W.N., Schuller, D.J., Thorsteinsson, M.V., Kerby, R.L., Roberts, G.P., and Poulos, T.L. (2000) Structure of the CO sensing transcription activator CooA. *Nature* **7**: 876-880.

Lee, M., Arosio, P., Cozzi, A., and Chasteen, N.D. (1994) Identification of the EPR-active iron-nitrosyl complexes in mammalian ferritins. *Biochemistry* **33**: 3679-3687.

Letoffe, S., Ghigo, J.M., and Wandersman, C. (1994) Iron acquisition from heme and hemoglobin by a *Serratia marcescens* extracellular protein. *Proc. Natl. Acad. Sci. U. S. A.* **91**: 9876-9880.

Letoffe, S., Nato, F., Goldberg, M. E., and Wandersman, C. (1999) Interactions of HasA, a bacterial haemophore, with haemoglobin and with its outer membrane receptor HasR. *Mol. Microbiol.* **33**: 546-555.

Letunic, I., Goodstadt, L., Dickens, N.J., Doerks, T., Schultz, J., Mott, R., Ciccarelli, F., Copley, R.R., Ponting, C.P., and Bork, P. (2002) Recent improvements to the SMART domain-based sequence annotation resource. *Nucleic Acids Res.* **30**: 242-244.

Li, T., Quillin, M.L., Phillips, G.N., Jr., and Olson, J.S. (1994) Structural determinants of the stretching frequency of CO bound to myoglobin. *Biochemistry* **33**: 1433-1446.

Liao, J.C., Hein, T.W., Vaughn, M.W., Huang, K.T., and Kuo, L. (1999) Intravascular flow decreases erythrocyte consumption of nitric oxide. *Proc. Natl. Acad. Sci. U. S. A.* **96**: 8757-8761.

Lindahl, P.A., Day, E.P., Kent, T.A., Orme-Johnson, W.H., and Münck, E. (1985) Mossbauer, EPR, and magnetization studies of the *Azotobacter vinelandii* Fe protein. Evidence for a $[4Fe\text{-}4S]^{1+}$ cluster with spin S = 3/2. *J. Biol. Chem.* **260**: 11160-11173.

Ling, J., Li, T., Olson, J.S., and Bocian, D.F. (1994) Identification of the iron-carbonyl stretch in distal histidine mutants of carbonmonoxymyoglobin. *Biochim. Biophys. Acta.* **1188**: 417-421.

Liu, L., Zeng, M., Hausladen, A., Heitman, J., and Stamler, J.S. (2000) Protection from nitrosative stress by yeast flavohemoglobin. *Proc. Natl. Acad. Sci. U. S. A.* **97**: 4672-4676.

Liu, X., Samouilov, A., Lancaster, J.R., Jr., and Zweier, J.L. (2002) Nitric oxide uptake by erythrocytes is primarily limited by extracellular diffusion not membrane resistance. *J. Biol. Chem.* **277**: 26194-26199.

Lo, W.-J., Lee, Y.-P., Tsai, J.-H.M., Tsai, H.-H., Hamilton, T.P., Harrison, J.G., and Beckman, J.S. (1995) Infrared absorption of cis- and trans-alkali-metal peroxynitrites (MOONO, M=Li, Na, and K) in solid argon. *J. Chem. Phys.* **103**: 4026-4034.

Lukat-Rodgers, G.S., and Rodgers, K.R. (1997) Characterization of Fe(II) FixL-nitric oxide adducts by resonance Raman spectroscopy. *Biochemistry* **36**: 4178-4187.

Makinen, M.W., and Churg, A.K. (1983) Structural and analytical aspects of the electronic spectra of hemoproteins. In *Iron Porphyrins*. Vol. 1. Lever, A.B.P. and Gray, H.B. (eds). Reading, MA: Addison-Wesley Publishing Company, pp. 141-236.

Mayhew, S.G. (1978) The redox potential of dithionite and SO_2^- from equilibrium reactions with flavodoxins, methyl viologen and hydrogen plus hydrogenase. *Eur. J. Biochem.* **85**: 535-547.

McDonald, C.C., Phillips, W.D., and Mower, H.F. (1965) An electron spin resonance study of some complexes of iron, nitric oxide, and anionic ligands. *J. Am. Chem. Soc.* **87**: 3319-3326.

McLean, K.J., Cheesman, M.R., Rivers, S.L., Richmond, A., Leys, D., Chapman, S.K., Reid, G.A., Price, N.C., Kelly, S.M., Clarkson, J., Smith, W.E., and Munro, A.W. (2002) Expression, purification and spectroscopic characterization of the cytochrome P450 CYP121 from *Mycobacterium tuberculosis*. *J. Inorg. Biochem.* **91**: 527-541.

McMillin, D.R. (2000) Electronic absorption spectroscopy. In *Physical Methods in Bioinorganic Chemistry*. Vol. 1. Que, L.J. (ed). Sausalito, CA: University Science Books, pp. 1-58.

Membrillo-Hernandez, J., Ioannidis, N., and Poole, R.K. (1996) The flavohaemoglobin (Hmp) of *Escherichia coli* generates superoxide in vitro and causes oxidative stress in vivo. *FEBS Lett.* **382**: 141-144.

Merryweather, J., Summers, F., Vitello, L.B., and Erman, J.E. (1998) Metmyoglobin/fluoride: effect of distal histidine protonation on the association and dissociation rate constants. *Arch. Biochem. Biophys.* **358**: 359-368.

Miller, J.H. (1972) *Experiments in Molecular Genetics.* Cold Springs Harbor, NY: Cold Springs Harbor Laboratory Press.

Miyatake, H., Mukai, M., Adachi, S., Nakamura, H., Tamura, K., Iizuka, T., Shiro, Y., Strange, R.W., and Hasnain, S.S. (1999) Iron coordination structures of oxygen sensor FixL characterized by Fe K-edge extended x-ray absorption fine structure and resonance Raman spectroscopy. *J. Biol. Chem.* **274**: 23176-23184.

Moncada, S., Palmer, R.M., and Higgs, E.A. (1991) Nitric oxide: physiology, pathophysiology, and pharmacology. *Pharmacol. Rev.* **43**: 109-142.

Nakamura, H., Saito, K., and Shiro, Y. (2001) Quantitative measurement of radioactive phosphorylated proteins in wet polyacrylamide gels. *Anal. Biochem.* **294**: 187-188.

Nakano, M.M., Marahiel, M.A., and Zuber, P. (1988) Identification of a genetic locus required for biosynthesis of the lipopeptide antibiotic surfactin in *Bacillus subtilis*. *J. Bacteriol.* **170**: 5662-5668.

Nakano, M.M., Hoffmann, T., Zhu, Y., and Jahn, D. (1998) Nitrogen and oxygen regulation of *Bacillus subtilis nasDEF* encoding NADH-dependent nitrite reductase by TnrA and ResDE. *J. Bacteriol.* **180**: 5344-5350.

Nakano, M.M., and Zuber, P. (1998) Anaerobic growth of a "strict aerobe" (*Bacillus subtilis*). *Annu. Rev. Microbiol.* **52**: 165-190.

Nakano, M.M. (2002) Induction of ResDE-dependent gene expression in *Bacillus subtilis* in response to nitric oxide and nitrosative stress. *J. Bacteriol.* **184**: 1783-1787.

Nakano, M.M. (2006) Essential role of flavohemoglobin in long-term anaerobic survival of *Bacillus subtilis*. *J. Bacteriol.* **188**: 6415-6418.

Nakano, M.M., Geng, H., Nakano, S., and Kobayashi, K. (2006) The nitric oxide-responsive regulator NsrR controls ResDE-dependent gene expression. *J. Bacteriol.* **188**: 5878-5887.

Newton, G.L., Rawat, M., La Clair, J.J., Jothivasan, V.K., Budiarto, T., Hamilton, C.J., Claiborne, A., Helmann, J.D., and Fahey, R.C. (2009) Bacillithiol is an antioxidant thiol produced in *Bacilli*. *Nat. Chem. Biol*. **5**: 625-627.

Ohta, T., Yoshimura, H., Yoshioka, S., Aono, S., and Kitagawa, T. (2004) Oxygen-sensing mechanism of HemAT from *Bacillus subtilis*: a resonance Raman spectroscopic study. *J. Am. Chem. Soc.* **126**: 15000-15001.

Olson, J.S., Foley, E.W., Rogge, C., Tsai, A.L., Doyle, M.P., and Lemon, D.D. (2004) No scavenging and the hypertensive effect of hemoglobin-based blood substitutes. *Free Radic. Biol. Med.* **36**: 685-697.

Orme-Johnson, W.H., and Orme-Johnson, N.R. (1982) Iron-sulfur proteins: The problem of determining cluster type. In *Iron-sulfur Proteins*. Vol. 4. Spiro, T.G. (ed). New York: Wiley-Interscience, pp. 67-96.

Overton, T.W., Whitehead, R., Li, Y., Snyder, L.A., Saunders, N.J., Smith, H., and Cole, J.A. (2006) Coordinated regulation of the *Neisseria gonorrhoeae*-truncated denitrification pathway by the nitric oxide-sensitive repressor, NsrR, and nitrite-insensitive NarQ-NarP. *J. Biol. Chem.* **281**: 33115-33126.

Overton, T.W., Justino, M.C., Li, Y., Baptista, J.M., Melo, A.M., Cole, J.A., and Saraiva, L.M. (2008) Widespread distribution in pathogenic bacteria of di-iron proteins that repair oxidative and nitrosative damage to iron-sulfur centers. *J. Bacteriol.* **190**: 2004-2013.

Park, H., Suquet, C., Satterlee, J.D., and Kang, C. (2004) Insights into signal transduction involving PAS domain oxygen-sensing hemoproteins from the X-ray crystal structure of *Escherichia coli* Dos heme domain (*Ec* DosH). *Biochemistry* **43**: 2738-2746.

Pendrak, M.L., Yan, S.S., and Roberts, D.D. (2004) Sensing the host environment: recognition of hemoglobin by the pathogenic yeast *Candida albicans*. *Arch. Biochem. Biophys.* **426**: 148-156.

Petryka, Z., Nicholson, D.C., and Gray, C.H. (1962) Isomeric bile pigments as products of the in vitro fission of haemin. *Nature* **194**: 1047-1048.

Podust, L.M., Ioanoviciu, A., and Ortiz de Montellano, P.R. (2008) 2.3 Å X-ray structure of the heme-bound GAF domain of sensory histidine kinase DosT of *Mycobacterium tuberculosis*. *Biochemistry* **47**: 12523-12531.

Protchenko, O., and Philpott, C.C. (2003) Regulation of intracellular heme levels by HMX1, a homologue of heme oxygenase, in *Saccharomyces cerevisiae*. *J. Biol. Chem.* **278**: 36582-36587.

Puig, S., Askeland, E., and Thiele, D.J. (2005) Coordinated remodeling of cellular metabolism during iron deficiency through targeted mRNA degradation. *Cell* **120**: 99-110.

Ray, G.B., Li, X.-Y., Ibers, J.A., Sessler, J.L., and Spiro, T.G. (1994) How far can proteins bend the FeCO unit? Distal polar and steric effects in hemoproteins and models. *J. Am. Chem. Soc* **116**: 162-176.

Reents, H., Gruner, I., Harmening, U., Bottger, L.H., Layer, G., Heathcote, P., Trautwein, A.X., Jahn, D., and Hartig, E. (2006) *Bacillus subtilis* Fnr senses oxygen via a [4Fe-4S] cluster coordinated by three cysteine residues without change in the oligomeric state. *Mol. Microbiol.* **60**: 1432-1445.

Reiter, C.D., Wang, X., Tanus-Santos, J.E., Hogg, N., Cannon, R.O., 3rd, Schechter, A.N., and Gladwin, M.T. (2002) Cell-free hemoglobin limits nitric oxide bioavailability in sickle-cell disease. *Nat. Med.* **8**: 1383-1389.

Reynolds, M. F., Parks, R. B., Burstyn, J. N., Shelver, D., Thorsteinsson, M. V., Kerby, R. L., Roberts, G. P., Vogel, K. M., and Spiro, T. G. (2000) Electronic absorption, EPR, and resonance Raman spectroscopy of CooA, a CO-sensing transcription activator from *R. rubrum*, reveals a five-coordinate NO-heme. *Biochemistry* **39**: 388-396

Roberts, D.M., Liao, R.P., Wisedchaisri, G., Hol, W.G., and Sherman, D.R. (2004) Two sensor kinases contribute to the hypoxic response of *Mycobacterium tuberculosis*. *J. Biol. Chem.* **279**: 23082-23087.

Rock, J.D., Thomson, M.J., Read, R.C., and Moir, J.W. (2007) Regulation of denitrification genes in *Neisseria meningitidis* by nitric oxide and the repressor NsrR. *J. Bacteriol.* **189**: 1138-1144.

Rodionov, D.A., Dubchak, I.L., Arkin, A.P., Alm, E.J., and Gelfand, M.S. (2005) Dissimilatory metabolism of nitrogen oxides in bacteria: comparative reconstruction of transcriptional networks. *PLoS Comput. Biol.* **1**: e55.

Rouault, T.A. (2006) The role of iron regulatory proteins in mammalian iron homeostasis and disease. *Nat. Chem. Biol.* **2**: 406-414.

Rousset, M., Montet, Y., Guigliarelli, B., Forget, N., Asso, M., Bertrand, P., Fontecilla-Camps, J.C., and Hatchikian, E.C. (1998) [3Fe-4S] to [4Fe-4S] cluster conversion in *Desulfovibrio fructosovorans* [NiFe] hydrogenase by site-directed mutagenesis. *Proc. Natl. Acad. Sci. U. S. A.* **95**: 11625-11630.

Russwurm, M., and Koesling, D. (2004) NO activation of guanylyl cyclase. *EMBO J.* **23**: 4443-4450.

Santos, R., Buisson, N., Knight, S., Dancis, A., Camadro, J.M., and Lesuisse, E. (2003) Haemin uptake and use as an iron source by *Candida albicans*: role of CaHMX1-encoded haem oxygenase. *Microbiology* **149**: 579-588.

Sardiwal, S., Kendall, S.L., Movahedzadeh, F., Rison, S.C., Stoker, N.G., and Djordjevic, S. (2005) A GAF domain in the hypoxia/NO-inducible *Mycobacterium tuberculosis* DosS protein binds haem. *J. Mol. Biol.* **353**: 929-936.

Schmitt, M.P. (1997) Utilization of host iron sources by *Corynebacterium diphtheriae*: identification of a gene whose product is homologous to eukaryotic heme oxygenases and is required for acquisition of iron from heme and hemoglobin. *J. Bacteriol.* **179**: 838-845.

Schwartz, C.J., Giel, J.L., Patschkowski, T., Luther, C., Ruzicka, F.J., Beinert, H., and Kiley, P.J. (2001) IscR, an Fe-S cluster-containing transcription factor, represses expression of *Escherichia coli* genes encoding Fe-S cluster assembly proteins. *Proc. Natl. Acad. Sci. U. S. A.* **98**: 14895-14900.

Sciotti, M.A., Chanfon, A., Hennecke, H., and Fischer, H.M. (2003) Disparate oxygen responsiveness of two regulatory cascades that control expression of symbiotic genes in *Bradyrhizobium japonicum*. *J. Bacteriol.* **185**: 5639-5642.

Sham, S., Calzolai, L., Wang, P.L., Bren, K., Haarklau, H., Brereton, P.S., Adams, M.W., and La Mar, G.N. (2002) A solution NMR molecular model for the aspartate-ligated, cubane cluster containing ferredoxin from the hyperthermophilic archeaon *Pyrococcus furiosus*. *Biochemistry* **41**: 12498-12508.

Shiloh, M.U., Manzanillo, P., and Cox, J.S. (2008) *Mycobacterium tuberculosis* senses host-derived carbon monoxide during macrophage infection. *Cell Host Microbe* **3**: 323-330.

Silchenko, S., Sippel, M.L., Kuchment, O., Benson, D.R., Mauk, A.G., Altuve, A., and Rivera, M. (2000) Hemin is kinetically trapped in cytochrome b_5 from rat outer mitochondrial membrane. *Biochem. Biophys. Res. Commun.* **273**: 467-472.

Singh, A., Guidry, L., Narasimhulu, K.V., Mai, D., Trombley, J., Redding, K.E., Giles, G.I., Lancaster, J.R., Jr., and Steyn, A.J. (2007) *Mycobacterium tuberculosis* WhiB3 responds to O_2 and nitric oxide via its [4Fe-4S] cluster and is essential for nutrient starvation survival. *Proc. Natl. Acad. Sci. U. S. A.* **104**: 11562-11567.

Sitter, A.J., Shifflett, J.R., and Terner, J. (1988) Resonance Raman spectroscopic evidence for heme iron-hydroxide ligation in peroxidase alkaline forms. *J. Biol. Chem.* **263**: 13032-13038.

Skaar, E.P., Gaspar, A.H., and Schneewind, O. (2004) IsdG and IsdI, heme-degrading enzymes in the cytoplasm of *Staphylococcus aureus*. *J. Biol. Chem.* **279**: 436-443.

Skaar, E.P., Gaspar, A.H., and Schneewind, O. (2006) *Bacillus anthracis* IsdG, a heme-degrading monooxygenase. *J. Bacteriol.* **188**: 1071-1080.

Sousa, E.H., Tuckerman, J.R., Gonzalez, G., and Gilles-Gonzalez, M.A. (2007) DosT and DevS are oxygen-switched kinases in *Mycobacterium tuberculosis*. *Protein Sci.* **16**: 1708-1719.

Spiro, T.G. (1983) The resonance Raman spectroscopy of metalloporphyins and hemoproteins. In *Iron Porphyrins*. Vol. 2. Lever, A.B.P. and Gray, H.B. (eds). Reading, MA: Addison-Wesley Publishing Company, pp. 89-160.

Spiro, T.G., Czeruszewicz, R.S., and Han, S. (1988) Iron-sulfur proteins and analog complexes. In *Biological Applications of Raman Spectroscopy*. Vol. 3. Spiro, T.G. (ed). New York: Wiley-Interscience, pp. 523-553.

Spiro, T.G., and Li, X.Y. (1988) Resonance Raman spectroscopy of metalloporphyrins. In *Biological Applications of Raman Spectroscopy. Vol. 3. Resonance Raman spectra of hemes and metalloproteins*. Vol. 3. Spiro, T.G. (ed). New York: John Wiley & Sons, pp. 1-37.

Spiro, T.G., and Czeruszewicz, R.S. (2000) Resonance Raman spectroscopy. In *Physical Methods in Bioinorganic Chemistry*. Vol. 1. Que, L., Jr. (ed). Sausalito, CA: University Science Books, pp. 59-119.

Stone, J.R., Sands, R.H., Dunham, W.R., and Marletta, M.A. (1995) Electron paramagnetic resonance spectral evidence for the formation of a pentacoordinate nitrosyl-heme complex on soluble guanylate cyclase. *Biochem. Biophys. Res. Commun.* **207**: 572-577.

Strickler, S.J., and Kasha, M. (1963) Solvent effects on the electronic absorption spectrum of nitrite ion. *J. Am. Chem. Soc.* **85**: 2899-2901.

Suits, M.D., Pal, G.P., Nakatsu, K., Matte, A., Cygler, M., and Jia, Z. (2005) Identification of an *Escherichia coli* O157:H7 heme oxygenase with tandem functional repeats. *Proc. Natl. Acad. Sci. U. S. A.* **102**: 16955-16960.

Sun, J., Wilks, A., Ortiz de Montellano, P.R., and Loehr, T.M. (1993) Resonance Raman and EPR spectroscopic studies on heme-heme oxygenase complexes. *Biochemistry* **32**: 14151-14157.

Sun, J., Loehr, T.M., Wilks, A., and Ortiz de Montellano, P.R. (1994) Identification of histidine 25 as the heme ligand in human liver heme oxygenase. *Biochemistry* **33**: 13734-13740.

Takahashi, S., Wang, J., Rousseau, D.L., Ishikawa, K., Yoshida, T., Takeuchi, N., and Ikeda-Saito, M. (1994) Heme-heme oxygenase complex: structure and properties of the catalytic site from resonance Raman scattering. *Biochemistry* **33**: 5531-5538.

Takahashi, S., Ishikawa, K., Takeuchi, N., Ikeda-Saito, M., Yoshida, T., and Rousseau, D.L. (1995) Oxygen-bound heme-heme oxygenase complex: Evidence for a highly bent structure of the coordinated oxygen. *J. Am. Chem. Soc.* **117**: 6002-6006.

Tamura, K., Nakamura, H., Tanaka, Y., Oue, S., Tsukamoto, K., Nomura, M., Tsuchiya, T., Adachi, S., Takahashi, S., Iizuka, T., and Shiro, Y. (1996) Nature of endogenous ligand binding to heme iron in oxygen sensor FixL. *J. Am. Chem. Soc.* **118**: 9434-9435.

Thomas, D.D., Liu, X., Kantrow, S.P., and Lancaster, J.R., Jr. (2001) The biological lifetime of nitric oxide: implications for the perivascular dynamics of NO and O_2. *Proc. Natl. Acad. Sci. U. S. A.* **98**: 355-360.

Tomita, T., Hirota, S., Ogura, T., Olson, J.S., and Kitagawa, T. (1999) Resonance Raman investigation of Fe-N-O structure of nitrosylheme in myoglobin and its mutants. *J. Phys. Chem. B* **103**: 7044-7054.

Tomita, T., Gonzalez, G., Chang, A.L., Ikeda-Saito, M., and Gilles-Gonzalez, M.A. (2002) A comparative resonance Raman analysis of heme-binding PAS domains: heme iron coordination structures of the *Bj*FixL, *Ax*PDEA1, *Ec*Dos, and *Mt*Dos proteins. *Biochemistry* **41**: 4819-4826.

Tsai, J.-H.M., Harrison, J.G., Martin, J.C., Hamilton, T.P., van der Woerd, M., Jablonsky, M.J., and Beckman, J.S. (1994) Role of conformation of peroxynitrite anion (ONOO-) with its stability and toxicity. *J. Am. Chem. Soc.* **116**: 4115-4116.

Tsubaki, M., Srivastava, R.B., and Yu, N.T. (1982) Resonance Raman investigation of carbon monoxide bonding in (carbon monoxy)hemoglobin and -myoglobin: detection of Fe-CO stretching and Fe-C-O bending vibrations and influence of the quaternary structure change. *Biochemistry* **21**: 1132-1140.

Tucker, N.P., Hicks, M.G., Clarke, T.A., Crack, J.C., Chandra, G., Le Brun, N.E., Dixon, R., and Hutchings, M.I. (2008) The transcriptional repressor protein NsrR senses nitric oxide directly via a [2Fe-2S] cluster. *PLoS ONE* **3**: e3623.

Tuckerman, J.R., Gonzalez, G., Dioum, E.M., and Gilles-Gonzalez, M.A. (2002) Ligand and oxidation-state specific regulation of the heme-based oxygen sensor FixL from *Sinorhizobium meliloti*. *Biochemistry* **41**: 6170-6177.

Uchida, T., Ishikawa, H., Ishimori, K., Morishima, I., Nakajima, H., Aono, S., Mizutani, Y., and Kitagawa, T. (2000) Identification of histidine 77 as the axial heme ligand of carbonmonoxy CooA by picosecond time-resolved resonance Raman spectroscopy. *Biochemistry* **39**: 12747-12752.

Uchida, T., and Kitagawa, T. (2005) Mechanism for transduction of the ligand-binding signal in heme-based gas sensory proteins revealed by resonance Raman spectroscopy. *Acc. Chem. Res.* **38**: 662-670.

Unno, M., Matsui, T., Chu, G.C., Couture, M., Yoshida, T., Rousseau, D.L., Olson, J.S., and Ikeda-Saito, M. (2004) Crystal structure of the dioxygen-bound heme oxygenase from *Corynebacterium diphtheriae*: Implications for heme oxygenase function. *J. Biol. Chem.* **279**: 21055-21061.

Van Wart, H.E., and Zimmer, J. (1985) Resonance Raman evidence for the activation of dioxygen in horseradish oxyperoxidase. *J. Biol. Chem.* **260**: 8372-8377.

Vanin, A.F., Serezhenkov, V.A., Mikoyan, V.D., and Genkin, M.V. (1998) The 2.03 signal as an indicator of dinitrosyl-iron complexes with thiol-containing ligands. *Nitric Oxide* **2**: 224-234.

Vogel, K.M., Kozlowski, P.M., Zgierski, M.Z., and Spiro, T.G. (1999) Determinants of the FeXO (X = C, N, O) vibrational frequencies in heme adducts from experiment and density functional theory. *J. Am. Chem. Soc.* **121**: 9915-9921.

Voskuil, M.I., Schnappinger, D., Visconti, K.C., Harrell, M.I., Dolganov, G.M., Sherman, D.R., and Schoolnik, G.K. (2003) Inhibition of respiration by nitric oxide induces a *Mycobacterium tuberculosis* dormancy program. *J. Exp. Med.* **198**: 705-713.

Wanat, A., Gdula-Argasinska, J., Rutkowska-Zbik, D., Witko, M., Stochel, G., and van Eldik, R. (2002) Nitrite binding to metmyoglobin and methemoglobin in comparison to nitric oxide binding. *J. Biol. Inorg. Chem.* **7**: 165-176.

Wayne, L.G., and Hayes, L.G. (1996) An in vitro model for sequential study of shiftdown of *Mycobacterium tuberculosis* through two stages of nonreplicating persistence. *Infect. Immun.* **64**: 2062-2069.

Wayne, L.G., and Sohaskey, C.D. (2001) Nonreplicating persistence of *Mycobacterium tuberculosis*. *Annu. Rev. Microbiol.* **55**: 139-163.

Wegele, R., Tasler, R., Zeng, Y., Rivera, M., and Frankenberg-Dinkel, N. (2004) The heme oxygenase(s)-phytochrome system of *Pseudomonas aeruginosa*. *J. Biol. Chem.* **279**: 45791-45802.

Wilks, A., Black, S.M., Miller, W.L., and Ortiz de Montellano, P.R. (1995) Expression and characterization of truncated human heme oxygenase (hHO-1) and a fusion protein of hHO-1 with human cytochrome P450 reductase. *Biochemistry* **34**: 4421-4427.

Wilks, A., and Moënne-Loccoz, P. (2000) Identification of the proximal ligand His-20 in heme oxygenase (Hmu O) from *Corynebacterium diphtheriae*. Oxidative cleavage of the heme macrocycle does not require the proximal histidine. *J. Biol. Chem.* **275**: 11686-11692.

Woodward, L. A. (1967) General introduction in *Raman Spectroscopy: Theory and Practice.* Szymanski, H. A. (ed.) New York: Plenum Press, 1-43.

Wolff, N., Izadi-Pruneyre, N., Couprie, J., Habeck, M., Linge, J., Rieping, W., Wandersman, C., Nilges, M., Delepierre, M., and Lecroisey, A. (2008) Comparative analysis of structural and dynamic properties of the loaded and unloaded hemophore HasA: functional implications. *J. Mol. Biol.* **376**: 517-525.

World Health Organization Report (2006) Global tuberculosis control-surveillance, planning, financing.

Wu, G., Cruz-Ramos, H., Hill, S., Green, J., Sawers, G., and Poole, R.K. (2000) Regulation of cytochrome *bd* expression in the obligate aerobe *Azotobacter vinelandii* by CydR (Fnr). Sensitivity to oxygen, reactive oxygen species, and nitric oxide. *J. Biol. Chem.* **275**: 4679-4686.

Yamamoto, K., Ishikawa, H., Takahashi, S., Ishimori, K., Morishima, I., Nakajima, H., and Aono, S. (2001) Binding of CO at the Pro2 side is crucial for the activation of CO-sensing transcriptional activator CooA. ^{1}H NMR spectroscopic studies. *J. Biol. Chem.* **276**: 11473-11476.

Yeh, S.R., Couture, M., Ouellet, Y., Guertin, M., and Rousseau, D.L. (2000) A cooperative oxygen binding hemoglobin from *Mycobacterium tuberculosis.* Stabilization of heme ligands by a distal tyrosine residue. *J Biol Chem* **275**: 1679-1684.

Yeo, W.-S., Lee, J.-H., Lee, K.-C., and Roe, J.-H. (2006) IscR acts as an activator in response to oxidative stress for the *suf* operon encoding Fe-S assembly proteins. *Molec. Microbiol.* **61**: 206-218.

Yoshimura, H., Yoshioka, S., Kobayashi, K., Ohta, T., Uchida, T., Kubo, M., Kitagawa, T., and Aono, S. (2006) Specific hydrogen-bonding networks responsible for selective O_2 sensing of the oxygen sensor protein HemAT from *Bacillus subtilis.* *Biochemistry* **45**: 8301-8307.

Yukl, E.T., Ioanoviciu, A., de Montellano, P.R., and Moënne-Loccoz, P. (2007) Interdomain interactions within the two-component heme-based sensor DevS from *Mycobacterium tuberculosis*. *Biochemistry* **46**: 9728-9736.

Yukl, E.T., Ioanoviciu, A., Nakano, M.M., de Montellano, P.R., and Moënne-Loccoz, P. (2008) A distal tyrosine residue is required for ligand discrimination in DevS from *Mycobacterium tuberculosis*. *Biochemistry* **47**: 12532-12539.

Yukl, E.T., Elbaz, M. A., Nakano, M.M., and Moënne-Loccoz, P. (2008) Transcription factor NsrR from *Bacillus subtilis* senses nitric oxide with a 4Fe-4S cluster. *Biochemistry* **47**: 13084-13092.

Yukl, E.T., de Vries S., and Moënne-Loccoz, P. (2009) The millisecond intermediate in the reaction of nitric oxide with oxymyoblobin is an iron(III)-nitrato complex, not a peroxynitrite. *J. Am. Chem. Soc.* **131**: 7234-7235.

Zhu, W., Wilks, A., and Stojiljkovic, I. (2000) Degradation of heme in gram-negative bacteria: the product of the hemO gene of *Neisseriae* is a heme oxygenase. *J. Bacteriol.* **182**: 6783-6790.

BIOGRAPHICAL SKETCH

Erik Yukl was born on March 4, 1983, in Baker City, Oregon. In 2005 he received a B. S. degree in Chemistry with an emphasis on biochemistry from Pacific University. In the fall of 2005, he began his graduate studies in the Department of Science and Engineering within the School of Medicine at Oregon Health and Science University.

Publications:

Bauman, A. T., Yukl, E. T., Alkevich, K., McCormack, A. L., Blackburn, N. J. (2006) The hydrogen peroxide reactivity of peptidylglycine monooxygenase supports a Cu(II)-superoxo catalytic intermediate. *J. Biol. Chem*. **281** (7), 4190-4198.

Kim, D. Yukl, E. T., Moënne-Loccoz, P., de Montellano, P. R. (2006) Yeast heme oxygenases: Functional expression and characterization of Hmx1 from *Saccharomyces cerevisiae* and *Candida albicans. Biochemistry* **45** (49), 14772-14780.

Bauman, A. T., Jaron, S., Yukl, E. T., Burchfiel, J. R., Blackburn, N. J. (2006) pH dependence of peptidylglycine monooxygenase: mechanistic implications of Cu-Methionine binding dynamics. *Biochemistry* **45** (37), 11140-11150.

Whittaker, M. M., Pan, H. Y., Yukl E. T., Whittaker, J. W. (2007) Burst kinetics and redox transformations of the active site manganese ion in oxalate oxidase: implications for the catalytic mechanism. *J. Biol. Chem*. **282** (10), 7011-7023

Ioanoviciu, A., Yukl, E. T., Moënne-Loccoz, P., de Montellano P. R. (2007) DevS, a heme-containing two-component oxygen sensor of *Mycobacterium tuberculosis*. *Biochemistry* **46** (14), 4250-4260.

Yukl, E. T., Ioanoviciu, A., de Montellano. P. R., Moënne-Loccoz, P. (2007) Interdomain interactions within the two-component heme-based sensor DevS from *Mycobacterium tuberculosis*. *Biochemistry* **46** (34), 9728-9736.

Yukl, E. T., Ioanoviciu, A., Nakano, M. M., Ortiz de Montellano, P. R., Moënne-Loccoz, P. (2008) A distal tyrosine residue is required for ligand discrimination in DevS from *Mycobacterium tuberculosis*. *Biochemistry* **47** (47), 12532-12539.

Yukl, E. T., Elbaz, M. A., Nakano, M. M., Moënne-Loccoz, P. (2008) Transcription factor NsrR from *Bacillus subtilis* senses nitric oxide with a 4Fe−4S Cluster. *Biochemistry* **47** (49), 13084-13092.

Alontaga, A. Y., Rodriguez, J. C., Schönbrunn, E., Becker, A., Funke, T., Yukl, E. T., Hayashi, T., Stobaugh, J., Moënne-Loccoz, P., Rivera, M. (2009) Structural characterization of the hemophore HasAp from *Pseudomonas aeruginosa*: NMR spectroscopy reveals protein−protein interactions between holo-HasAp and hemoglobin. *Biochemistry* **48** (1) 96-109.

Yukl, E. T., de Vries, S., Moënne-Loccoz, P. (2009) The millisecond intermediate in the reaction of nitric oxide with oxymyoglobin is an iron(III)-nitrato complex, not a peroxynitrite. *J. Am. Chem. Soc.* **131 (**21), 7234-7235.